NTNU – Trondheim
Norwegian University of
Science and Technology

Bacterial Microarrays by Microcontact Printing

Development of a Method for Immobilizing
Live Bacteria on Microarrays

Vegar Ottesen

Nanotechnology
Submission date: June 2014
Supervisor: Marit Sletmoen, IFY
Co-supervisor: Nina Bjørk Arnfinnsdottir, IFY

Norwegian University of Science and Technology
Department of Physics

This work is dedicated to the memory of John Arthur Ottesen (1922-2008)
He kindled my love of science and silently cheered me on toward my dreams.

Cover art was taken by Vegar Ottesen on a Leica SP5 confocal microscope. The image shows fluorescently labeled *Pseudomonas putida* KT2440 adhering to text spelling NTNU, written in polydopamine, deposited by microcontact printing. The image is digitally edited for aesthetic purposes and should therefore not be considered a scientific image.

Abstract

Traditional microbiological experimental methods generally reveal population-wide statistics and are not capable of revealing variations between individual cells. In an effort to address this, a cheap, quick and easy means of producing micro-arrays with live bacteria immobilized on the array's coordinates has been developed. To achieve this, microcontact printing (μCP) was used to print circular polydopamine (PD) "islands" onto a surface coated with either poly(ethylene glycol) (PEG) or poly(vinyl alcohol) (PVA). The bacteria, *Pseudomonas putida* KT2440 were successfully immobilized on approximately 97% of the printed islands. The portion of islands with immobilized bacteria and the average number of bacteria per island depends on island diameter. A Live/Dead® *Bac*Light™ assay revealed that over 99% of the immobilized bacteria survive the immobilization on the array. Qualitative analysis suggests the bacteria survive for hours after immobilization, provided nutrients are available. The developed method may, by revising the stamp design and/or choice of elastomer, likely be optimized to immobilize only one bacterium per array coordinate.

Sammendrag

Tradisjonelle eksperimentelle metoder i mikrobiologi avdekker normalt statistiske data om en hel mikrobiell populasjon, og er ikke i stand til å avdekke informasjon om heterogenitet innad i en populasjon. Denne avhandlingen presenterer en eksperimentell metode for å feste levende bakterier på mikro-arrays for å kunne studere bakteriell heterogenitet. Arrayene ble produsert ved microcontact printing av sirkulære «øyer» av polydopamin (PD) på et underlag dekket med poly(etylen glykol) (PEG) eller poly(vinyl alkohol) (PVA). Bakterier av arten *Pseudomonas putida* KT2440, ble immobilisert på omtrent 97% av de trykte PD-øyene. Andelen av øyer med immobiliserte bakterier såvels som antallet bakterier per øy avhenger av øyenes diameter. Et Live/Dead® *Bac*Light™ assay avdekket at over 99% av de immobiliserte bakteriene overlevde isolerings- og immobiliserings-prosessen. Kvalitativ analyse av bakterier isolert over tid tyder på at bakteriene overlever i flere timer på arrayene, forutsett at næring er tilgjengelig. Den utviklede metoden presentert i denne avhandlingen kan, ved revisjon av stempeldesign og/eller valg av elastomer, trolig optimeres slik at hver adhesive øy med høyere sannsynlighet immobiliserer kun èn bakterie.

Preface

This work is submitted in partial fulfillment of the requirements for a Siv.Ing. degree in Nanotechnology from NTNU. The work presented herein was performed at the Department of Physics, division of biophysics and medical technology at NTNU. Experimental work was done at the lab and microscopy facilities in the biophysics division, at NTNU nanolab cleanroom facilities and at the department of biotechnology, NTNU.

Some of the work presented in this thesis is also included in a draft for scientific publication with working title "Design of Bacterial Microarrays". This article was authored by Nina Bjørk Arnfinnsdottir, Vegar Ottesen, Rahmi Lale and Marit Sletmoen.

Acknowledgements

I wish to extend my deepest thanks to my supervisor *Marit Sletmoen* for her open door and readily provided advice throughout the completion of both my master thesis and preceding project work. Special thanks are also due my co-supervisor *Nina Bjørk Arnfinnsdottir* for engaging conversations on related and unrelated topics. Moreover, both *Nina* and *Marit* were excellent co-workers during the work on the publication mentioned previously in this preface. It has been a true joy working with them both.

I would also like to extent special gratitude to post-doctoral fellow *Rahmi Lale* for his assistance on questions related to microbiology and biotechnology as well as for supplying microbes and growth medium for my experiments.

Thanks are also extended to *Katarzyna Maria Psonka-Antonczyk* for valuable input on cleaning processes and permission to use an AFM image she recorded in this thesis. Additionally, thanks are due *Kai Müller Beckwith* and *Pawel Tadeusz Sikorski* for access to lab facilities with spin coating equipment. For their friendly and readily provided assistance and training on microscopes and lab equipment thanks are also extended to *Astrid Bjørkøy*, *Gjertrud Maurstad* and *Kristin Grendstad Sæterbø* .

Last, but certainly not least, I would extend my sincerest gratitude to my dear wife and friend *Kelly McCammon Ottesen* for her continued friendship, love and support.

Contents

Acronyms

AFM *atomic force microscope* 38, 53, 77, 78

BSA *bovine serum albumin* 18, 35, 36, 38, 68, 72

BSE *back-scattered electrons* 28–30, 34, 44, 50

CLSM *confocal laser scanning microscope* . 21–23, 26, 27, 34, 39, 43, 73, 77, 84

DOF *depth of field* 77

DOPA *3,4-dihydroxy-L-phenylalanine* 15, 16

DPSS *diode-pumped solid-state laser* 54, 56, 60, 61, 63, 68, 115

ECM *extra-cellular matrix* 15

FITC *fluorescein isothiocyanate* 35, 37, 42

LB-medium *lysogeny broth growth medium* 37–39, 60, 63, 66, 83–85

LPS *lipo-polysaccharide* 14

MAP *mussel adhesive protein* 15, 16, 71

MFP *mussel foot protein* 15

NA *numerical aperture* 77

PBS *phosphate buffered saline* 35, 36

PD *polydopamine* . .iii, v, 15, 16, 18, 38, 39, 42, 52, 53, 58, 60, 61, 63, 66–68, 71–73, 75–79, 82, 83, 85, 87, 89, 92, 111, 115

PDMS *polydimethylsiloxane* 7–10, 31, 32, 34, 76, 80, 82, 87

PEG *poly(ethylene glycol)* . . iii, v, 15–19, 35, 36, 39, 46, 51, 53, 56, 58, 61, 66, 67, 70–73, 75, 77, 78, 87, 89, 92

PEI *polyethyleneimine* 35–38, 68, 72, 89, 92

PLL *poly-L-lysine* 35–38, 68, 72, 89, 92

PMT *photomultiplier tube* 26, 27, 46, 54, 56, 60, 61, 63, 115

PVA *poly(vinyl alcohol)* . . iii, v, xvi, 16–18, 35, 42, 58, 60, 63, 67, 70–73, 75, 79, 87, 92, 111, 115

SAM *self-assembling monolayer* 18

SE *secondary electrons* 29, 30

SEM *scanning electron microscope* 28–30, 34, 43, 49

tris *tris(hydroxymethyl)aminomethane* 37, 38, 92

List of Figures

List of Tables

Introduction

1

It is unlikely that van Leeuwenhoek could have fathomed in 1675 the vast scope and impact his discovery would have on human civilization. Since the discovery of microbes, or "animalcules" as they were first known, it has been found that microbial organisms are the most abundant and may well be considered the most diverse life-forms on this planet. Abundant, even in other species. It is now known that healthy human bodies have approximately ten times more bacteria than human cells [1, 2]. Of life's three domains, eukaryotes, archaea and bacteria, bacteria are the oldest, most prevalent across vastly different environments and the most numerous. Organisms from this domain can be both beneficial and detrimental to the good health and survival of more complex organisms such as plants or animals, including humans. Bacteria are of increasing interest to the medical field as global travel grows more widespread, vaccine denial gains ground and antibiotics resistance continues to increase [3, 4]. Chemical industries may also find bacteriology of increasing interest as biotechnology finds more applications for organisms tailored to specific tasks, such as enzyme production for industrial and medical purposes.

Traditional methods for studying bacteria and other microorganisms often rely on microbial colonies large enough to be visible to the naked eye, or nutrient liquid so densely packed with bacteria that it is visibly turbid [1]. Such traditional methods are often more qualitative than quantitative and, due to their reliance upon large numbers, cannot uncover information on variation within the microbial population [1, 2, 5]. While traditional methodology can uncover information about averages within a given population, such as the average expression of a gene or an average response to a given stimulus, they are not suited for the study of heterogeneity within the populations studied.

To effectively study bacterial heterogeneity, it is desirable to follow a large quantity of single bacteria over a period of time. A researcher may find intended heterogeneity studies facilitated by introduction of order, which may enable and/or empower software assisted analysis. A concept which may address both of these concerns has been in use since 1983, when Tse-Wen Chang manually created antibody microarrays for immunoabsorbance studies [6]. Since then microarrays as a concept have seen widespread use in for example genomics, being the concept behind several commercial actors providing microchips with DNA microarrays for medical and research purposes.Examples

of such commercial actors include Affymetrix and Illumina. Conceptually, organizing what is to be studied into arrays is simple. For studies of cells, bacterial or otherwise, the concept has not seen much use. While microarray ordering of live bacterial cells is not untouched by the scientific literature, the described techniques for obtaining such arrays often require extensive lab expertise, expensive equipment and/or components and mastery of difficult and time-consuming processes [7–14]. For viable implementation of the microarray concept in most bacteriological labs a cheap, robust, non-toxic and easily implemented method needs to be developed.

Microcontact printing (µCP) is a soft-lithography method which utilizes polymer, typically elastomer stamps to pattern a substrate. Due to the flexible nature of elastomer stamps, the method can, in principle, pattern a very large variety of surfaces, flat, curved or rough [15, 16]. Moreover, the method is chemically versatile and can readily print a large variety of chemicals (inks) onto these substrates [17]. Production of the stamps used in µCP does require a master, also known as a mold, which is typically produced by photolithography in a cleanroom environment. However, once such a master is produced, it may be re-used a number of times, producing multiple batches of stamps. Each stamp, in turn may be cleaned and re-used multiple times. These factors combine to make µCP an excellent candidate for production of microarrays, even in sparsely stocked labs.

This thesis aims to describe a cheap, rapidly implemented and robust method for the production of bacterial microarrays using model organisms as a template. Examining the efficiency of the described method, the current thesis discusses the viability of bacteria immobilized on the array as well as the ability of the developed method to immobilize bacteria on the printed patterns. Finally we propose possible applications of the developed method for any future work based on, or further refining, the technique.

Theory

2

This master thesis is a continuation of the work presented by Ottesen [18]. Much of the same theory therefore still applies. What follows is for that reason a modification of the text presented in that work.

2.1 Photolithography

As the name suggests photolithography utilizes light, commonly ultraviolet (UV) or deep UV (DUV), to create a pattern on a surface. This is done by use of a photoresist, a chemical compound that either polymerizes or depolymerizes when exposed to light of a specific wavelength. Such resists come in two forms; *Positive* resists depolymerizes where exposed, solubilizing the resist. *Negative* resists polymerizes where exposed, reducing solubility.

By controlling which areas of a substrate coated with such a resist are exposed to light with one can control where the polymerization/depolymerization occurs, and thereby controlling which areas of the photoresist will be removed when the substrate is developed. The process, as applied in the work documented herein, is shown in Figure 2.2, and will shortly be discussed in more detail. Photolithography is much used in semiconductor manufacturing, but also has applications in various other fields, including but not limited to soft lithography, specifically micro-contact printing.

2.1.1 The Method, Step by Step

The substrate to be patterned is first cleaned and later dehydrated to ensure an even, uncontaminated and dry surface. The cleaning and dehydration ensures a surface with minimal contaminants and good adhesive properties for the photoresist. Once cleaned and dehydrated, the substrate will be covered with a thin film of photoresist. While various coating methods exist, spin coating is commonly used as it can provide uniform films with an easily controlled thickness. This control of the film thickness is achieved by controlling spin parameters such as angular velocity, (angular) acceleration and time.

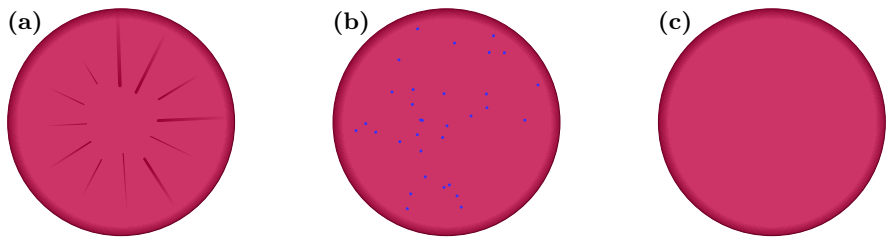

Figure 2.1: Wafers displaying three select artifacts related to spin coating. Streaks or "comets" as seen in (a) may appear as a result of letting the resist stay too long on the wafer prior to spinning. Pinholes in the resist, as seen in (b), may appear due to particles on the wafer or in the resist. Edge beads, shown as a darkened band near the edge of all of these figures, may, as seen in in (c), persist even though the coating may otherwise be pristine. This phenomenon occurs due to interactions on the wafer edge during the spin process, and the artefact consists of a thicker layer of resist near the edge. This may, especially in contact mode photolithography, interfere with the process, degrading resolution. Edge beads may be reduced by increasing spin acceleration, but removal of the challenges represented by this artefact necessitates the use of edge bead removal processes if deemed necessary to improve resolution. Further artefacts are discussed in Quirk and Serda [19].

As seen in Figure 2.1 the quality of the resist coating is dependent on the clean nature of the wafer and the resist both, as well as the chosen spin speed, acceleration and the timing involved in the spin coating process. These steps are important as inadequate attention at this first stage of the process will have ramifications that can render the end product useless. As may be inferred from this discussion, photolithography is a sensitive technique best performed in cleanrooms. For this reason the semiconductor industry has not only automated this process, but conducts it in a strictly controlled, isolated atmosphere, devoid of human beings precisely for the purpose of cleanliness [19].

Once coated, solvent is usually evaporated from the substrate by heating it for a specified and resist-dependent time (See Figure 2.2(b)). This improves the photoresist adhesion and increases film density by removing solvents that are normally present. For the positive photoresists used in this project it also starts a cross-linking process which hardens the film. These cross-links are photochemically unstable and are broken if exposed to UV light of a manufacturer-specified wavelength.

By covering the coated substrate with a mask[1] during exposure it is possible to define which areas are exposed by obscuring portions of the exposed substrate. By limiting exposure to certain areas the operator can decide where cross-links are broken, meaning the areas exposed to UV light can then be dissolved and removed from the substrate by submersion in a developer bath.

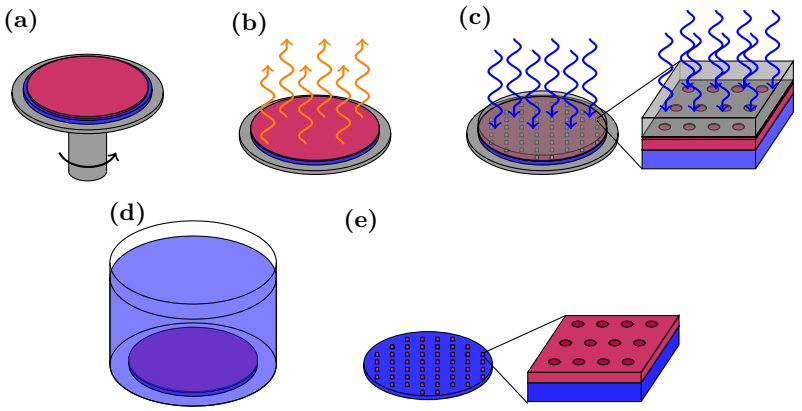

Figure 2.2: Photolithography in five steps, as utilized in this project. (a), Spin Coating: A cleaned substrate is spin-coated with a photoresist. (b), Pre-bake: Said substrate is heated on a plate in order to evaporate most of the solvent in the resist, hardening it and ensuring adhesion to the surface. The orange arrows denote heat and evaporated solvent. The time and temperature depend on the photoresist as well as the intended product. (c), Exposure: The coated substrate is exposed to UV-light (illustrated as blue arrows) with areas covered by a partially opaque mask remaining un-exposed. (d), Development: The exposed substrate is introduced to a developer which dissolves photoresist which is not crosslinked. (e), Finished product: After development the substrate is rinsed, dried and inspected for faults with applicable microscopy techniques. This figure shows a pattern of circular wells in the photoresist layer. Cleaning and dehydration bake, as well as any steps not applied in this project, are not shown.

[1] In this case a mask is composed of a transparent material such as glass or quartz with opaque patterns in for example chrome.

2.1.2 The Product

As seen in Figure 2.2 the product of a photolithographic process consists of a substrate, e.g. an Si wafer, with select areas being covered with a hardened photoresist of a given thickness. How small the features may be depends on a variety of the factors including the size of the features on the mask, the wavelength of the light used and the thickness of the resist. Near the lower end of the resolutions technically possible a host of interactions come into play, which make determining the best possible resolution a non-trivial matter, but resolutions on the sub-micrometer level are achievable given equipment and lab environments of sufficient quality.

Utilization of photolithographically created patterns are many. By coating the surface of this product with a thin metal film, and later dissolving the hardened photoresist, a network of metal, for example serving as wires, may be created. Moreover, the resist may serve as protection against etchants, providing the opportunity to etch grooves or holes where the substrate is not covered by the resist pattern. While these and other opportunities for further processing abound, one in particular is of interest for this project; the use of the photoresist pattern to cast soft polymer products such as stamps. These may then be used in various soft-lithography processes, such as a mold for casting stamps for microcontact printing (µCP).

2.2 Microcontact Printing

Micro-contact printing (µCP) is a form of soft lithography where an elastomer stamp with features (punches) on the micro or nanometer scale is used to deposit an ink such as a chemical substance or small micro or nanoscopic particles onto a surface of interest. The use of elastomers in stamp construction imbue the technique with the ability to imprint non-flat surfaces where many other lithography techniques, such as photolithography, require flat, even surfaces.

The elastomer stamps used in µCP are normally cast in a 'master', also called a mold which was created by another lithography technique such as photolithography or similar technique. Once a master is prepared it is possible to re-use it several times, producing several batches of stamps in the lifetime of the master.

The procedure to create stamps on such a master is outlined in Figure 2.3, which is seen in conjunction with Figure 2.2 which shows the creation of the master.

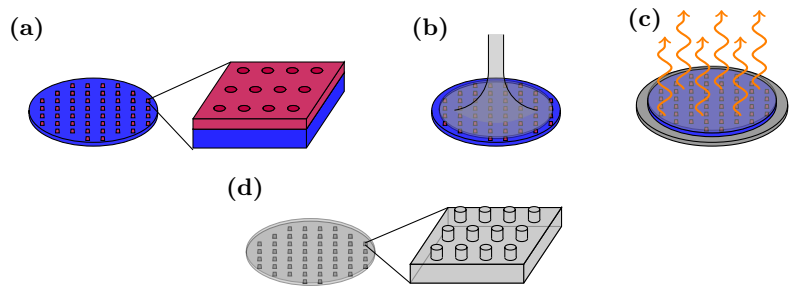

Figure 2.3: Production of polydimethylsiloxane (PDMS) stamps on master. Subfigure (a) shows the master produced with photolithography. (b) shows a de-gassed mixture of PDMS and curing agent is poured onto the master. The PDMS is then left to cure, often with applied heat as shown in subfigure (c), though other options do exist [20]. Once cured, the PDMS may be peeled off the master, subfigure (d) shows stamps with rods, cast on a master with wells.

Moreover, while the production of the master may require cleanroom techniques, as described in chapter 2.1,soft lithography does not have such requirements. Once the stamps are produced, the technique is no longer dependent on cleanroom techniques to yield good results. Naturally, the quality of the results are highly dependent on the polymer of which the stamps are constructed.

2.2.1 Polydimethylsiloxane (PDMS)

PDMS, see Figure 2.4, is the most common elastomer used to create the stamps used in µCP [20]. The polymer has several advantages leading to its widespread use. The polymer typically has a Young's modulus around 1.5 MPa, which means it is flexible enough to form consistent contact with rough surfaces. It also has the mechanical strength to support micrometer or, with certain chemical modifications to increase the Young's modulus, sub-micrometer features. The transparent nature of PDMS, it has a refractive index $\eta = 1.41$, allows for application of optical methods to alter the ink or simply inspect the process. Additionally, PDMS is both cheap and the process of casting the stamps, shown in Figure 2.3, is - once a master is acquired - both cheap, safe and easy. Post production modification of the stamps is also fairly simple. The PDMS is naturally hydrophobic, as can be inferred from Figure 2.4, yet can be made hydrophilic by for example treating the stamp with UV-light or oxygen plasma. This leads to radicals or hydroxy groups on the stamp surface, which confers hydrophilicity and grants an opportunity to functionalize the surface with molecules of interest by way of applicable chemistry [20].

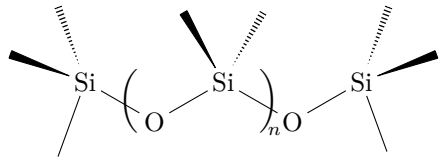

Figure 2.4: Poly(dimethyl)siloxane (PDMS) molecular structure.

Note, however, that stamps of this polymer will contain trace amounts of curing agent and PDMS chains of low molecular weight, both of which may lead to artefacts. This challenge may be reduced by thorough cleaning of the stamps with solvents such as ethanol [21].

2.2.2 Casting With PDMS

Once curing agent and PDMS is mixed, curing begins. This process can be completed in room temperature, in which case the process will take approximately 48 hours. Alternately, heat may be applied to reduce the time requirements down to as little as 10 minutes, if the temperature is set to 150°C [22]. Curing PDMS at high temperatures Note that increasing curing temperatures also increases PDMS shrinkage, which even at 65°C exceeds 1% [23].

2.2.3 Stamping Using Microcontact Printing

In principle, and to a large part in practice, stamping using µCP is simple. The stamp is coated ("inked") with an ink of interest, and then pressed against an intended substrate. Inking of the stamps may be achieved by use of a stamp pad, or by submersion of the stamp or its pattern in an ink solution. Both are illustrated in Figure 2.5. The ink may in principle be anything of interest provided the molecules or particles printed are not too large or reacts with the stamp itself. Where this is a likely occurrence the experimenter may opt for another elastomer as a construction material. The first application of µCP in 1994 consisted of patterning gold with alkanethiol self-assembling monolayers (SAMs) [15]. Since that time a large variety of applications have been found. In their review of µCP from 2007, Ruiz and Chen list examples (with ample citations) which include patterning of *"water, salt, organic solvents, metals, polymers, DNA, proteins and cells."* [17]. The purpose of these patterns may be as diverse as the molecules of which they are printed, ranging from resists for etching purposes, to localized polymerization, or (as previously argued) cellular microarrays [20, 24].

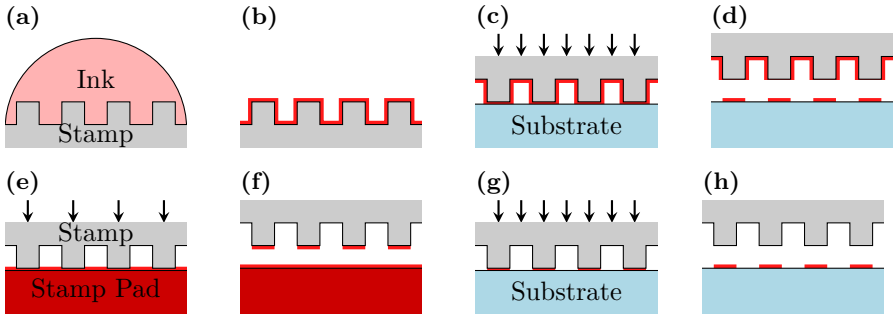

Figure 2.5: Two means of stamping. The stamp may be coated by submerging the stamp's features in a solution of ink and then curing it, as seen in (a) and (b). Alternately one may gently press the stamp against a stamp pad containing the intended ink, as seen in (e). Once coated the stamp may be pressed against a surface of interest (c), (g), depositing ink according to the stamp's pattern ((h), (d)).

2.2.4 Micro-Contact Printing Challenges and Artefacts

As a soft elastomer PDMS may deform sufficiently to alter the printed pattern, sometimes significantly. Four commonly encountered deformations, roof collapse, buckling, edge collapse and lateral collapse are shown in Figure 2.6.

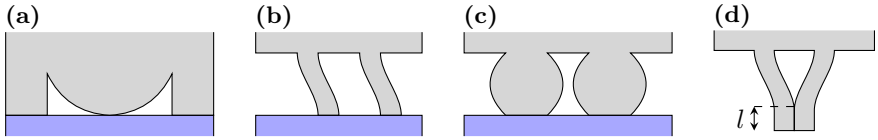

Figure 2.6: PDMS stamp deformations. Subfigure (a) shows roof-collapse, where the top of the stamp contacts the stamped substrate. Subfigure (b) shows buckling, where features deform when pressure is applied. Subfigure (c) shows sidwall collapse, a scenario where the walls of the feature will swell out due to compression and increase the surface area of the feature in contact with the substrate. Subfigure (d) shows lateral collapse, where adjacent features adhere to one another over a distance l without applied force.

Roof Collapse

If the stamp's aspect ratio $A = {}^{h}/_{2a}$, see Figure 2.7, is too low the "roof" of the stamp may come into contact with the substrate. If that happens the contact area may increase due to forces between surface of the stamp and the surface of the stamped substrate [25, 26]. The same effect can occur if the stamping is performed with too much force. Hui et al. [26] describe the conditions necessary to avoid roof collapse as

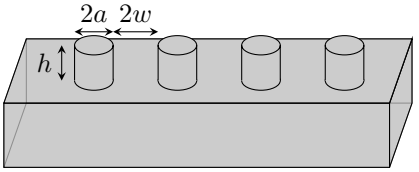

Figure 2.7: The dimensions of a stamp's feaures. Note that if these are non-cylindrical $2a$ becomes the width of the features, regardless of the feature's shape.

$$v_{max} = \frac{4\sigma_\infty}{\pi E^*}(w+a)\cosh^{-1}\left[\sec\left(\frac{w\pi}{2(w+a)}\right)\right]. \tag{2.1}$$

Here v_{max} is the maximal vertical displacement, $E^* \equiv {}^{E}/_{(1-v^2)}$ where E is the Young's modulus, and σ_∞ is the pressure applied on the stamp in ${}^{\mathrm{N}}/_{\mathrm{m}^2}$. The pressure is assumed to be evenly distributed. w, a and h are annotated on Figure 2.7. The annotations are identical to the ones used in reference [26].

Lateral Collapse

Antithetically to roof collapse, lateral collapse can occur if the aspect ratio is too high. In this scenario two features stick together over a length l, as seen in Figure 2.6(d). In this event we observe that lateral stability may be expressed as

$$\frac{2}{h}\left[\frac{3E^*a^3w^2}{2\gamma_s}\right]^{1/4} > 1, \tag{2.2}$$

where γ_s is the surface energy in ${}^{\mathrm{N}}/_{\mathrm{m}}$ and the other parameters are as described for Equation 2.1 and discussed in reference [26]. Note that as is the case for roof collapse, once contact occurs between features forces in the interface between the two contacting features may increase the contact area [25].

Buckling

For high aspect ratios we increase the chances of the features buckling under pressure. Specifically we can anticipate buckling if these criteria are not met:

$$-\frac{1.47\sigma_\infty h^2}{\pi^2 E^* a^2} < \frac{1}{1+{}^{w}\!/_{a}}, \tag{2.3}$$

where all parameters are previously defined. It should be specified that equation 2.3 is sensitive to boundary conditions explained in [26], and should therefore not be taken as an exact condition.

Sidewall Collapse

Sidewall collapse S_c occurs when

$$S_c = K \tag{2.4}$$

$$K_I = K|_{A\to 0,\, {}^{A}\!/_{P}\to 0} = \frac{2\pi AP}{3(P+1)^2}\left[-\log\left\{\cos\left(\frac{\pi P}{2(P+1)}\right)\right\}\right] \tag{2.5}$$

$$K_{II} = K|_{A\to\infty} = \frac{4P}{3(P+1)^2}. \tag{2.6}$$

where K is the stiffness of the elastomer. $A = {}^{h}\!/_{w}$ and $P = {}^{a}\!/_{w}$, or the aspect and pattern ratios respectively. K is between K_I and K_{II} and converges to

$$K = \frac{A+P+0.6}{(K_I(A,P)^{-1}+K_{II}(A,P)^{-1})(A+P)}, \tag{2.7}$$

as shown in reference [27].

2.3 Microbiology

While bacteria are nearly omnipresent on the earth, only a few species have been used as model species for microbiology and biotechnology. Two of these will be discussed here, *Escherichia coli* and *Pseudomonas putida*. Both species have simple nutritional requirements and are well studied [1, 28]. While the two organisms are different phylogenetic orders (Enterobacteria and Pseudomonadales respectively) it can be said about them both that sudden changes in temperature may lead to an adjustment period which may last several hours before the bacteria adjust to the new environmental temperature and continue growing with a new, temperature dependent generation time [1, 29, 30].

2.3.1 *Escherichia coli* and Culturing Thereof

Escherichia coli (*E. coli*) is often used as a model organism in molecular biology and biotechnology. The species is an approximately 2 µm long, peritrichously flagellated Gram negative rod. It is metabolically diverse, mesophilic and facultatively aerobic. In terms of habitat, it is found in the intestinal tract of nearly all humans and other warm-blooded animals. Its ability to grow at a convenient rate, with a generation time between 20 to 60 minutes, on a wide variety of nutrient sources at temperatures ranging from 8°C to a maximum of 48°C with an optimal temperature of approximately 39°C are all reasons why the bacterium is a model organism frequently used in biotechnology and microbiology [1, 31].

2.3.2 *Pseudomonas putida* and Culturing Thereof

P. putida is a soil bacterium in the Proteobacteria phylum. The bacteria are lopotrichous Gram negative rods. It grows optimally near 30°C, with a generation time of 41 ± 4 minutes [29]. *P. putida* may be grown aerobically or anaerobically in simple growth media due to its diverse metabolism [28, 32, 33]. The organism is known to form a beneficial relationship with several agricultural plants, as well as having beneficial abilities with respect to biodegradation [28, 33, 34]. The bacterium is, for the aforementioned reasons, used as a model organism in biotechnology and microbiology.

2.4 Bacterial Adhesion

About bacterial adhesion in general it may be said that while virtually all surfaces, natural or artificial, exposed to a solution with bacteria present will eventually have bacteria adhere to it, and a biofilm will eventually form unless something prevents this [35]. Adhesion strategies do vary somewhat from genus to genus, but initial attachment initiates when a bacterium randomly collides with a compatible surface [1, chapter 23.4]. Exactly what happens in the moment of adhesion, when the bacterium collides and sticks, is not fully understood and likely quite complex [36, chapter 20, 37].

2.4.1 Promoting Bacterial Adhesion

As bacteria typically are capable of adhering to virtually any surface, permitting the adhesion of bacteria may seem trivial. If an experimenter should wish to promote adhesion selectively, and encourage it in order to increase the likelihood of a bacterium or multiple bacteria adhering to a specific spot certain strategies may be employed.

Surface Charge

Bacterial surfaces are, with some notable exceptions[2], negatively charged when in an aqueous solution, whether the bacterium is Gram positive or negative. For Gram negative bacteria the presence of lipo-polysaccharide (LPS) in the outer membrane is the main contributor to this negative charge, whereas for Gram positive bacteria the ample presence of teichoic acids is what confers an overall negative charge.

The surface charge of the bacteria contributes to both attraction and repulsion of bacteria to/from surfaces of interest. Electrostatic interactions are, in addition to van-der Waals forces and hydrogen bonds, central in the adhesion of bacteria to solid surfaces [36, chapter 13.4, 39, 40, 41, 37]. As surface charge is readily manipulable, for example by coating the surface with a charged polymer, researchers can and do utilize it to better control cellular adhesion of both eukaryotes and prokaryotes [9, 14, 38].

[2] For example *Stenotrophomonas maltophilia* at physiological pH [38].

Mussel Adhesive Protein (MAP) and Derivatives.

In their native habitat(s) mussels are able to adhere to a practically any organic or inorganic surface in a variety of challenging conditions, submerged in salt or fresh water and subjected to changing currents and tides [42, 43]. Insufficiently powerful adhesion would, for the mussel, mean waves or currents would tear it free of its holdfast to be dashed against rocks or carried away to other locations where survival might not be possible for the small animal. To adhere to a variety of surfaces in difficult aqueous environments mussels have evolved a family of proteins known as mussel adhesive protein (MAP) or mussel foot protein (MFP). MAP extracts retain the adhesive properties and creates good adhesion to most surfaces, even ones otherwise resistant to adhesion, such as poly(ethylene glycol) (PEG) [43].

MAPs extracted from mussels are available commercially. An example is BD CellTak^{TM}. CellTak^{TM} is intended as a cellular adhesive. Such extracts contain elements from the mussel's extra-cellular matrix (ECM), which can be of significance for studies of animalian cells [44]. The extracts are, however, somewhat expensive. Moreover, while MAPs contain many different amino-acids one chemical motif has shown itself to be of significance to the adhesion; catechols. Specifically 3,4-dihydroxy-L-phenylalanine (DOPA).

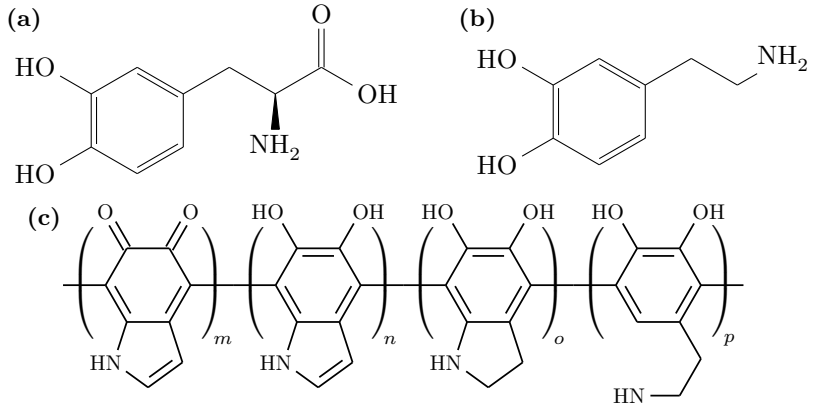

Figure 2.8: The molecular structure of DOPA (a), dopamine (b), and polydopamine (PD), as suggested by Liebscher et al. [45] (c).

As may be seen in Figure 2.8, a close chemical analog to DOPA is dopamine. When polymerized, dopamine, or rather *poly*dopamine, shows many of the same adhesive properties MAP does. Dopamine, often in the form of dopaminehydrochloride, is commercially available, inexpensive and polymerization is easily initiated. It is also highly versatile, chemically speaking. The molecule can, as may be evident by Figure 2.8(b), interact supramolecularly by π-stacking, charge transfer and hydrogen bonding [46]. This versatility empowers the polymer as an adhesive. With the variety of possible interactions available, PD - or DOPA in MAPs - can serve as versatile adhesives capable of binding even to surfaces that display significant anti-adhesive properties, such as PEG [47].

PD is a complex polymer, and the nature of its composition is subject to debate among chemists; while Figure 2.8(c) shows one possible polymeric structure suggested by Liebscher et al. [45], Dreyer et al. [46] suggests a different basis for polymerization wherein hydrogen bonding and π-stacking is suggested. Whichever is the case, polymeric dopamine is rich on catechol and amine groups, and binds amine, thiol and catechol moieties as well as metal ions and -particles [48–51].

Besides the chemical variability with respect to adhesion, even submerged in water, PD is known to have very low toxicity and high degree of biocompatibility [52–54]. The numerous possibilities for adhesion offered by PD also offer possibilities for cellular adhesion, and has been shown to be biocompatible [14, 55, 56]. The polymer has been used as a cellular adhesive for eukaryotic as well as for bacterial cells [57].

2.4.2 Adhesion Prevention

As discussed in Chapter 2.4 microbes, including bacteria, are capable of adhering to most surfaces [35]. In order to reduce or prevent adhesion of bacteria it is therefore necessary to treat a surface in a manner which prevents adhesion. When considering readily available, non-toxic alternatives two chemical compounds stand out, PEG and poly(vinyl alcohol) (PVA). Both of these two amphiphilic polymers are used to reduce cellular (bacterial or otherwise) adhesion [14, 58].

Polyethylene Glycol (PEG)

PEG, seen in Figure 2.9(a), has garnered much interest as a “stealth” coating for drug delivery purposes. By stealth in this situation it is understood that

the polymer's amphiphilic nature can provide a sterically induced exclusion zone, provided the polymer is coating the surface of interest densely enough. Such an exclusion zone may prevent access to the coated surface. This can prevent the binding of molecules such as proteins or sugars to the coated surface, even if interactions would normally have occurred. It is this sterical prevention of molecular recognition, conferring a degree of stealth with regards to microbial and immunological recognition both, coupled with the high degree of biocompatibility which has lead to the widespread use of the polymer in various biomedical research applications [59].

The efficacy of PEG coatings depend primarily on two factors; the coating density and the polymer length. While PEG may form both hydrogels and polymer brushes when coating a surface, this thesis considers only the latter. When tethered to the coated surface by one end, PEG may form brushes only when the polymer density be sufficient to make the brush conformation favorable [60]. Once the polymer brush has formed, a protein, sugar or other molecule of sufficient size passing through the brush will result in a large loss of entropy in the brush. This loss of entropy makes penetrating the brush and adhering to the coated surface thermodynamically unfavorable [14]. Even so, if the brush is too thin, the Debye length associated with the coated surface may "bleed" through and allow for adhesion by electrostatic interaction. Likewise, should the brush be insufficiently dense, small proteins may traverse it and adhere to the surface underneath. Furthermore, insufficiently thick and dense brushes may also be compressed, leading to interactions between the surface and the particle or organism responsible for said compression. These scenarios and how the brush should be organized (How thick and dense it needs to be) in order to prevent these different scenarios are described in Barbey et al. [61] and, more specifically on electrostatic interactions, in Pasche et al. [62].

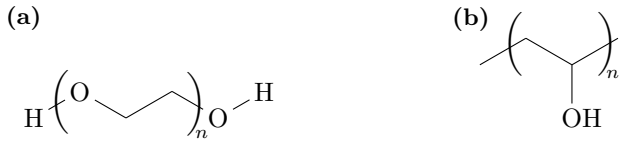

Figure 2.9: Polyethylene Glycol (PEG), (a) and Polyvinyl Alcohol (PVA), (b).

While non-toxic, highly resistant to adhesion and readily available, PEG may, with time, oxidate and lose it's effectiveness. Various causes depending on environment may lead to oxidation of PEG chains' terminal hydroxy group to an aldehyde group, opening for conjugation of the degraded PEG molecule to corresponding amine groups on proteins. For the most part, this becomes an issue at elevated temperatures, and in the presence of metal catalysts or alcohol dehydrogenase [63–65].

Poly(vinyl Alcohol) (PVA)

PVA hydrogels are known to resist protein adhesion, and has been used to endow surfaces with properties preventing protein adsorption as well as cellular (bacterial and otherwise) adhesion [66–69]. As a hydrogel, long term adhesion of PVA to a surface can be achieved by use of an adhesive such as glutaraldehyde or PD, though if the film duration is not crucial, a thermal curing can be undertaken to create a temporary relationship between the PVA hydrogel and the surface it coats [69].

Bovine Serum Albumin (BSA)

bovine serum albumin (BSA) is at times used as a cell repellent for studies involving animalian cells [14, 70]. The protein may be used to prevent cellular adhesion, as it can reduce nonspecific protein adhesion to the coated surface [71]. The protein also exhibits a negative charge at physiological pH [72], which may repel bacteria which largely have negative net surface charge. While it is also known to be resistant to bacterial adhesion [73], the molecule can still interact with bacteria to an extent which makes it useful as a molecule permitting bacterial motility and slight adhesion, while not irreversibly binding surface structures of the bacteria [7].

Silanization. A Surface Coating Mechanism.

Coating a surface with PVA can be done by thermal curing, as mentioned above. For PEGylation a number of possibilities exist, one of which is silanization.

Silanization is a process first used in 1946 by which surfaces which present hydroxy groups to the environment (Such as glass, silica or metal oxides) may be covered with (and covalently bound to) self-assembling monolayers (SAMs) of chemicals grafted to a suitable silane [74, 75]. The method, with proposed reaction schemes presented in Figure 2.10, utilizes silanes with group(s) attached

which can bind to hydroxy groups on a surface [76]. Beside these functional groups most silanes also carry a side chain, for example a PEG-chain as seen in Figure 3.3(b).

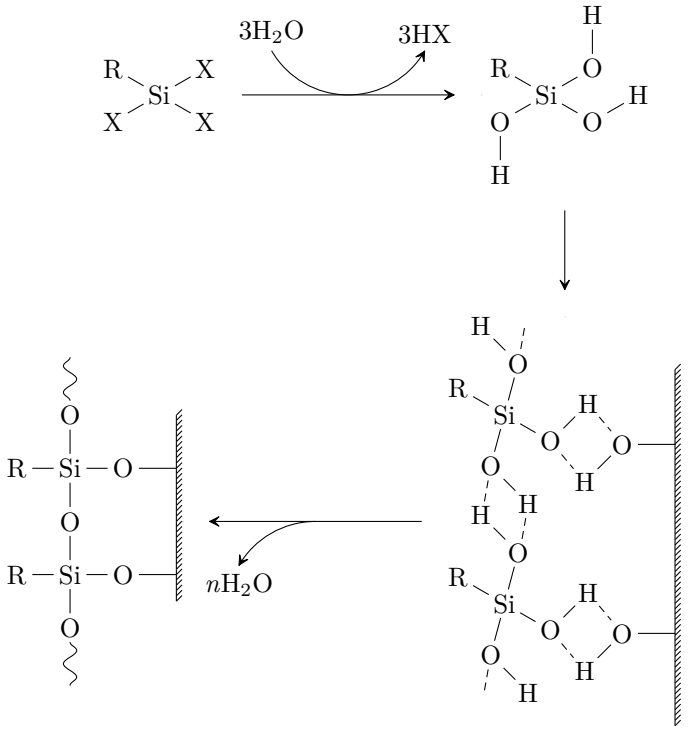

Figure 2.10: Classical hydrolysis reaction scheme for surface silanization using trialkoxy or trichloro silanes [77, 78]. These reactive moieties (chlorine or alkoxy groups) are labeled X in this reaction scheme.

As for the groups that mediate adhesion to the surface, several moieties can be used. To limit the scope of this text only trialkoxy and trichlorine will be discussed. Of the aforementioned, trichlorosilanes were the first silanes discussed in literature [74]. While other reaction schemes are proposed for the reactions, silanization by such silanes are classically thought to follow the reaction scheme in Figure 2.10, forming covalent Si-O-M bonds to the surface and to other silane monomers. Given that M can be Si or a metal such as Fe or Al, the coating mechanism is versatile and may well be used to form durable coatings on surfaces including glass, mica and metal (oxide) surfaces. The reaction binding silanes can be initiated by water, especially for chloro-silanes, which when exposed to moisture will react with the surface and/or one another. While water can initiate and run this process for either group of silanes, a base or acid catalyst should be used to catalyze silanization by alkoxy-silanes [75]. As water alone can run the reaction, silanes will, with time and moisture, polymerize, thus rendering the chemical unable to bind to surfaces presenting hydroxyl groups.

2.5 Confocal Laser Scanning Microscopy (CLSM)

Confocal Laser Scanning Microscopy is, in its basic forms, a diffraction limited optical method with a main focus on fluorescence, utilizing an epi-illumination setup with one or more lasers as the light source(s). Note that in principle other light sources than lasers can be used.

The basic function of confocal laser scanning microscope (CLSM) is illustrated in Figure 2.11. Note how the aperture before the detector is placed in the focal plane, thus blocking the majority of the light from areas other than the focal plane in the sample itself. This pinhole thus limits the observed volume to one point, the size of which is determined by the pinhole in front of the detector (B_2 in Figure 2.11).

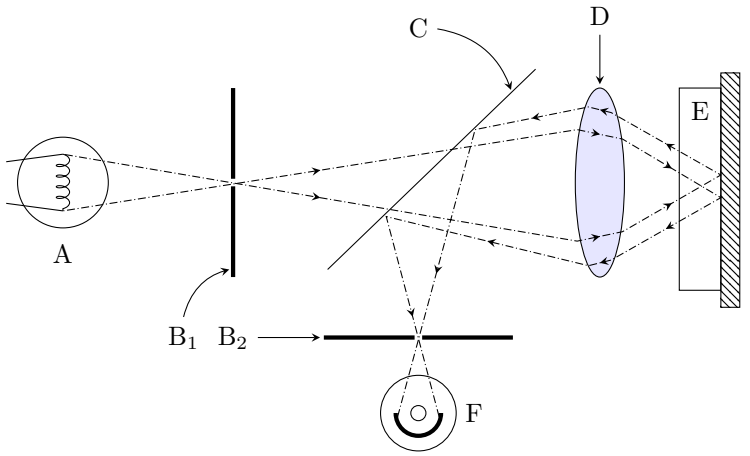

Figure 2.11: Conceptual sketch of principle behind Confocal Microscopy. **A**: Light source, commonly a laser. **B**: Apertures (Pinholes). **C**: Dichromatic or partial mirror. **D**: Objective and condenser in one single lens/system of lenses. **E**: Sample. **F**: Detector (Photomultiplier tube, avalanche photodiode or similar). Figure adapted from original patent, source [79].

Images larger than the focal volume are obtainable by either moving the sample or the excitation light beam across the sample in a raster pattern. By collecting data from points along the raster scan, computers can generate a micrograph for the microscopist. Such pattern scans are performed by computer controlled electro-mechanical systems discussed in Pawley [80, chapter 9].

2.5.1 Resolution Limit

By introducing the pinholes to the light path in the confocal setup we limit the area (and volume) observed. Should we use an otherwise perfect optical setup with flawless lenses this means the resolution the system can achieve is diffraction-limited. That is to say that given a circular aperture the resolution is limited to a volume defined by a diffraction pattern. This volume is described by equations 2.8 and 2.9, which the show the light's intensity distributions in the plane (Equation 2.8) or axially (Equation 2.9), for an idealized, aberration-free system.

Hence, we can see that in an aberration free system the defining sizes for planar and axial resolutions respectively,

$$r_{airy} = \frac{1.22\lambda}{2\mathrm{NA}} \tag{2.8}$$

$$z_{min} = \frac{2\lambda\eta}{(\mathrm{NA})^2}, \tag{2.9}$$

are determined by the wavelength of the light both from the laser and re-emitted from the sample (λ), the numerical aperture (NA) of the objective ($\mathrm{NA}=\eta\sin\theta$) and the refractive index of the object medium (η) [80, Ch. 1]. As equations 2.8 and 2.9 reveal, the point in the sample that is and can be registered may be substantially smaller in the plane than is possible to achieve along the z-axis.

2.5.2 Fluorescence

While the CLSM can indeed utilize reflected light from portions of the sample it is commonly used to study samples by utilization of fluorescence. In this setup the sample to be studied is dyed with a fluorophore, bound to a molecule or substance one intends to study.

CLSM is a technique relying heavily on fluorescence. The use of lasers, which have well defined wavelengths, and the utilization of the confocal principle,

confers two major benefits over conventional wide-field fluorescence microscopy. First, the use of lasers as opposed to mercury lamps means the operator can excite specific fluorophores while not exciting others. While wide-field microscopes can employ filters to accomplish similar results, a CLSM can employ multiple lasers at the same time without the need for filters, thereby giving excellent control over which fluorophores (if multiple are present) to excite and which to leave untouched. Secondly, the confocal principle means fluorescence from areas outside the focal volume can be excluded by introduction of the pinhole. Such fluorescence can reduce clarity in wide-field images, especially of thick samples. Additionally, the fact that CLSMs scan the sample with the laser beam(s) means each point on the sample is only exposed to the beam for a short time during each image acquisition. This limited exposure means bleaching is less of a problem in CLSMs than in conventional wide-field microscopes, which illuminate the entire sample continuously. Bleaching occurs when fluorophores are chemically altered by the light exposure, irreversibly altering or more commonly eliminating the fluorescence capabilities of the fluorophore. Certain fluorophores are more easily bleached than others, and thus require extra care to limit exposure to light, especially light with wavelengths within the excitation spectrum.

Provided the wavelength of the photons in the incident laser beam corresponds to the excitation wavelength of the chosen fluorophore, this will be excited to a higher energy state, and upon de-excitation to the ground state may emit a photon of a higher wavelength, within the fluorophore's emission spectrum. With the exception of multi-photon techniques the emission wavelength is always longer than the excitation wavelength, a phenomenon known as Stokes-shift (See Figure 2.12(b)). In reality, the curves are rarely such neat normal distributions, of course. For that reason, the excitation and emission spectra of four relevant fluorophores are shown in Figure 2.12(c). How likely an emission by fluorescence is once a molecule has reached an excited state depends on the likelihood of de-excitation following a radiative pathway, see Figure 2.12. This is normally simplified to a quantum yield Q of the system,

$$Q = \frac{\text{photons}_{\text{absorbed}}}{\text{photons}_{\text{emitted}}}, \tag{2.10}$$

which is found in relevant literature, such as data-sheets from the producer of the relevant fluorophore.

When a fluorophore emits a photon, these will not be emitted with a specific directionality, but rather escape the molecule in a random direction. Some few of them will retrace the path taken by the laser. As can be inferred by Figure 2.11, those photons will, by lenses and mirrors, be guided to the detector. This process can be said to begin when the photons encounter the dichroic mirror. While this mirror is supposed to be reflective only to the light emitted from the sample, some few reflected photons with the excitation wavelength are likely to also be reflected along with emitted photons. In order to reduce the number of these that reach the detector a filter - either low/long pass filter transmitting lower frequencies/longer wavelengths - or a band-pass filter transmitting a given, finite spectrum. The photons that successfully traverse this optical pathway then encounter a pinhole, (Marked B_2 in Figure 2.11). The remaining portion which successfully pass the pinhole are then counted by a detector. The data from this detector is translated to an image for the microscopist.

If the microscopist should wish to analyze the sample using reflected light the setup can be altered to accommodate this. The pinholes remain in place, and a filter selecting for the wavelength of the laser light may be inserted to reduce light from other sources, though this is not strictly speaking necessary. The major change consists of a change of mirrors, from the dichroic mirrors with a reflectivity dependent on wavelength, to a partial mirror, reflecting a given portion of the light that encounters it, for example 50%.

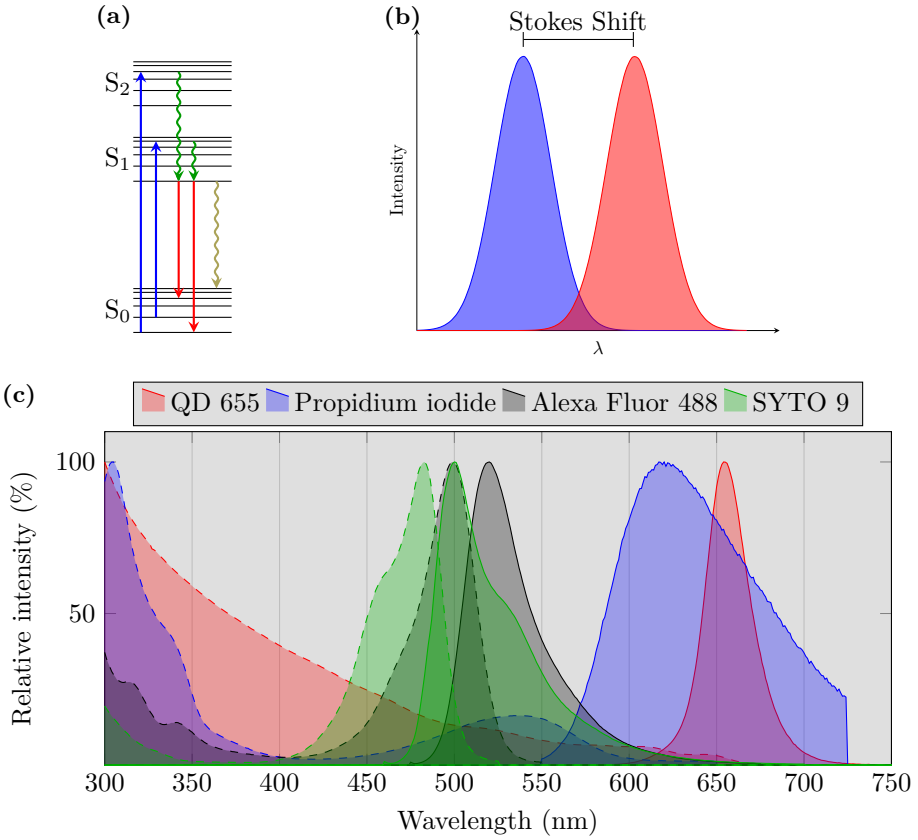

Figure 2.12: (a) Jablonski energy diagram showing energy transitions in a fluorophore related to fluorescence. → denotes excitation light and → denotes emission light. Conversely, ⇝ denotes internal conversions of energy levels from vibrational states (S_2) to lower energy states or within the same singlet state (S_n). ⇝ denotes non-radiative de-excitation processes. The figure does not show phosphorescence. (b) is a sketch illustrating Stokes-shift, the increase in wavelength between excitation and emission bands in fluorescence. The blue curve illustrates the spectrum of wavelengths corresponding to available energy transitions that can lead to excitation of the fluorophore. The red curve illustrates the spectrum within which the fluorophore can emmit light. More information on these phenomena may be found in Pawley [80]. Subfigure (c) shows the Excitation (Dotted lines) and Emission (whole lines) spectra of the main fluorophores used in the report. Subfigure (c) was produced using data from Life Technologies Fluorescence SpectraViewer [81].

2.5.3 Detectors

The typical intensity of the light emitted by the sample which reaches the detectors in a CLSM is low due to the filters and, in particular, the pinhole. Moreover, it is desirable to keep the intensity of the excitation light low to reduce photo bleaching, heating and other detrimental effects high intensity light can have on the sample. For these reasons, detectors which are capable of giving a comparatively strong signal per collected photon are used. Two detectors commonly used in CLSMs include photomultiplier tube (PMT) and avalanche photodiodes. The oldest of these is the PMT, and the concept for this is shown in Figure 2.13.

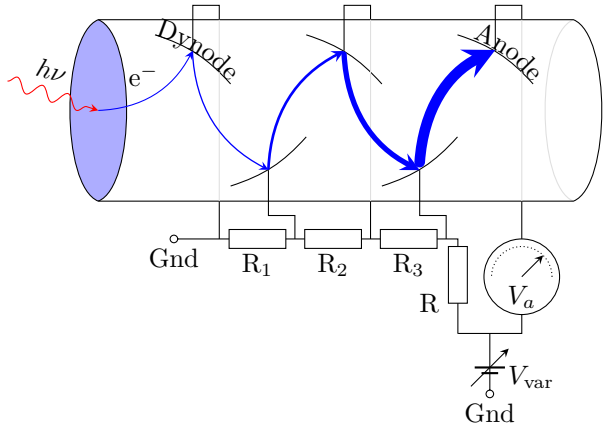

Figure 2.13: A conceptual drawing showing the principle behind the photo multiplier tube (PMT). A photon (red wavy line) encounters a photocathode (Light blue end of cylinder) and triggers the release of a so-called photoelectron (blue line). This electron progresses through the vacuum in the PMT, being drawn to the first in a series of dynodes by the positive potential applied to it. Encountering the dynode the electron carries enough energy to knock off a number of electrons from it. These are drawn to the next dynode in the PMT, which is at a higher positive potential, where each electron knocks off a number of more electrons. This cascade continues until the electrons arrive at the anode. Once there the electrons, now significantly more than the photon initially released, will be counted by a voltage meter, V_a. Thus, the PMT is capable of converting a small optical signal to a stronger electric signal.

By adjusting the voltage across V_{var}, the amplification of the PMT may be changed. Note that as the voltage V_{var} increases, so does the noise in the system, as more quantum events (which may or may not be triggered by photoelectrons) will result in an ejected electron and following cascade. The noise levels in the system may be compensated for by tuning the offset. The offset is the level interpreted as zero by the electronics and software that receives the PMT's signal. While increased offset reduces background noise, it also reduces the perceived signal strength from the rest of the sample, meaning weakly fluorescing portions of the sample may be excessively dimmed, even to the point of not registering. [80, 82]

Another detector which may be utilized, especially for longer wavelengths of light and low intensities, even for CLSM applications, is the avalanche detector. Unlike the PMT, avalanche detectors are solid state semiconductor devices. As the name implies, a photon encountering the device will lead to multiple electron-hole pairs forming, thereby resulting in a detectable signal. These detectors are especially well suited for low light levels and long wavelengths [80, 83].

A hybrid technology also exists. Known as Hybrid Detectors (HyD), these detectors consist of an avalanche diode located in a vacuum tube with a photocathode in one end. This photocathode converts incoming photons to photoelectrons, as was the case for PMTs. The resulting photoelectron will traverse the vacuum and encounter the avalanche diode, introduced in place of the PMT's dynodes and anode. The benefits inherent in this setup include a reduction from the multiple amplification steps necessary in PMTs, to one single amplification step. As a consequence, noise is also reduced. Secondly, the HyDs have the advantage over avalanche diodes in durability as well as lower noise and faster photon count rates [84].

2.6 Scanning Electron Microscopy

A scanning electron microscope (SEM) uses an electron beam as the probe used to retrieve information about the sample. Electrons can be seen as very light, charged particles that readily interact with both matter and electromagnetic fields. These properties are used in electron microscopes where the microscope's electron beam is focused, spread, tilted or otherwise manipulated using a series of electromagnetic or electrostatic[3] lenses and stigmators. The highly reactive properties of the electrons is also why the sample and any space traversed by the electron beam needs to be in a vacuum.

Once the electrons encounter the sample they will, provided the sample is thick enough, eventually interact with its constituent atoms, or their related charge. A variety of interactions are possible, each resulting in one of several possible signals, as outlined in Figure 2.14. Each of these signals carry different information about the sample.

2.6.1 Interaction Volume

When an electron microscope's electron beam reaches the sample this beam will penetrate with a depth R that is highly dependent on the sample density (ρ), and the energy E_0 of the incident beam. These parameters (ρ and E_0) define the size of interaction volume seen in Figure 2.14(b). Mathematically this can be approximated to

$$R \approx \frac{aE_0^b}{\rho}, \tag{2.11}$$

where $a \approx 10$ µg/cm^2 and $b \approx 1.35$ [85, chapter 5]. The depth R does not distinguish between the different signals that can result from electron-matter interactions. Note that the volumes of origin from the different signals vary greatly [85, chapter 5].

[3] Electrostatic lenses are primarily used in specialized instruments constructed to study magnetic samples.

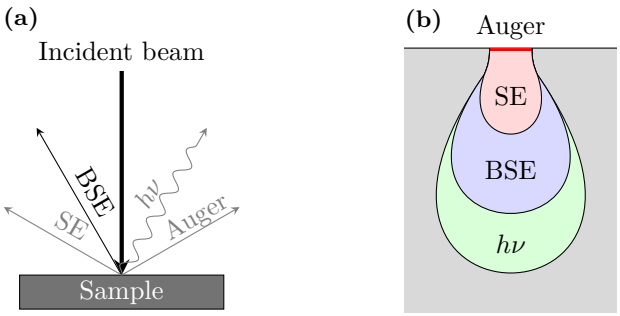

Figure 2.14: (a) show the most commonly used signals present in a SEM. Note that signals that are not of interest to this thesis are gray, these will not be discussed at any length. (b) illustrates the so-called interaction volume, the volume within which the signals observed by the microscopist originates. The following interactions are color-coded in: Auger electrons in the upper few Å (here: Bright red line), followed by secondary electrons (secondary electrons (SE)), shown as a red bulge, being generated within the top two nanometers of the sample. The back-scattered electrons (BSE)s (blue) originate from approximately half the interaction volume, while the characteristic x-rays (green) are emitted from a significantly larger volume. The electron beams, incident and otherwise, are not shown.

2.6.2 Backscattered Electrons (BSE)

BSEs are electrons that after interacting with the sample are elastically[4] scattered at angles greater than 90° relative the incident beam. Most of these electrons achieve such high angles through various scattering events in the sample, resulting in a cumulative energy loss of slight note. Adapting Egerton [85, equation 4.15] we find the probability an electron has of becoming backscattered can be written as

$$P(BSE) \propto Z^2, \tag{2.12}$$

where Z is the atomic number of the sample, supposing the area observed consists of only one element.

[4] This is an approximation, some energy is transferred to the sample.

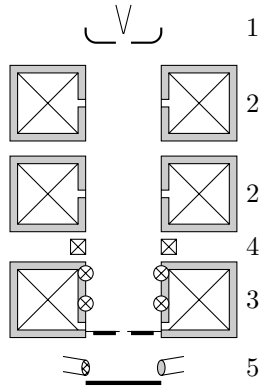

Figure 2.15: Simple conceptual sketch showing component train in a SEM. The detectors may include an SE detector, a BSE detector and an x-ray detector, although less conventional detectors also exist. The electron beam is not shown. The numbered components are: **1**: Wehnhelt cap and filament (Electron gun). **2**: Condenser Lenses. **3**: Objective lens (large) and scanning coils (small circles). **4**: Stigmator. **5** Sample and any detectors the instrument may have.

2.6.3 The Instrument

SEMs, see Figure 2.15, works by focusing an electron beam onto a sample of interest and scanning it across the sample in a raster pattern. This is achieved by constructing a column wherein electromagnetic lenses, scanning coils
As the electron beam sweeps across the sample one or more of the resulting signals - as previously discussed - can be picked up by relevant detectors and a computer converts the raw data to information the microscopist can analyze, for example an image.

Experimental

3

For all procedures: ensure that the constituent parts of the different processes are not exposed to a contaminating environment. Use gloves, even when not required for safety reasons, to keep the sample as free from contamination as possible. It should be noted that the contents of this chapter may have similarities to reference [18], as this thesis is a continuation of the work presented therein.

3.1 Stamp Production

The stamps are produced by casting PDMS in a mould/master created by photolithography. Production of stamps was in its entirety conducted at NTNU's nanolab facilities. The photolithographic process was performed in nanolab's ISO 5 section whereas the casting of the PDMS stamps was performed under ISO 7 conditions.

3.1.1 Photolithographic Process

Materials. 4-inch wide, 525 µm thick Silicon wafers from Siltronix. Polos Spin 150 Spin coater, MA/BA6 Mask Aligner from SUSS microtech, Shipley Microposit S1818 photoresist, MF 26 A developer and a 5-inch quartz-chrome mask designed using Clewin 4.3.5.0 software. The mask was manufactured by Computographics.

Method. Having designed a pattern, described in Figure 3.2 and received the resulting mask from its producer, Computographics, the process of creating the master is described below.

The Si wafer was first cleaned by spraying the wafer surface generously with acetone, isopropanol, ethanol and D-I water in that order. Breaks between sprays was shortened to the smallest achievable interval. After cleaning the wafer was blow-dried with gaseous Nitrogen and transferred to a hotplate at 180°C for 5 minutes in order to dehydrate the surface. Once dried, the Si-wafer was placed and centered on the vacuum chuck in the spin coater. Photoresist was carefully applied onto the wafer by a disposable plastic Pasteur pipette held in close proximity to the wafer, right above the wafer center point.

An even pressure was exerted on the pipette to ensure an even, uninterrupted stream of photoresist onto the wafer surface. In the event that bubbles were formed, these were promptly extracted by pipette. The spin coater was engaged, rotating at 3500 rpm for 40 s. After spin coating the wafers were soft baked at 115°C for 60 s. After coating the wafer was transferred to the mask aligner and exposed to 225 $\mathrm{mJ\,cm^{-2}}$ using i-line UV (λ =365 nm). After exposure wafers were developed in MF 26 A for 110 s, and transferred to DI-water for more than 30 s. The master was then dried using nitrogen gas.

3.1.2 Stamp Casting

Materials. Acetone, Ethanol and Sylgard® 184 silicone elastomer kit from Dow Corning was used. Aluminum foil, a curing oven and the master produced by photolithography was used in the curing itself, while the finished product was inspected using a Hitachi Dektak 150 stylus profilometer and an epi-illumination optical microscope.

Method. The master was placed, pattern up, on top of the aluminum foil. The aluminum foil was then folded into a cup containing the master, as illustrated in figure 3.1.

The PDMS precursor and curing agent from the Sylgard® 184 kit were mixed in a 10:1 weight ratio, stirred for five minutes, poured onto the master and degassed while on the master at 2.4 bar for 30 minutes, after which the master with PDMS was transferred to the curing oven, set to 80°C for 2 hours. 30 g of precursor was used per four inch master.

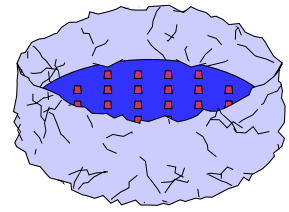

Figure 3.1: The aluminum foil is folded into a shallow cup or beaker with slight dents around the edge serving to secure the master against the bottom of the aluminum cup.

After curing, the aluminum foil was peeled from the now solid PDMS. Once this was removed the flexible PDMS was carefully peeled from the mold and inspected by bright field light microscopy.

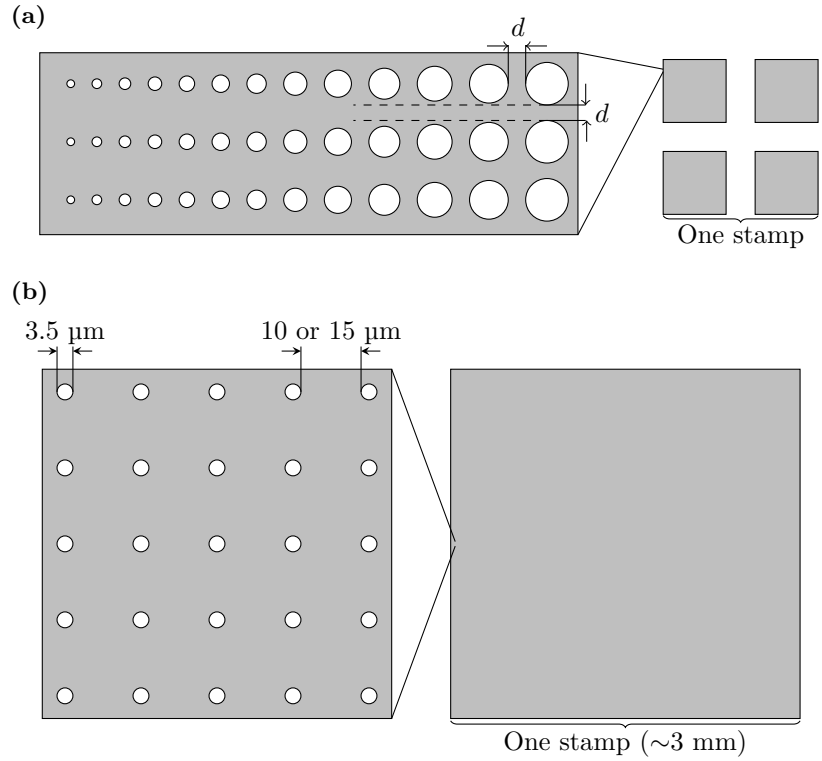

Figure 3.2: (a) shows the prototype mask design. The repeated pattern across this mask consists of thirteen circular holes of increasing radius in an opaque background. The radius of the holes ranges from 0.4 µm to 2.2 µm. The stamps are produced with a distance d =3, 4, 6 and 8 µm. The circles are to scale, other dimensions are not to scale. This dot pattern is repeated vertically as shown, the distance d being the minimal distance between the largest circles vertically, as well as between the circles of different stacks. Such stacks are then repeated between 8 (for the stamps with $d = 8$ µm) and 24 (for the stamps with $d = 3$ µm) times in each of a stamp's quadrants. The mask contains patterns for 185 stamps total.
(b) shows Stamp Design II. Punches on this mask has a diameter of 3.5 µm and are spaced equidistantly with a spacing of 10 or 15 µm. Each individual stamp measures 9 mm^2. The mask may yield 116 stamps with 15 µm separation and 98 stamps with 10 µm separation.

3.2 Stamp Inspection

Materials. Finished PDMS stamps. A Cressington 208 HR B sputter coater and a Hitachi TM3000 tabletop SEM sporting a BSE detector. QD655 ITK Amino quantum dots from Life Technologies. Mili-Q water. Nitrogen gas at 2.6 quality from Yara Praxair. Cover slips. 100 or 20 g weights. A CLSM.

Methods. One stamp was cut from the PDMS disc and sputter coated with a 10 to 20 nm thick Au coating. The stamp was then inspected in the tabletop SEM. A number of other stamps were cut from the PDMS disc, and 20 µL 10 nM QD655 (diluted in mili-Q water) was applied to each stamp. The stamps were left to incubate for ten minutes after which excess QD655 solution was withdrawn with a micropipette and the stamps blown dry with nitrogen gas. The ready stamps were gently placed pattern down on cover slips. Another cover slip was gently placed on the stamp's unpatterned side. A weight was placed on top of the stamp/cover slip structure. For prototype stamps a 100 g weight was used. For stamp design II 20 g was used. The stamps were allowed to remain in contact with the substrate for ten minutes. After the ten minutes have passed the weight was removed and the stamped area was marked using a permanent marker. Once the patterned area was marked the stamp was carefully removed. The patterned cover slip was transferred to a confocal microscope, and the stamped pattern was observed using a laser and detector setup in-line with the fluorophore's excitation and emission spectrum, detailed in Figure 2.12.

3.3 Substrate Preparation

3.3.1 Cleaning

Materials. Substrates for µCP processing consisted of 20×20 mm glass cover slips and WillCo-dishes. 1 M hydrochloric acid (HCl), 96% methanol, nitrogen gas at 2.6 quality from Yara Praxair, milli-Q water, lens paper.

Method. Cover slips and WillCo Dish glass bottoms were cleaned by 15 minutes submersion in a 1:1 volumetric mixture of HCl and Methanol. After submersion the slides were rinsed by subjecting them to jets from a pasteur pipette with milli-Q water and dried with Nitrogen. The slips were stored in plastic boxes with lid on at all times to reduce contamination from the environment. Lens paper was used to line the box and separate the slides.

Once cleaned, the WillCo dish bottoms were assembled into complete WillCo Dishes according to the instructions available on the WillCo Wells website [86]. Once completely assembled, cleaned WillCo-d ishes were stored with their lids on.

3.3.2 Coating

Materials. 22 kDa polyvinyl alcohol (PVA, see Figure 3.3(a)) from BDH Chemicals. 5 kDa methoxyl silane polyethylene glycol (PEG) from nanocs (Figure 3.3(b)). BSA from Sigma Aldrich. fluorescein isothiocyanate (FITC)-labeled poly-L-lysine (PLL), mw 15 000-30 000 from Sigma Aldrich. Polyethyleneimine (PEI), mw 750 000, 50 wt% in H_2O from Sigma Aldrich. phosphate buffered saline (PBS) from Sigma Aldrich. Acetic acid. Milli-Q water. A hot-plate with adjustable temperature and spin coater with adjustable rotation speed were also used.

Method. Once cleaned the cover slips or WillCo-dish bottoms were coated with either PVA, PEG or BSA

Coating with PVA. Cleaned cover slips were spin-coated with a solution of 1 wt% solution of PVA at approximately 3000 rpm for 10 seconds, or until the dispersion of Newton Rings could no longer be observed. Spin coating was followed by curing on a hot-plate at 130°C for 30 minutes.

Coating with PEG. Cleaned surfaces (Cover slips and WillCo dishes) were PEGylationPEGylated using a Silane PEG with a MW of 5 kDa obtained from Nanocs (Figure 3.3(b)). PEG powder was added to 1 mM acetic acid at a concentration of 2 mg/ml, and vortexed. Immediately after vortexing, the resulting solution was added to a clean glass slide, and left to incubate for 30 minutes. After incubation slides were rinsed with milli-Q water and blown dry with N_2 (g). In the case where WillCo dishes were used, assembly was done prior to PEGylation.

Coating with BSA. 1 mg BSA was dissolved in 1 ml PBS with a pH of 7.4. PBS was prepared according to instructions from the manufacturer, Sigma Aldrich. The resulting solution was added to cleaned cover slips, and left to incubate for 20 minutes. After incubation the cover slip was rinsed with milli-Q water and blown dry with N_2 (g).

Coating with PLL or PEI. PLL was diluted to 1 $\mathrm{mg\,ml^{-1}}$ in milli-Q water. PEI was diluted to 1 wt% in milli-Q water. Borosilicate cover slips were incubated with one of the resulting solutions for 10 minutes and blown dry with N_2 (g).

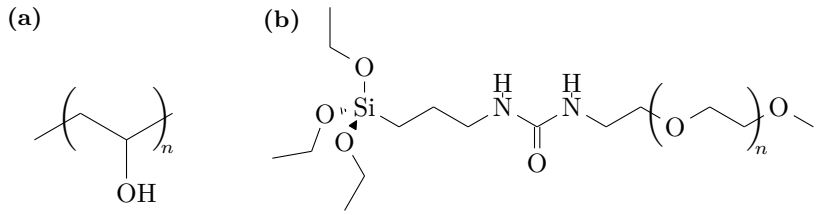

Figure 3.3: The two substrate coatings used, Poly(vinyl Alcohol) (PVA) (a) and methoxyl triethoxysilane-*g*-poly(ethylene glycol) (b).

3.4 Sample Preparation

Materials. Dopamine hydrochloride from Sigma Aldrich. Tris from Sigma Aldrich. FITC-labeled PLL, mw 15 000-30 000 from Sigma Aldrich. PEI, mw 750 000, 50 wt% in H_2O from Sigma Aldrich. Nitrogen gas at 2.6 quality from Yara Praxair, lysogeny broth growth medium (LB-medium), *P. putida* overnight culture, DI-water, Skotch tape, double sided tape, plastic dishes.

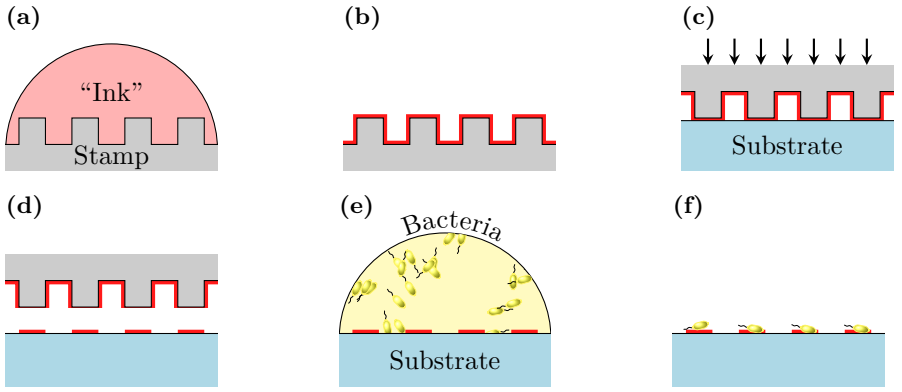

Figure 3.4: In figure (a) we see a 2D profile of a stamp coated with an ink of choice. Once incubated for a preset amount of time, see Chapter 3.4 for parameters, the stamp is blown dry with N_2, leaving an adsorbed layer coating the stamp, shown in figure (b). The cured stamp can then be pressed against the intended substrate (See figure (c)), depositing the ink with which it is coated wherever contact is made, as shown in figure (d). Once stamped, the substrate is covered with bacteria in solution and left to cure for a time, shown in figure (e). After curing the substrate is dried by touching a paper towel to the bacteria in solution and thereby removing the liquid by capillary suction, leaving bacteria deposited onto the substrate surface, as seen in figure (f). Note that multiple "inks" may be added successively by adding a new ink to an already coated stamp.

Method. A stamp was cut from the disc of stamps yielded by the casting process using a scalpel. The resulting stamps measure approximately 5 mm by 5 mm. Dust was removed from the stamp by repeated application and withdrawal of Skotch tape. Once cleaned in this way, the stamp was affixed to onto a double sided tape, in the bottom of a plastic dish, with the stamp's patterned side up and away from the tape. The plastic dish's lid was kept closed when no work was done to prevent contamination.

Coating with PD. To minimize the effort of PD application, a stock solution of 200 mg/mL dopamine hydrochloride in H_2O was prepared. A number of Eppendorf tubes containing 5 µL stock solution were prepared and frozen along with the stock solution. To activate polymerization 1 ml 10 mM tris(hydroxymethyl)aminomethane (tris) (pH 8.5) was addded to one of these Eppendorf tubes, which was then vortexed. The stamp features were covered with the polymerizing solution using a micro-pipette immediately following vortexing. The lid of the plastic dish was kept closed whenever possible to keep contaminants away from the stamp. The stamps were left to incubate for 30 minutes. For samples intended for atomic force microscope (AFM)-inspection incubation was done with the stamp atop a drop of polymerizing PD to reduce sedimentation of any large particulates onto the stamp pattern. After incubation excess PD was removed with a micropipette, and the stamp was blown dry using N_2 (g).

Coating with PLL or PEI. For stamping of PLL or PEI onto BSA this is performed on clean stamps. For co-deposition of PD with either PLL or PEI this step follows the PD-coating step above. PLL was dissolved in milli-Q water to a concentration of 1 mg/ml and vortexed. PEI was simmilarly diluted and vortexed. The stamp features were coated with approximately 20 µL solution and left to incubate for ten minutes. After incubation excess solution was removed by micropipette and the stamp was blown dry with nitrogen gas.

Stamping. Dried and coated stamps were gently placed with the pattern side towards the chosen and coated substrate. A cover slip was placed atop the stamps un-patterned side. Unless otherwise stated, a 100 g weight (for prototype stamps) or 20 g weight (for stamp design II) was gently placed atop the stamp. The weight was left on the stamp for 10 minutes. After which the weight was removed from the stamp, and the underside of the sample (though

not directly under the pattern) was marked with a permanent marker. Once marked, the stamp was gently withdrawn.

Adding Bacteria. Bacteria are added to the stamped pattern in LB-medium, as shown in Figure 3.4(e). It is left to incubate for 5 minutes after which it was rinsed by submerging the sample in DI-water for a second or two and then withdrawn. Submersion and retraction was performed twice per sample. Once rinsed the sample was either left to air-dry, it was covered with nutrient media (LB) or it was stained with a Live/Dead assay.

3.4.1 Live-Dead Assay

Materials. Live/Dead® *Bac*Light™ Bacterial Viability Kit (L13152) from Life Technologies. Milli-Q water. Fresh overnight *P. putida* KT2440 culture. LB-medium medium.

Method. PEG-coated WillCo dishes were prepared as described in Chapter 3.3.1 and 3.3.2. PD microarrays were prepared as described in Chapter 3.4.

Using gloves at all stages for personal safety, the Live/Dead® *Bac*Light™ assay was prepared according to the product datasheet [87]: One part of component A was mixed one part component B and two parts milli-Q water and vortexed.

Once the Live/Dead assay dye mixture is ready, bacteria were added to the prepared PD microarrays. After incubating for five minutes and rinsing the arrays, as described in Chapter 3.4, 200 µL dye mixture was added to each sample, the WillCo dish lids were closed and the closed dishes wrapped in aluminum foil. The samples were transferred to a CLSM for inspection. Note that the dyes used, SYTO 9 and propidium iodide, are potentially toxic and need to be handled with care [87]. For this reason gloves were always used when handling samples dyed with these stains.

Some samples were tested after bacteria had been isolated on the arrays for a time. In this case the arrays were prepared as described earlier in this thesis, cleaned and submerged in LB-medium at room temperature for a specific time, during which the WillCo dishes' lids were closed. After the alotted time (0, 30, 60, 120 and 180 minutes) the arrays were cleaned as before and the Live/Dead assay was added to the arrays.

Results

4

While this chapter will detail instrument settings used to achieve a given image, certain features such as the photomultiplier gain and offset will not be specified. Four main stamp designs will be used throughout the section and referred to by names dictated by their design. Specifically two pillar-based stamp designs, a grid stamp design and a line stamp design. Where post-processing by LAS AF Lite is indicated, version 3.2.9652.0 is used. Where post processing by ImageJ is indicated version 1.47v (64 bit, Windows version) has been used. All scale bars added, and some processing has been done (where and as indicated), using Ti*k*Z/PGF version 2.10 in TEX Live 2013. With respect to the scale-bars on images from confocal microscopes, the length of these are accurate to the fifth decimal place, supposing the data from the microscope is accurate and Ti*k*Z does not introduce unknown errors. Note that the document's results portion is primarily intended to be perused on-screen. The images recorded or taken by Ottesen are included in high quality, and the PDF file produced permits the user to magnify these to the extent that the original image files permit.

4.1 Starting Point

The images in this section were recorded prior to the beginning of Ottesen's master project, were themselves included in Ottesen [18], and are included to give perspective to the included and discussed work. Figure 4.1 shows results obtained prior to (Figure 4.1(a)) and during (Figure 4.1, (b) and (c)) Ottesen's project work in 2013.

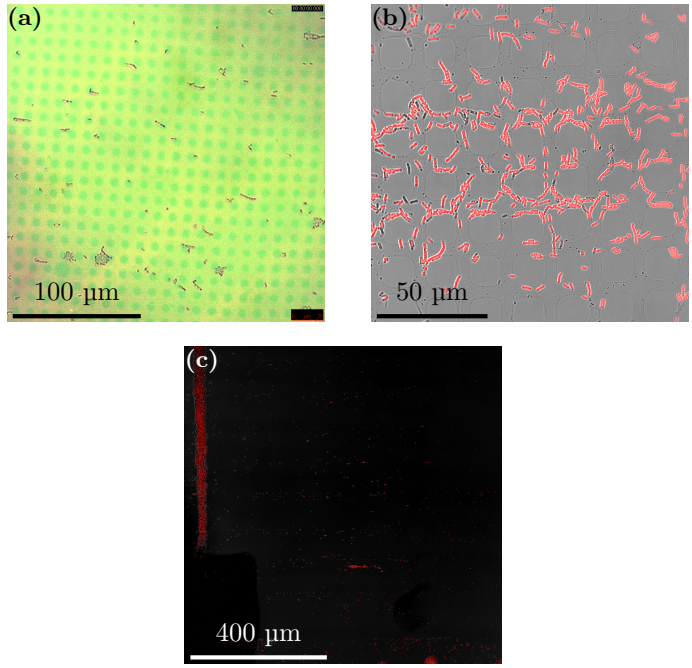

Figure 4.1: Previous attempts at creating bacterial arrays using *E. coli* DH5alpha. (a) *E. coli* on a Alexa Fluor 546 labelled BSA grid stamped onto a FITC labelled PLL surface, the image is supplied by Nina Bjørk Arnfinnsdottir. (b) *E. coli* on PD pattern stamped onto PVA treated glass slide. (c) *E. coli* stamped onto glass. (a) and (b) use a stamp design which deposits the ink in a grid with holes in it, whereas (c) uses the prototype stamp design discussed in this thesis. Both figures are from Ottesen's project paper [18]

4.2 Stamp Inspection

The surface of stamps produced using the first mask design, hereafter referred to as the prototype stamp design, were sputter-coated with gold and subsequently inspected in SEM (Figure 4.2). Stamps from the same master were also used to print patterns of quantum dots. The printed patterns were imaged by CLSM (Figure 4.4). Based on the CLSM images, the diameter of the fluorophore islands were determined (Table 4.1 and Figures 4.5). SEM inspection of stamps produced using the second mask design, hereafter referred to as stamp design II, are presented in Figure 4.6. These SEM micrographs were used to determine the diameter of the stamp punches (Table 4.2). Quantum dots were printed using stamp design II (Figure 4.7)

4.2.1 Prototype stamp design

Some prototype stamps were sputter coated and examined in a Hitachi TM3000 Tabletop SEM (Figure 4.2). To ensure stamp-to-pattern fidelity stamps were also coated with fluorophores, and patterns were stamped on glass (figures 4.3 and 4.4). The images in Figure 4.4 were used to determine the diameter of the islands deposited by the stamps. Island area was measured using ImageJ's built-in "Analyze Particles" functionality. Threshold for island identification was set using ImageJ's built-in function, employing the MaxEntropy Over/Under algorithm. Island radius was subsequently calculated from measured area, using the assumption that each island was perfectly circular. Data from this is tabulated in Table 4.1 and plotted in Figure 4.5.

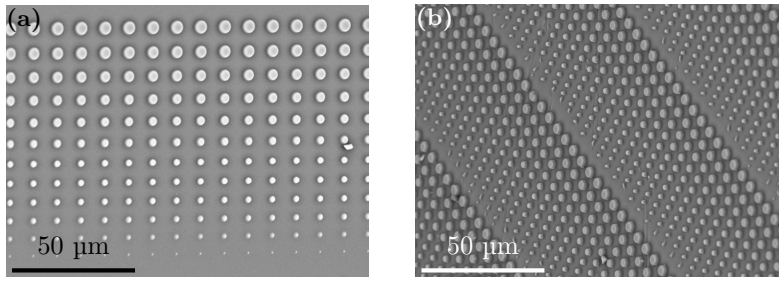

Figure 4.2: Figures (a) and (b) show gold coated stamps manufactured from the prototype design shown in Figure 3.2(a). Image recorded on a Hitachi TM3000 Tabletop SEM using it's solid state BSE detector. Images have been cropped to remove the SEM software's built-in scale bar and image name.

Figure 4.3: Image showing QD655 stamped with a prototype stamp. The image is stitched together from multiple micrographs, and shows the entire patterned area left from one prototype stamp. A Leica TCS SP5 was used to obtain these images. The objective used was a Leica HCX PL APO CS 10.0x0.40 dry UV. An Argon laser emitting with a wavelength of 458 nm was used. Recording was done using a HyD, registering light with a wavelength between 611 and 695 nm. The image was automatically stitched together from several images using the LAS AF software on the Leica SP5 microscope.

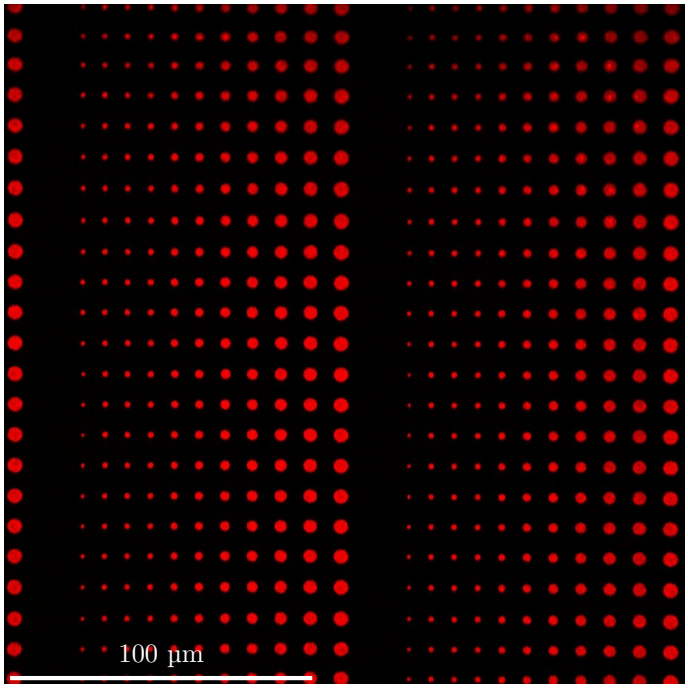

Figure 4.4: Fluorophores stamped onto glass using prototype stamp design.This image was taken on a Zeiss 510 Meta. The objective used was a Zeiss Plan neofluar 20.0x 0.5 l. An Argon laser emitting with a wavelength of 458 nm was used. Recording was done using a PMT, registering light with a wavelength between 588.7 and 662.0 nm. Island area was measured using ImageJ's built-in "Analyze Particles" functionality. Threshold for island identification was set using ImageJ's built-in function, employing the MaxEntropy Over/Under algorithm. Island radius was subsequently calculated from measured area, using the assumption that each island was perfectly circular. The fluorophore used was a 10 nM dilution of QD655® ITK™ PEG amine from Life Technologies.

Table 4.1: Designed (d_D) versus measured diameter (d_M) of islands formed by deposited quantum dots. The data for this table was determined based on the image displayed in 4.4 and five similar micrographs shown in Appendix A. The data is visualized in Figure 4.5.

Island	d_D	d_M	Standard deviation
1	4.40	5.18	$6.58 \cdot 10^{-2}$
2	4.00	4.77	$6.05 \cdot 10^{-2}$
3	3.60	4.36	$5.76 \cdot 10^{-2}$
4	3.20	3.93	$5.87 \cdot 10^{-2}$
5	2.80	3.56	$4.84 \cdot 10^{-2}$
6	2.40	3.11	$4.76 \cdot 10^{-2}$
7	2.00	2.66	$7.15 \cdot 10^{-2}$
8	1.80	2.35	$4.45 \cdot 10^{-2}$
9	1.60	2.31	$4.41 \cdot 10^{-2}$
10	1.40	2.23	$4.29 \cdot 10^{-2}$
11	1.20	1.46	0.15
12	1.00	NaN	NaN
13	0.80	NaN	NaN

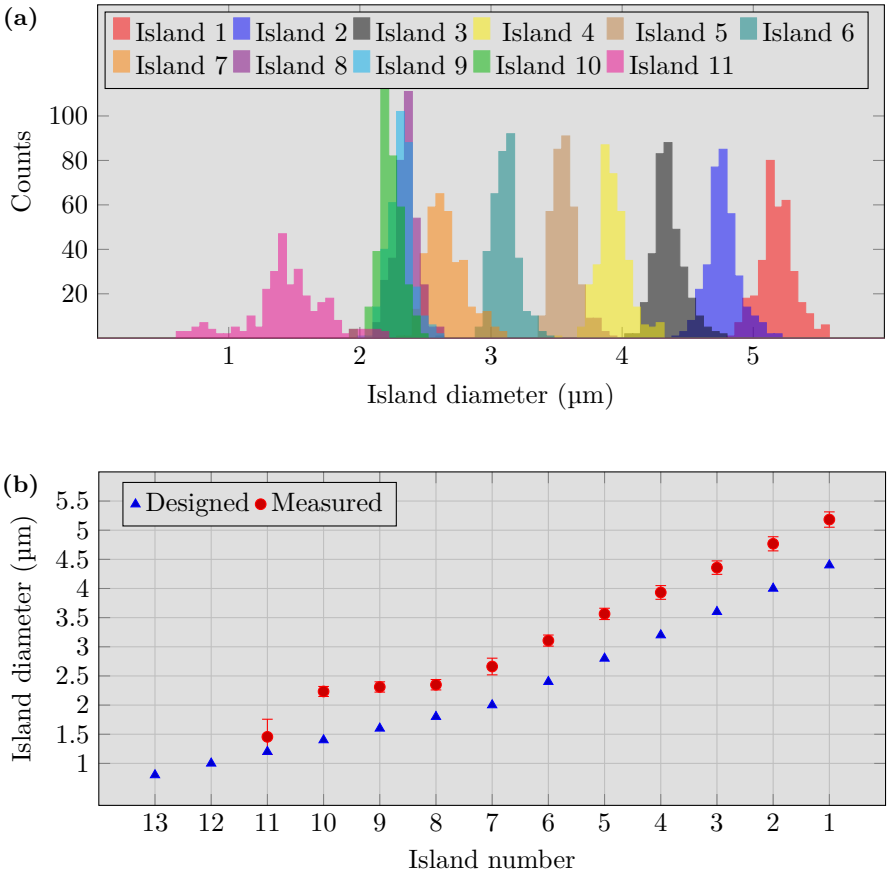

Figure 4.5: The diameter of islands produced using the prototype stamp design. (a) histograms with semitransparent bars presenting the diameter of printed islands. (b) shows a plot comparing the measured diameter of printed islands (red) with the diameter of holes in the prototype mask design (blue). This plot is generated using data seen in Table 4.1, which was collected from micrographs shown in Figure 4.4 and Appendix A. The islands are numbered according to decreasing diameter, viz. the largest island is numbered 1, whereas the smallest designed island is numbered 13.

4.2.2 Stamp Design II

The second stamp design, hereafter referred to as stamp design II, was made based on data gathered with respect to the prototype arrays' ability to isolate single bacteria on each array coordinate. SEM micrographs of the new stamps are seen in Figure 4.6. Punch diameter was determined from SEM micrographs (Table 4.2). Quantum dot islands were printed with the stamp design (Figure 4.7) and island size distribution was plotted in histograms using the same technique as was used for the prototype design (Figure 4.8).

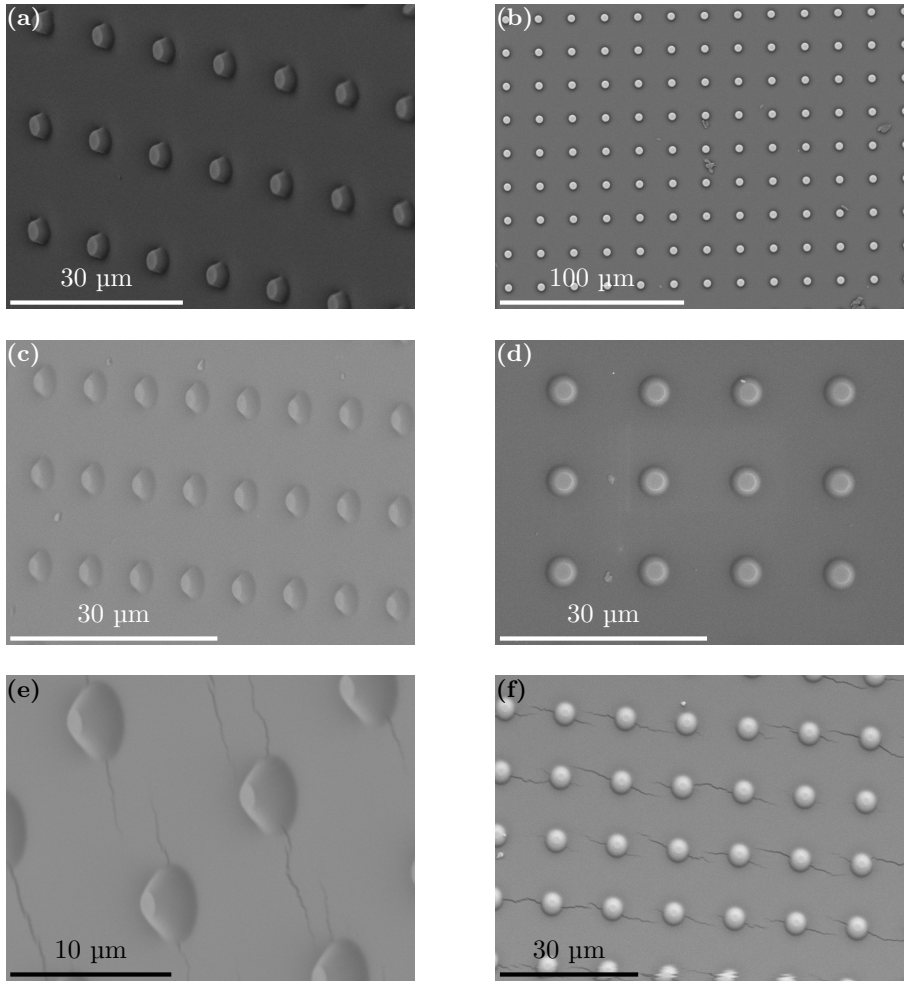

Figure 4.6: Electron micrographs taken at different angles showing gold-coated stamps. The design used was stamp design II (Figure 3.2(b)). (a) and (b) shows stamps cast on a master exposed to 220 $mJcm^{-2}$ ultraviolet radiation. (c) and (d) shows stamps cast on a master exposed to 180 $mJcm^{-2}$ ultraviolet radiation. Figures (e) and (f) shows stamps cast on a master exposed to 150 $mJcm^{-2}$ ultraviolet radiation. Image recorded on a Hitachi TM3000 Tabletop SEM using it's solid state BSE detector. Images have been cropped to remove the SEM software's built-in scale bar and image name.

Table 4.2: Stamp punch (pillar) diameter in µm for stamps cast on masters prepared with 220, 180 and 150 mJ/cm^2 respectively. Data acquired from Figure 4.6 (b), (d) and (f).

UV Dosage (mJ/cm^2)	220	180	150
Mean (µm)	3.83	2.49	1.69
Min (µm)	3.75	2.31	1.49
Max (µm)	3.87	2.63	1.87

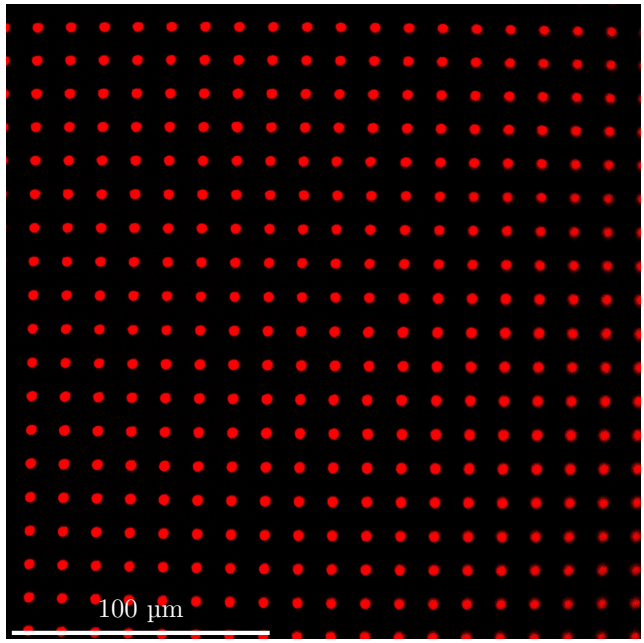

Figure 4.7: Microarray of quantum dots (QD655®) printed using new stamps, cast on high UV exposure master. A Leica TCS SP5 was used to obtain this image Recording was done using a HyD, registering light with a wavelength between 561 and 633 nm. An Argon laser emitting with a wavelength of 458 nm was used. The objective used was a Leica HCX PL APO CS 63.0x1.20 WATER UV. The fluorophore used was a 10 nM dilution of QD655® ITK™ PEG Amine from Life Technologies. The stamps used to print this image was cast on a master exposed to 220 mJcm^{-2}.

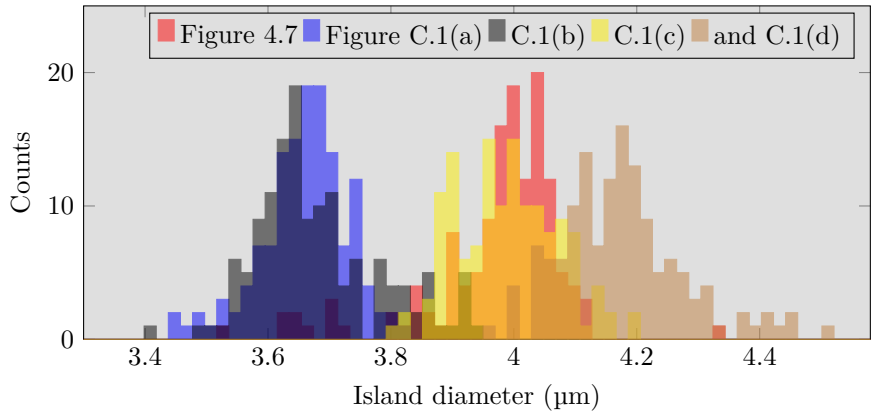

Figure 4.8: Island size distributions for stamps cast on masters prepared with high exposure dose (220 mJcm^{-2}). Island area was measured using ImageJ's built-in "Analyze Particles" functionality. Threshold for island identification was set using ImageJ's built-in function, employing the MaxEntropy Over/Under algorithm. Island radius was subsequently calculated from measured area, using the assumption that each island was perfectly circular. Data extracted from image in Figure 4.7 and four similar micrographs shown in Appendix C.

4.2.3 AFM Pattern Inspection

Katarzyna Maria Psonka-Antonczyk expressed interest in the roughness of the printed PD pattern and the PEGylated surface. She examined samples prepared using the prototype stamp by the author of this thesis using a Veeco Multimode V AFM, the result of which is shown in Figure 4.9. Note that as the author of the current thesis did not utilize this technique it is also not described in Chapter 2. The reader is instead referred to relevant literature [88–90].

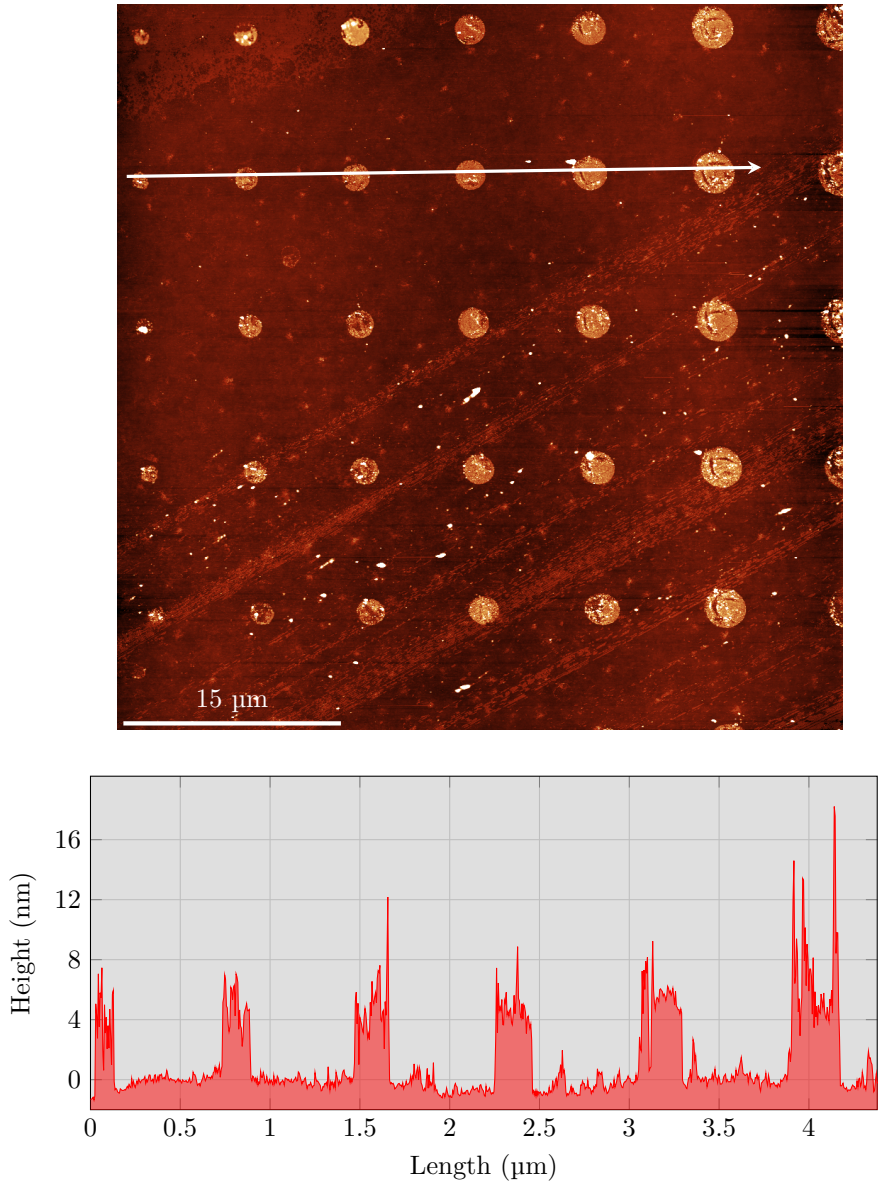

Figure 4.9: PD pattern printed with prototype stamp onto PEG, inspected with AFM. The plot shows a profile plot across 6 PD islands as indicated by an arrow across the micrograph proper. The micrograph was recorded by Katarzyna Maria Psonka-Antonczyk and is used with permission. Analysis was performed and profile plot extracted using Gwyddion 2.33 (64 bit).

4.2.4 Observed Aberrations

Figure 4.10 shows some of the aberrations, either from the microscopes, the stamping process or the integrity of the anti-adhesive coating encountered in several experiments.

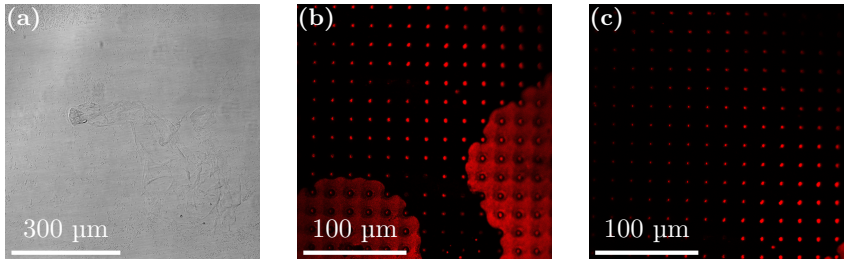

Figure 4.10: Various challenges faced during experimentation. 4.10(a) failure of deposited PVA film. The image shows a poorly reproduced pattern with *Pseudomonas putida* embedded in agar. (b) shows areas displaying roof collapse. (c) shows an uneven intensity distribution across the image with the upper right and lower left corners showing the lowest intensities and a maximum between them. For (b) and (c) the dye used was Alexa Fluor 488. (b) and (c) was recorded on a Leica TCS SP8. A White-light laser emitting with a wavelength of 488 nm was used. The objective used was a Leica HC PL APO CS2 63x/1.20 WATER. Recording was done using a HyD, registering light with a wavelength between 525 and 577 nm. For (a) no dye was used. (a) was recorded on a Leica TCS SP5. The objective used was a Leica HCX PL APO CS 10.0x0.40 dry UV. A diode-pumped solid-state laser (DPSS) laser emitting with a wavelength of 561 nm was used. Transmitted light was collected in a PMT and is shown as greyscale.

4.3 Bacterial Arrays

Bacteria from two model strains, *E. coli* DH5alpha and *P. putida* KT2440, were added to the arrays of bacterial adhesive and adhesion preventing chemicals yielded results that differed based on the dimensions of the printed islands, the bacterial strain used and the time bacteria were left to incubate on the arrays. Arrays were tested in air, submerged in growth medium and the survival of bacteria was tested using a LIVE/DEAD® *Bac*Light™ assay from Life Technologies.

4.3.1 Arrays Obtained Using the Protoype Stamp Design

The prototype arrays were inspired by Rozhok et al. [9]. The varying diameter of the islands, described earlier in this chapter, were meant to assist in identification of an optimal island size, immobilizing one bacterium per island while also immobilizing bacteria on as large a portion of the printed islands as possible. Data from Bacterial arrays, see Figure 4.11, was gathered and analyzed together with data from the stamp analysis seen earlier in this chapter to identify an optimal island diameter. The data is tabulated in Table 4.3 and plotted in Figure 4.12.

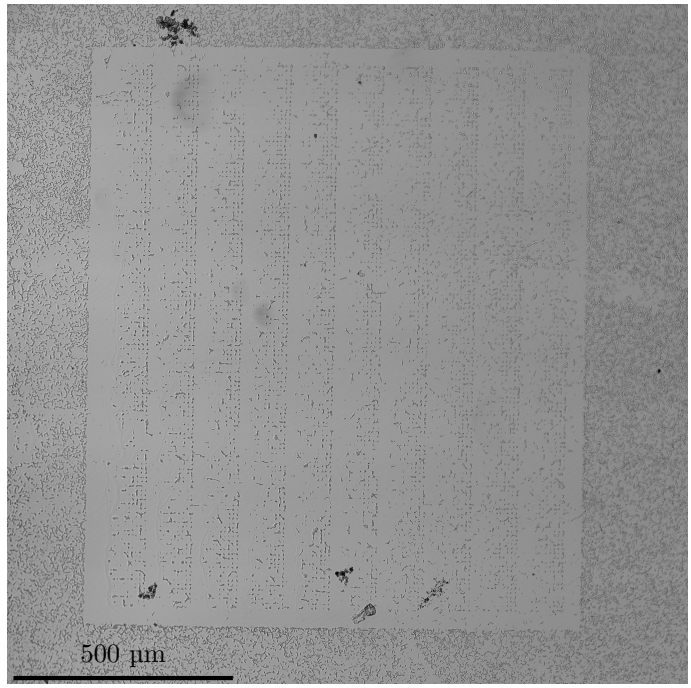

Figure 4.11: *Pseudomonas putida* adhering to polydopamine arrays printed onto PEG-coated cover slips using the prototype stamp design. Several columns of bacteria from this image and four similar arrays formed the basis for the plot presented in Figure 4.12 and in Appendix B. A Leica TCS SP5 was used to obtain this image. Transmitted light was collected in a PMT and is shown as greyscale. A DPSS laser emitting with a wavelength of 561 nm was used. The objective used was a Leica HCX PL APO CS 10.0x0.40 dry UV.

Table 4.3: Number of bacteria per island. $Nb_B \geq 1$, one or more bacteria adhering. $Nb_B = 1$ only one bacterium adhering. The data was acquired by observing the array seen in Figure 4.11 and four other micrographs shown in Appendix B, counting islands with bacteria and with only one bacterium. Note that areas with significant bacterial adhesion outside the stamped pattern were omitted in the counting process.

Avg. d (µm)	$Nb_B \geq 1$ (%)	$\sigma_{\geq 1}$	$Nb_B = 1$ (%)	$\sigma_{=1}$
2.59	87	8.65	47	5.18
2.39	77	3.28	54	7.00
2.18	75	9.01	55	3.24
1.97	67	8.96	49	17.63
1.78	65	9.63	60	8.77

Nb_B: Number of bacteria per island

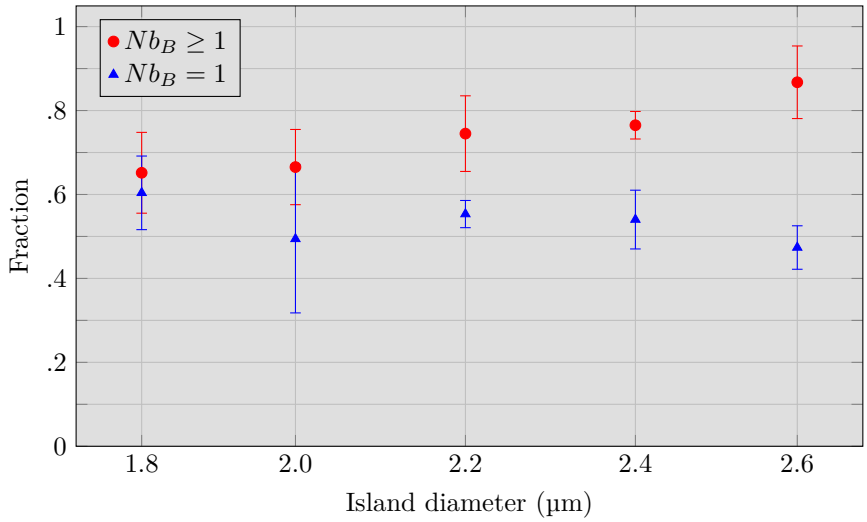

Figure 4.12: Fraction of islands with one or more than one bacteria adhering. The data were obtained based on inspection of the array presented in Figure 4.11 and four other micrographs showing one array each. Areas with significant bacterial adhesion outside the stamped pattern were omitted in the counting process.

4.3.2 Arrays Obtained Using Stamp Design II

The features of stamp design II were chosen based on results presented in Table 4.3. Whether printed on PVA or PEG, PD arrays of this design successfully resulted in immobilization of *P. putida*, whether the array was in air or submerged in liquid environments.

Dry Arrays

The arrays presented in this subsection were cleaned and air-dried following the procedure detailed in Chapter 3.4. A series of arrays were prepared and subjected to different incubation times, ranging from five to forty-five minutes (Figure 4.13). The arrays were imaged in dry condition. The arrays seen in Figure 4.14 were analyzed for adhesion statistics. The results of this analysis is seen in Table 4.4.

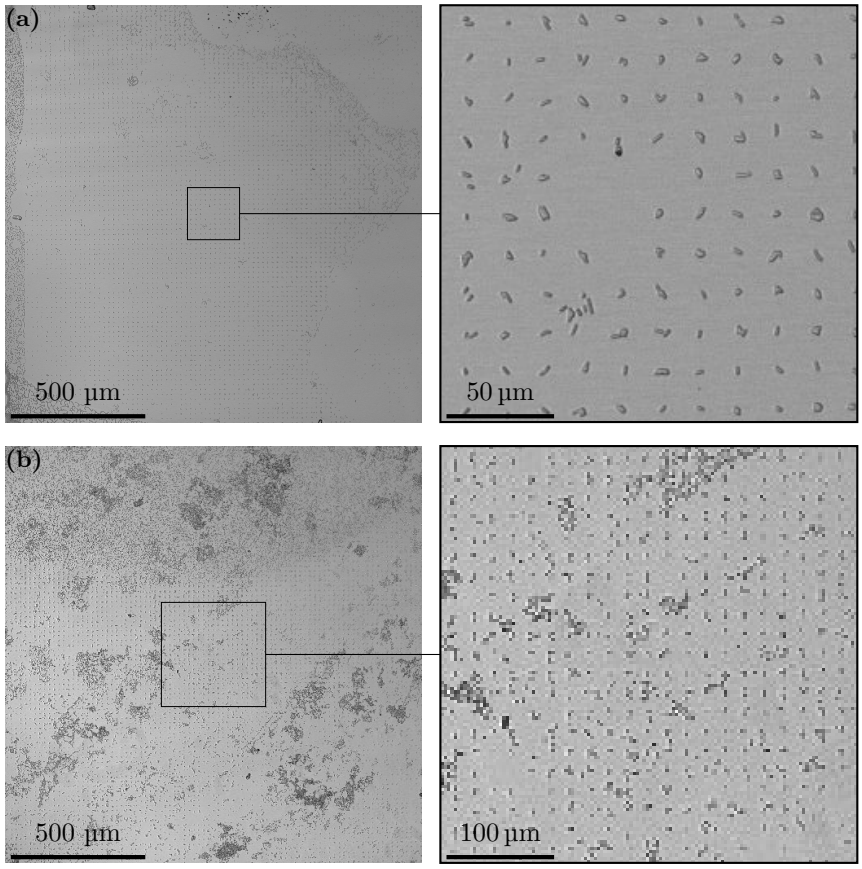
(a)
500 µm
50 µm
(b)
500 µm
100 µm

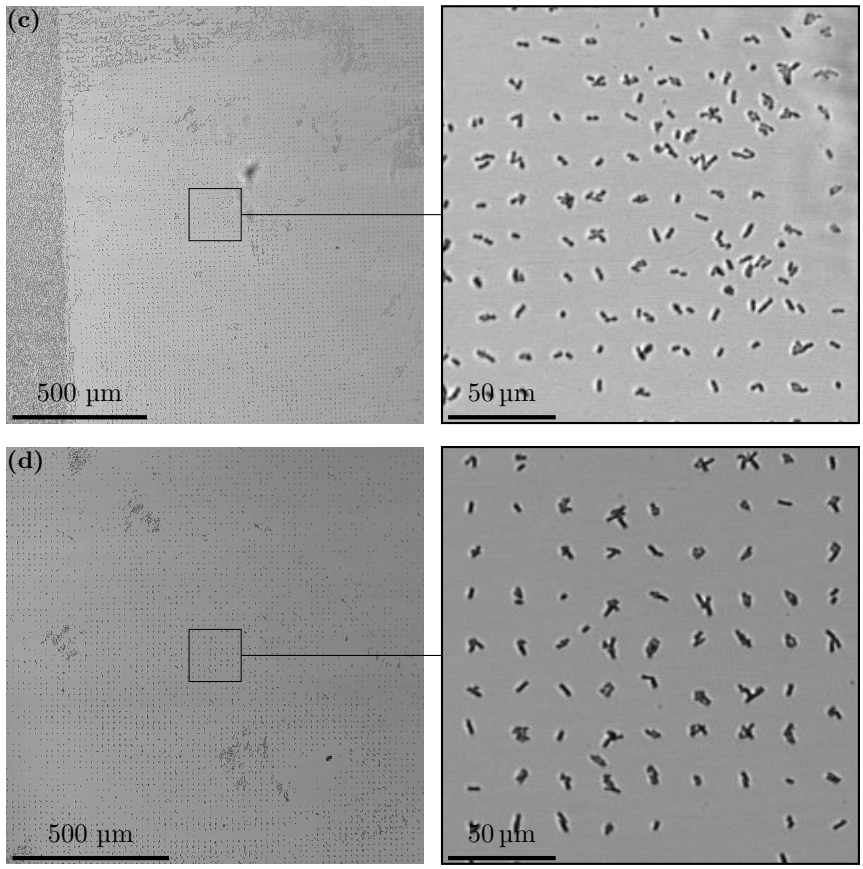

Figure 4.13: Micrographs depicting arrays after 5 (a), 10 (b), 20 (c) and 45 (d) minutes in *P. putida* overnight culture in LB-medium. These arrays consist of PD printed on PVA. A Leica TCS SP5 was used to obtain these images. The objective used was a Leica HCX PL APO CS 10.0x0.40 dry UV. A DPSS laser emitting with a wavelength of 561 nm was used. Transmitted light was collected in a PMT and is shown as greyscale.

Array Isolation Potential

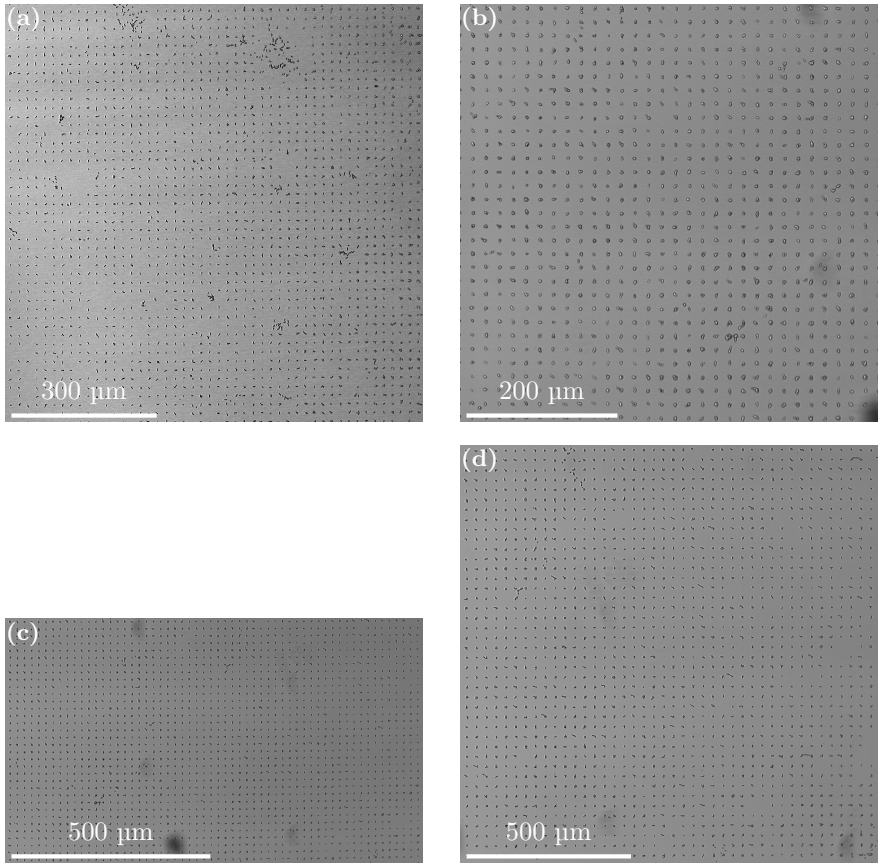

Figure 4.14: Select arrays used for assessing adhesion statistics. (a) shows an area excerpted from Figure 4.13(a). (b), (c) and (d) shows *P. putida* adhering to PD arrays printed on PEG-coated glass and manually analyzed. A Leica TCS SP5 was used to obtain these images. The objective used was a Leica HCX PL APO CS 10.0x0.40 dry UV. A DPSS laser emitting with a wavelength of 561 nm was used. Transmitted light was collected in a PMT and is shown as greyscale.

Table 4.4: Results from counts of bacterial arrays made with stamp design II. Arrays analyzed are found in Figure 4.14. Analysis was performed by manual counting. The columns labeled $Nb_B \geq 1$ refers to the number or percentage of islands with one or more bacteria adhering. The columns labeled $Nb_B = 1$ refers to the number or percentage of islands with one and only one bacterium adhering.

Figure	Total islands	$Nb_B \geq 1$	$Nb_B \geq 1$ (%)	$Nb_B = 1$	$Nb_B = 1$ (%)
4.14(a)	2 209	1 972	89.3	1 693	76.6
4.14(b)	961	958	99.7	370	38.5
4.14(c)	1 972	1 952	100.0	744	62.2
4.14(d)	1 764	1 725	97.8	532	30.2
4.15(a)	1 444	1 407	97.4	379	26.3
4.15(b)	576	560	97.2	123	21.4

Nb_B: Number of bacteria per island

Arrays in Growth Medium (LB)

By supplying the bacteria with nutrition in the form of liquid growth media it is possible to observe their behavior when in a nutrient rich and liquid evironment, yet immobilized on well defined coordinates. The result of a proof-of concept experiment is seen in Figure 4.15 and in Appendix D

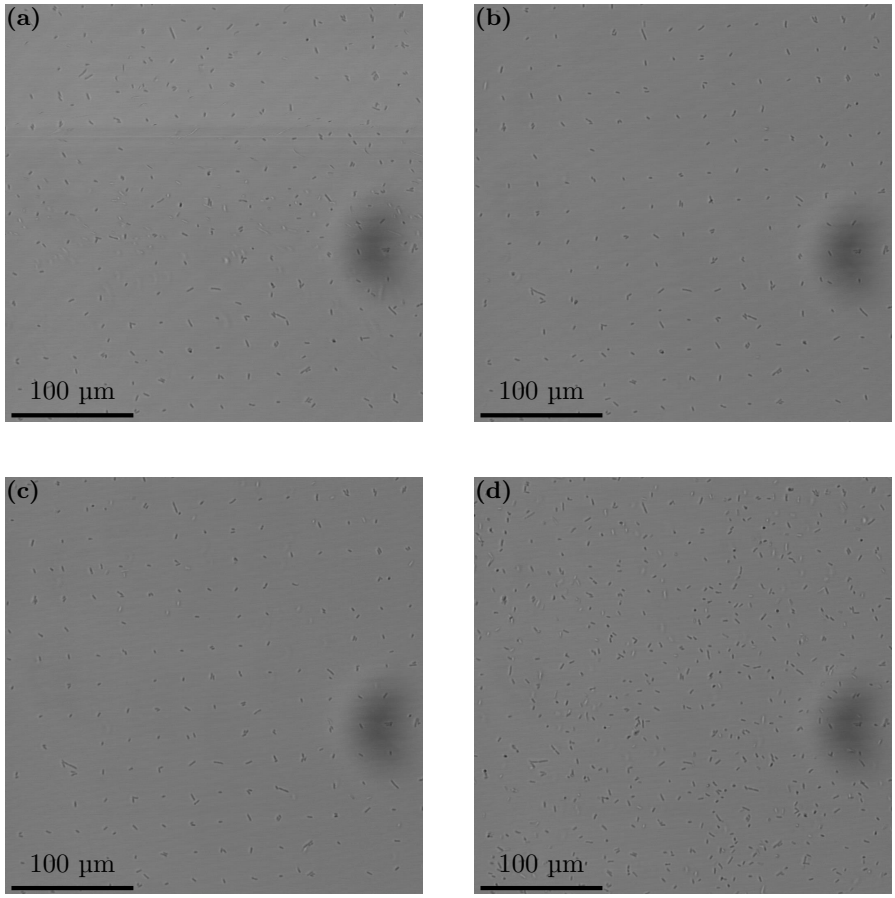

Figure 4.15: Images excerpted from timelapse recording of *P. putida* microarray submerged under LB-medium. Images show array immediately after submersion (a), after 22 minutes (b), 40 minutes (c) and 1 hour (d). The sample was dry for a short while (minutes) prior to submersion. These arrays consist of PD printed on PVA. A Leica TCS SP5 was used to obtain these images. Transmitted light was collected in a PMT and is shown as greyscale. The objective used was a Leica HCX PL APO CS 10.0x0.40 dry UV. A DPSS laser emitting with a wavelength of 561 nm was used.

4.4 Live/Dead Assay

To ascertain whether immobilized bacteria were alive at the point of immobilization and after a time spent immobilized on the arrays the LIVE/DEAD® *Bac*Light™ Bacterial Viability Kit (L13152) from Life Technologies was used. When using this kit cells with intact cell walls (live) are labeled with one dye (SYTO 9), and cells with permeable walls (dead) are labeled with a second dye (Propidium iodide). The fluorescence spectra of these dyes can be seen in Figure 2.12. The result is seen in Figure 4.16. The micrographs in Figure 4.16 which show well-defined microarrays were analysed to obtain quantitative estimates of the viability of bacteria immobilized on the arrays.

Table 4.5: Quantitative analysis of bacterial viability on arrays produced using stamp design II and subjected to Live/Dead assays. The analysis was performed on arrays presented in figures 4.15(a) and (b). Analysis was performed by manual counting.

Figure	Alive	% Alive	Dead	% Dead
4.15(a)	2 249	99.0	23	1.0
4.15(b)	825	99.5	4	0.5

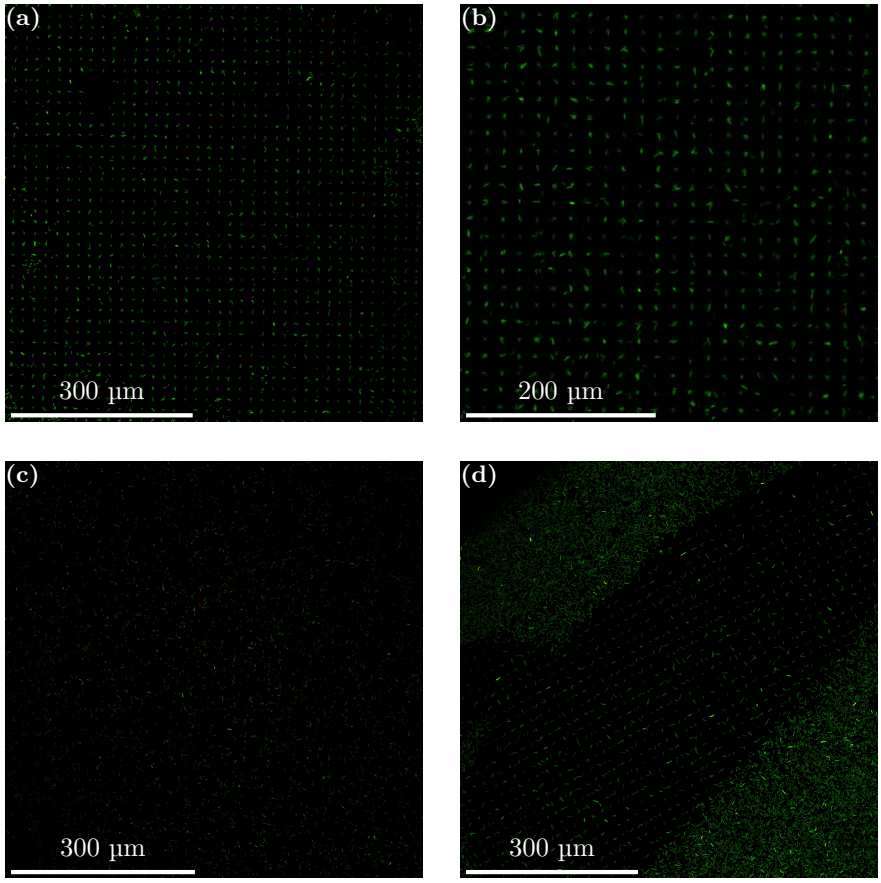
(a)
300 µm
(b)
200 µm
(c)
300 µm
(d)
300 µm

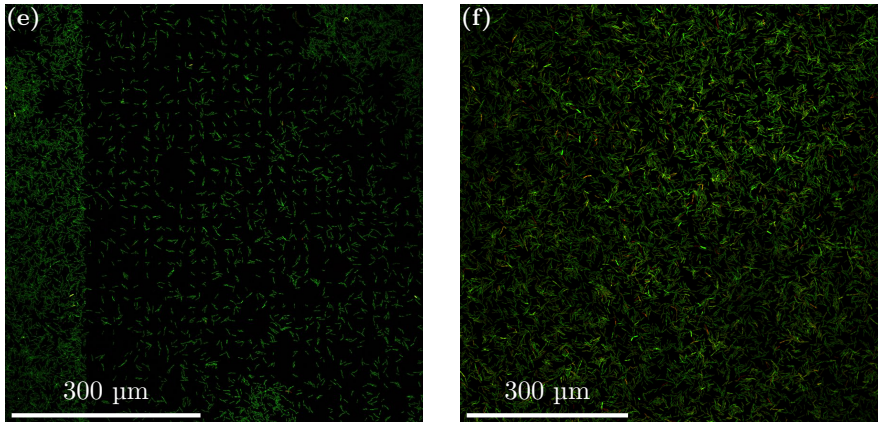

Figure 4.16: *P. putida* isolated on a PD coating, printed onto PEG. The arrays were then submerged in LB-medium for 0, 30, 60, 120 and 180 minutes, rinsed and labeled with LIVE/DEAD® *Bac*Light™ Bacterial Viability Kit (L13152) from Life Technologies. Live bacteria show up as green, dead bacteria show up as red. (a) and (b) were taken without LB-medium submersion. (c) was taken after 30 minutes, (d) after 60 minutes, (e) after 120 minutes and (f) after 180 minutes.A Leica TCS SP5 was used to obtain these images. The objective used was a Leica HCX PL APO CS 10.0x0.40 dry UV. An Argon laser emitting with a wavelength of 488 nm was used. The channels from these images are seen separately in Appendix E. Figures (d) through (f) are taken by Nina Bjørk Arnfinnsdottir

4.5 *Escherichia coli* arrays

Besides work done on *P. putida* KT2440 the arrays were also tested with *E. coli* DH5alpha. Images of arrays where *E. coli* have been attempted immobilized are presented in Figure 4.17.

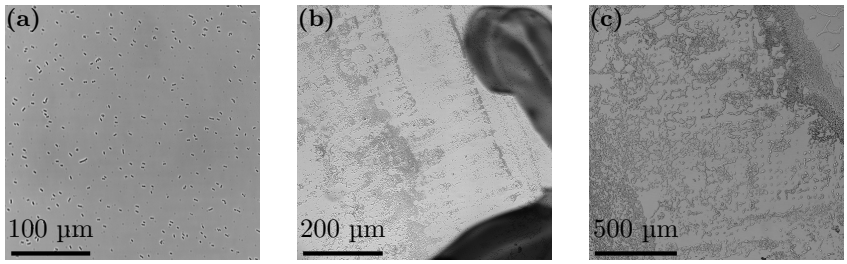

Figure 4.17: *E. coli* on PD printed onto PVA using stamp design II (a) and (b). *E. coli* on PD printed on PEG using the prototype design (b). The figure shows samples incubated for 5 minutes (a), 45 minutes (b) and 270 minutes (c). A Leica TCS SP5 was used to obtain these images. For (a) the objective used was a Zeiss HCX PL APO 40.0x1.10 WATER. For (b) and (c) the objective used was a Leica HCX PL APO CS 10.0x0.40 dry UV.

4.6 Charge Mediated Adhesion Control

P. putida was attempted immobilized on patterns (lines) of PD stamped onto BSA, or on positively charged arrays of PLL or PEI using BSA stamped onto the positively charged polymers PLL and PEI. The results are seen in Figure 4.18. The micrographs in Figure 4.18 are taken by Nina Bjørk Arnfinnsdottir.

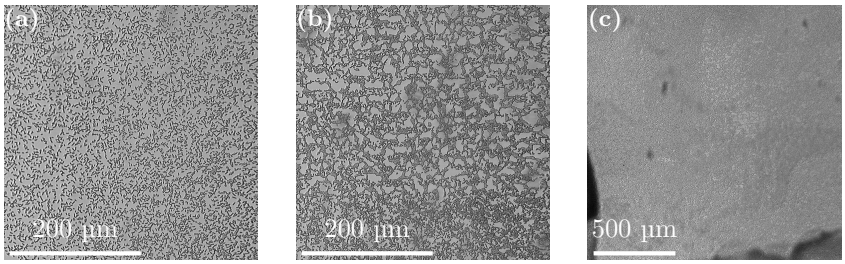

Figure 4.18: *P. putida* on PD lines stamped onto BSA (a). *P. putida* on BSA lines stamped onto PLL (b) *P. putida* on BSA lines stamped onto PEI (c). A Leica TCS SP5 was used to obtain these images. The objective used was a Leica HCX PL APO CS 10.0x0.40 dry UV. A DPSS laser emitting with a wavelength of 561 nm was used. The micrographs are recorded by Nina Bjørk Arnfinnsdottir.

Discussion

5

By immobilizing bacteria onto well defined arrays without inducing stress in the bacteria, a researcher may be able to conduct computer assisted studies into population heterogeneities. Microarrays, as a conceptual approach, have had significant impact on genetics where DNA microarrays have facilitated much research. The aim of this project has been the development of a method by which bacterial microarrays can be constructed cheaply, rapidly and easily. To achieve such a goal, microcontact printing (µCP) of a bacterial adhesive onto a chemical which prevents adhesion was the chosen approach.

A bacterial microarray based on bacterial adhesion must, necessarily, consist of areas that permit bacteria to adhere and areas where adhesion is difficult or impossible for the bacteria. In order to isolate a single bacterium per island, the size of this island must also be considered. The spacing between islands is important because bacteria may form bridges between islands, or they may seem to adhere between islands, adhering to multiple islands through extending protein structures such as pili, fimbria and flagella. These structures can extend multiple micrometers past the outer membrane or cell wall, and interact with the environment or other cells at a distance [1, 36]. It is therefore important to consider the geometry of the printed pattern as well as the chemical basis for adhesion and adhesion prevention when designing a means by which bacteria can be isolated onto arrays.

5.1 Chemical Regime

A chemical basis for adhesion would ideally affix the bacteria only to select areas without inducing bacterial stress or death. Literature can be found supporting several regimes, some of these work based on electrostatic adhesion, using the overall negative charge of a bacterium's surface as basis for the adhesive action [9, 14, 38]. Preventing bacterial adhesion is less simple, as many bacteria are skilled at adhering to practically any surface [35].

5.1.1 A Durable Adhesion Resistant Coating

Both poly(ethylene glycol) (PEG) and poly(vinyl alcohol) (PVA) provide anti-adhesive properties, which can be exemplified by Figure 4.11, where PEG is used and Figure 4.13 where PVA is used. While both anti-adhesive coatings work, and both amphiphilic polymers confer anti-adhesive properties by way of somewhat similar chemistry, the approaches we used in this project may be said to be fundamentally different where coating is concerned.

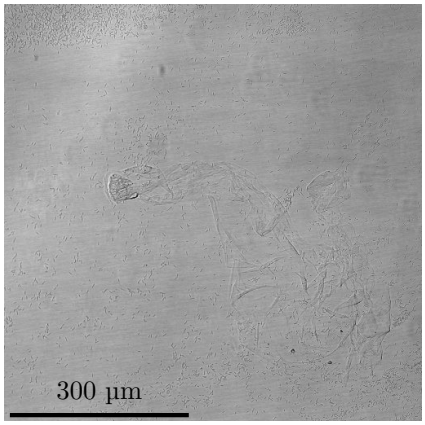

Figure 5.1: A defect in a poly(vinyl alcohol) (PVA) film. This image is also presented in Figure 4.10(a). It is repeated here for clarity. The image shows a poorly reproduced pattern with *Pseudomonas putida* embedded in a thin agar film coating the surface.

Poly(vinyl alcohol) (PVA) was the chemical we first considered using. It is cheap, readily available in large quantities and can coat a surface by thermal treatment of said surface. Coating is also simple, requiring only a spin coater and a hotplate for baking, as discussed in Chapter 3.3.2. The result is a hydrogel coating, annealed to the surface. A PVA coating prepared by this method has certain shortcomings, however. First, spin coating is a sequential process which may become a bottleneck if many samples are to be prepared at the same time. Secondly, the coating is not particularly durable and eventually peels off the substrate. Figure 5.1 demonstrates this shortcoming. Dust particles may aggravate the situation and cause film failure at the moment of coating. This may be remedied by the use of a linker, binding the hydrogel more firmly to the

substrate. As this would add a step in the production process, this was deemed undesirable.

PEG-silanes As an alternative to PVA as a surface coating, coating by PEG-silanes was evaluated. By silanizing the surfaces, covalent bonds will form between the PEG polymers and the substrate, creating a PEG brush which will prevent adhesion, provided it is sufficiently thick and dense, as discussed in Chapter 2.4.2. Silanization enables the experimenter to coat large or multiple areas simultaneously. The covalent bonds ensure that the film will remain tightly bound to the surface where less stable bonds may break with time or exposure to different environmental factors. While they provide an easy means of coating a surface, silanes may polymerize without addition of a catalyst triggering the silanization reaction, provided water is present, as may be inferred from the reaction scheme in Figure 2.10. Such polymerization will render the product unable to react further, rendering it useless for our purposes. During the thesis work, a batch of PEG-silanes was polymerized and gradual degradation of anti-adhesive properties were experienced until the silanes were too degraded to provide the anti-adhesive properties desired. A temporary change to PVA coating was therefore deemed necessary until new polymers could be ordered.

5.1.2 Polydopamine as Bacterial Adhesive

Polydopamine (PD), a mussel adhesive protein (MAP)-inspired adhesive, can readily adhere to most surfaces and bind amine groups, thiols, and metal ions, [48–51]. In the case of bacteria adhering to a PD film, we judge amine groups in the proteins expressed in the bacterium's cell wall (for Gram positive) or outer membrane (for Gram negative) is the most likely candidate for adhesion. Amine groups are present both at a terminal end of proteins (N-terminus), and as side chains in multiple amino acids. Thiols, being present only in the amino acid cysteine, are less abundant among amino-acids than amine groups, and fewer are likely available for interaction with the PD. How many amine and thiol groups the respective bacterium presents to the environment may well determine how likely the bacterium is to adhere to PD. Besides being capable of binding amine and thiol moieties PD is also capable of binding to PVA and PEG-coated surfaces [43]. This means the polymer can be used to pattern such surfaces and serve as a bacterial adhesive on surfaces which otherwise resist adhesion. This property was a major contributor to the choice in bacterial adhesive, though it was also selected due to its low price, the high availability of the chemical and its low toxicity [52–54].

5.1.3 Charge Mediated Adhesion

Initial experiments prior to Ottesen's commencement in this project were based on the charge of the bacteria in an attempt to control their adhesion. Bacteria have, generally speaking, a negative net surface charge [1, 36]. Based on this, positively charged polymers may be able to bind the bacteria to a pattern using electrostatic interactions. For this regime, bovine serum albumin (BSA), which can be used to reduce protein and cellular adhesion, was used as an adhesion resistant chemical [14, 70, 71, 73]. The positively charged poly-L-lysine (PLL) or polyethyleneimine (PEI) were used to promote adhesion. Surfaces prepared with this chemistry failed to isolate the bacterial strain used, *E. coli* DH5alpha (Figure 4.1(a)). Given that arrays of PD onto PEG or PVA also fail to isolate the same *E. coli* strand, the original chemical basis was re-tested, using *P. putida* KT2440 as a test organism. The results, shown in Figure 4.18, reveals that *P. putida* did not respond positively to the charge mediated regime initially explored, but that selective immobilization was successful if PD was deposited onto PEG or PVA alone, or co-deposited with a positively charged polymer, such as PLL or PEI. From co-deposition experiments performed in previous work, it is known that co-deposition of PLL or PEI with PD onto a surface coated with PVA or PEG is possible [18, 66]. When charged polymers such as PLL or PEI are co-deposited with PD, it is not known how significantly the charged polymers impact the adhesion. As co-deposition of charged polymers may permit other adhesion mechanisms than what is affforded by PD, it may be worth exploring if other species of bacteria are to be immobilized with the developed technique described in this thesis.

5.2 Stamp Design and Optimization

Combined with a new chemical regime (patterns of PD on PEG or PVA), a new stamp design was made to identify the optimal island size for isolation of single bacteria. This design is referred to as the prototype design in this text. The prototype design consists of thirteen equidistantly (along the horizontal axis) spaced circular pillar-like punches with a diameter increasing from 0.8 to 4.4 µm (Figure 5.2).

Figure 5.2: Prototype stamp pattern with designed island diameter, in µm, denoted below each island. Average measured island diameter, in µm, is denoted above each. Island separation d for the stamps used to create bacterial arrays was 8 µm. Island size is to scale (according to design), island separation is not to scale.

This design, inspired by Rozhok et al. [9], was designed to test two different pattern parameters; island size and island separation. The goal of the thesis work was to isolate a few or, ideally, a single bacterium per array coordinate. That is to say, create bacterial micro-arrays with cellular resolution. By varying both the spacing and the diameter of the punches, patterns which would allow identification of both the ideal island size and the ideal spacing between the islands could be created.

Once cast, pattern reproduction and island size were both considered by printing a fluorescent dye onto plain glass slides, and observing this by confocal laser scanning microscope (CLSM). The result, shown in Figure 5.3, reveals successful printing of large patterns using the prototype stamp. To measure the size of the deposited islands, these images were used in conjunction with ImageJ to measure the size of the printed islands, and from that calculate their diameter.

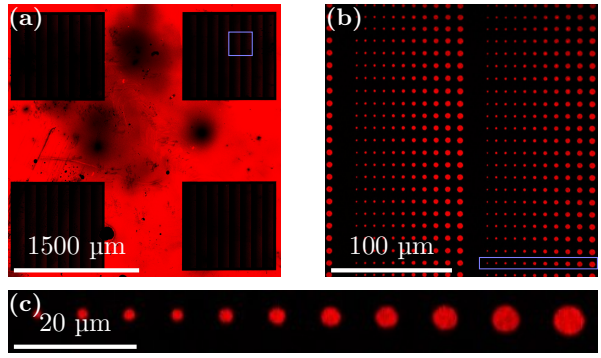

Figure 5.3: Fidelity of stamped prototype pattern. Entire stamped area (a), a subsection of the stamped area (b) a line of islands (c). This figure shows images from figures 4.3 and 4.4. The blue box in (a) shows an area corresponding to the pattern shown in (b) and the blue box in (b) shows the area magnified in (c)

5.3 Bacterial Arrays and Array Design Revision

Reproducible arrays of fluorescent ink demonstrated the viability of the stamps, but it does not demonstrate the efficacy of the technique when applied to isolate bacterial cells. In order to evaluate this, patterns of PD without a fluorescent label were printed onto surfaces functionalized with PEG or PVA. When *P. putida* in nutrient medium was subsequently added to the array, bacterial adhesion to the pattern was rapid, and bacterial arrays were produced with as little as five minutes incubation in bacterial solution (Figure 4.13).

5.3.1 Island Spacing

Prototype stamps were used to identify the optimal spacing between, and diameter of, the islands of bacterial adhesive. It is worth noting that the geometry used in the stamps means the vertical spacing between the islands will increase as the island diameter decreases. Horizontal spacing was, by design, equal between all islands. This difference in space led to an interesting observation; The horizontal spacing between islands did not appear to be sufficient, despite being at least four times the length of an individual non-filamentous *P. putida* KT2440 bacterium ($\sim$ 2 µm [91]). Bacterial bridges formed across the horizontal gaps on the stamp, or vertically between the largest islands especially, where the gaps were also small (Figure 5.4). Bridging appears less frequent in the larger, vertical gaps between small islands. This seems to suggest that the prototype design island spacing was insufficient, but close to functional for *P. putida*. A larger gap was deemed necessary to decrease the likelihood of such bridges forming on arrays printed using stamp design II. For this reason spacing of 10 and 15 µm was chosen in stamp design II to separate the islands: 10 µm, because it is approximately one *P. putida* bacterium's length above the maximum size available in the prototype design; 15 µm because 5 µm was thought to be a significant safety margin, in case 10 µm should prove unsatisfactory. It should be noted that these decisions are made on qualitative analysis of the situation. Given the presence of what appears to be filamentous *P. putida* on several of the collected micrographs, the supposed approximate length of one bacterium is likely not easily defined. Moreover, the size of a bacterium is difficult to clearly define regardless of whether the bacteria form filaments or not. This is due to the proteins, sugars and more presented to the environment by the bacterium which increases its effective size well beyond the membrane which is often used to describe a bacterium's size.

5.3.2 Island Diameter

To determine the optimal size of the islands of bacterial adhesive chemicals for isolation of single *P. putida* bacteria, multiple images were analyzed. Analysis was performed by manually counting the number of islands printed in each stamp column, which of these islands had no bacteria on them, and the number of islands with one and only one bacterium adhering. The results, seen in Chapter 4.3.1, revealed that the fifth largest island, intended to have a diameter of 2.8 µm, was close to ideal. Given that feature sizes on the stamp do not necessarily mirror the designed feature sizes exactly, this revelation alone would not tell us a definite size of this island; the results were compared with the island measurements presented in Chapter 4.2.1. The photolithography produced by photolithography may deviate from the design, depending on the UV dose used during exposure, and also upon the time spent in a developer bath. Moreover, polydimethylsiloxane (PDMS) may shrink during curing and swell if exposed to hydrophobic chemicals [23]. Beside this, the stamping process itself may well deform the stamps by application of forces, as discussed in Chapter 2.2.4, and further distort the intended features [25, 26].

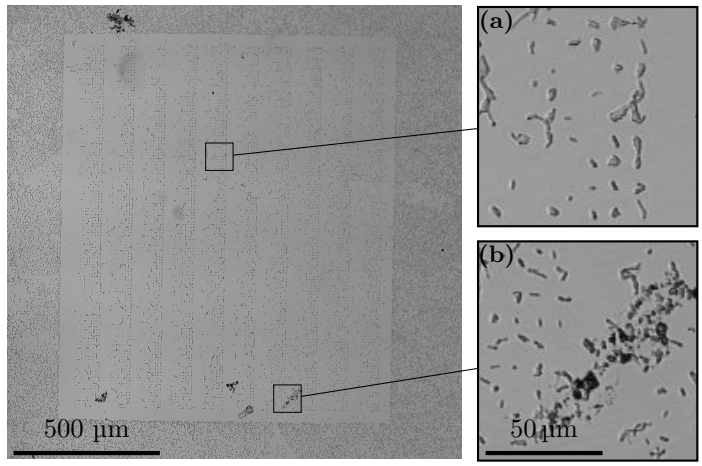

Figure 5.4: Bacterial microarray from Figure 4.11 reproduced for clarity. *P. putida* forms bridges across the gaps between islands (a) and adhering to areas outside the deposited PD (b). Both subfigures shown at 8 times magnification over main figure.

To determine the size of printed islands from the prototype design, images of stamped fluorophores, observed by CLSM, were analyzed using ImageJ, as detailed in Chapter 3.2. The area of each island was used as a basis for calculating the average diameter of each island size, using the assumption that each island was perfectly circular. This assumption has pitfalls, as it does not account for deviations from the intended shape of each pillar. However, significant deviations from circularity were removed from the set of islands examined prior to analysis. Errors may also be introduced by the sample's physical dimensions. µCP deposits very thin films of the printed inks, as may be seen from Figure 4.9, which in turn means portions of the stamped area may more easily be outside the objective's depth of field (DOF) than would be the case for thicker samples. A rather pronounced example of this is seen in the image presented in Figure 4.10(c). Blurring and fading of these areas may lead to inaccurate measurements, which may broaden or shift the apparent size distribution of the islands. This can be compensated for by opening the pinhole, letting more photons be counted. Since the film is thin, few photons will emerge from areas outside the intended area; signal strength is increased, though some blurring will still be present. This means we may retain a good microscopy image with larger pinholes than is likely for thicker samples. Further correction may be introduced by using a lens with relatively low numerical aperture (NA), which results in a larger DOF, keeping a larger part of the sample in focus at a given time.

5.3.3 Pattern Quality

From CLSM inspections of fluorophore patterns we know there is a high degree of stamp-pattern fidelity. What the CLSM inspections cannot reveal is the thickness and the uniformity of the deposited islands. Nor can said technique tell us much about surface topography. For such studies, a high-resolution technique, specifically atomic force microscopy (AFM), may reveal more information about the surface pattern than is retrievable by CLSM. Inspection by AFM of a PEG-coated surface stamped with a PD-coated prototype stamp yielded the pattern shown in Figure 4.9, the plot from which is repeated in figure 5.5 for clarity.

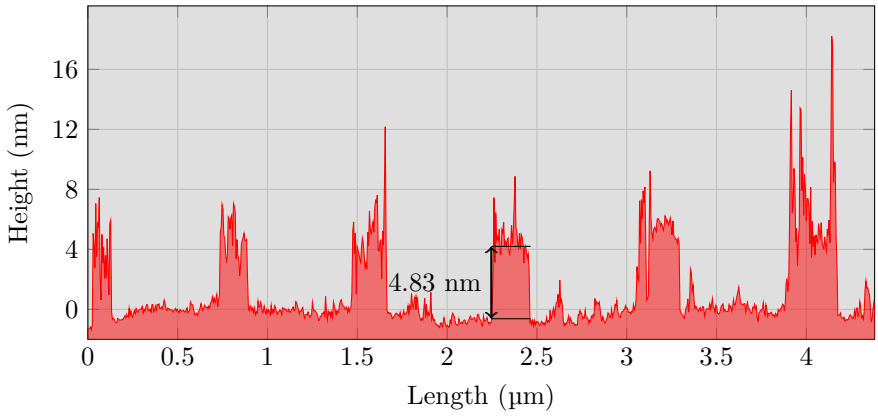

Figure 5.5: A profile plot across six PD islands on top of PEG. It is repeated from Figure 4.9 for clarity. The micrograph this plot is taken from is seen in Figure 4.9, was recorded by Katarzyna Maria Psonka-Antonczyk and is used with permission.

From the plot in Figure 5.5 we see that the thickness of the deposited PD islands is approximately 5 nm, and that the deposits are flat, uniform and fairly thin. The uniformity and thickness of the deposits suggests the technique developed herein may be suitable to observe bacteria isolated on the arrays by way of high resolution techniques such as AFM. The fairly low roughness of both the PEG brush and the PD islands should make distinguishing fine structures like flagella and fimbria possible using the developed technique. We also note the diameter of the islands as less than they should be, according to 4.1. There are several possible reasons; the stamps used in the two experiments are cast on different masters, and differences in exposure dosages and time spent in the developer bath may have altered the dimensions of the master features. Moreover, the photoresist used in casting of the respective masters was out of date (for fluorescence experiments) and freshly supplied by nanolab engineers (for AFM experiments). Moreover, in the preparation of the AFM samples, a lighter load was applied to the stamps which would cause less deformation of the punches, which in turn may have reduced the island size.

5.3.4 A New Design

By using the measured island diameter, seen in Table 4.1 and Figure 4.5(a), along with the data identifying which island is most likely to isolate one and only one bacterium, the dimensions of the ideal island size could be identified. This is shown in Chapter 4.3. A new design was made based on the results shown therein. Leaving the four quadrants separated by a thick support structure used in the prototype design, stamp design II measures approximately 9 mm^2 and have no support structures. This does yield much larger arrays when deposits are flawless on pristine surfaces, but it also makes the stamps more prone to roof collapse. This event was made more likely by the increased pillar spacing, as we can see from Equation 2.1 on page 11. A qualitative assessment was done in the lab to compensate for the new geometry; a change from the 100 g used in the prototype to 20 g yielded good results.

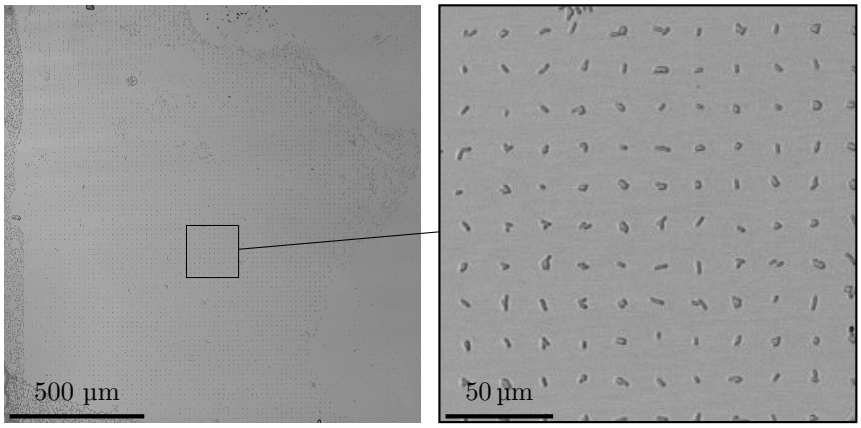

Figure 5.6: Figure 4.13(a) repeated for clarity. The micrograph displays *P. putida* adhering to a PD array printed onto PVA.

5.3.5 Microcontact Printing, Challenges

Data concerning the stamped patterns does reveal that reproducible arrays of bacteria adhering to reproducible patterns of PD were produced. There are, however, some challenges that relate to the current stamp design. Stamped patterns were on rare occasions not faithfully reproduced, and future applications

of this work may benefit from considering the optimization opportunities still afforded.

The Prototype Stamp Design

The prototype stamp design did not reproduce the smallest features at all. The MA6 mask aligner can, according to the producer, reproduce features down to 0.6 µm provided both that the photoresist is no thicker than 1 µm and the wafer is in hard, vacuum mediated contact with the photolithography mask. While tight contact between mask and wafer is possible by introducing an edge-bead removal process, a photoresist thickness of 1 µm or less would be ill-advised given that this would decrease the aspect ratio of the stamp features precariously, inviting roof collapse in the produced stamps. If patterns with such small features are desired, the prototype mask may be used, but it should be noted that a harder PDMS than Sylgard 184$^{\text{TM}}$ might benefit the experimenter by making the design less susceptible to deformation during the stamping process. Given the results described in Chapter 4.3.1, which reveal the five largest islands produce the best results for immobilizing a desirable number of bacteria per island, we judged the smallest islands superfluous.

Stamp Design II

Stamp design II, seen in Figure 3.2(b) on page 33, and discussed at some length above, consists of one large area (9 mm^2) with widely spaced pillars. Stamp design II has significantly lower punch density as the spacing between them has increased significantly from the prototype design. This means that the force experienced by one punch is a larger fraction of the total force applied to the stamp, leading to increased likelihood of stamp deformations, as described in Chapter 2.2.4.While the stamp design used produces patterns with fidelity, the new design has, for the aforementioned reasons, brought with it some challenges related to pattern reproduction.

Island size. The island size is crucial to whether one or multiple bacteria are isolated on a given island, as revealed by the arrays adhering to the prototype stamp design. When the mask for stamp design II was produced, the island size was set to the discovered ideal size. This does not mean these stamps automatically get the designed diameter. As can be understood from the results of island measurement, island size can be made to vary by altering different parameters in the photolithography process. Exposing the resist to high UV

dosage will, provided positive resists are used, increase depolymerization of the photoresist, thereby increasing feature size. Similarly, decreasing UV exposure will decrease depolymerization and thus decrease feature size.

During experimentation with stamp design II it was found that the island size was excessively large, as can be seen from the data in tables 4.4 and 4.5; the array islands with bacteria are likely to have more than one bacterium per coordinate. To alleviate this, new masters were produced using lower UV dosages than before. This did, as may be seen from Figure 4.6 and Table 4.2, result in reduced punch diameter, and subsequently it should also reduce island diameter. Note, however, the sloped sides of the punches in Figure 4.6(e), repeated here as Figure 5.7. Given that low-dosage stamps have such sloped sides, it is conceivable any force above a minimum to achieve stam-substrate contact will deform the punch, bringing portions of its walls into contact with the surface. Note also that smaller punches necessarily means a greater chance of other deformations as well.

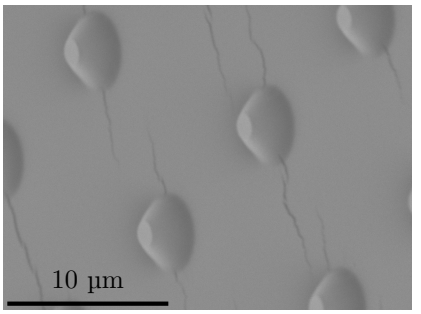

Figure 5.7: Figure 4.6(e) repeated for clarity. The image shows punches shaped like conical frustums with small apices and broad bases.

Considering Figure 5.8, which shows the same dataset shown in Figure 4.7 but split into one histogram from each contributing micrograph, we can see that there are differences within the same stamp batch. Given the size difference it does not appear likely these are due to minor differences in UV intensities across the master. Another possibility may be uneven force distribution during stamping, leading to different punch deformations across the stamps or from stamp to stamp. An aggravating factor may also have been the lack of support structures within the 9 mm^2 stamps. That there is a difference from micrograph to micrograph of patterns stamped with stamps from the same batch may indicate that there is a certain instability in stamp design II and that care should be taken when using stamps cast on a master of this design.

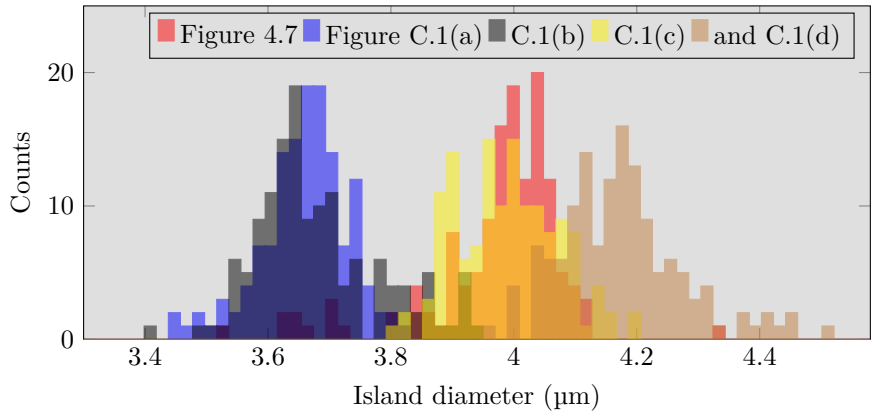

Figure 5.8: Figure 4.8 repeated for clarity. The figure shows size distributions for fluorophore islands, stamped using stamps of design II.

Despite the variations in island size we attempted to use stamps with reduced punch diameter to print arrays of PD on glass. Bacterial solution was added, and Live/Dead assays were performed. To minimize printing problems stamps were placed eight at a time onto the WillCo-dishes used; the stamps were made more rigid by application of a glass slide on their un-patterned side. Additionally, the weight used to stamp was reduced from 20 g per stamp to 20 g for all eight stamps combined. Despite these precautions the result was total or nearly total roof collapse, as may be seen in Figure 4.15(c), which shows an area where a pattern should exist. While this reveals the bacteria were alive on the PD coating, it also indicates that the stamps are insufficiently stiff to reliably produce patterns. The introduction of otherwise useless support structures in the pattern might alleviate this problem. Employing a mask design with smaller features and increasing the UV dosage might yield punches with straight, as opposed to sloped, sides. Such punch sides might reduce side wall collapse, which may be a contributing factor to the discussed challenge. The same result may be obtained by changing photoresist, though it is uncertain which resist is optimal for this purpose. Increasing the stiffness of the elastomer, for example by increasing the amount of curing agent used [92], or choosing a stiffer PDMS than Sylgard 184, might also raise the likelihood of producing functional stamps significantly.

5.4 Bacterial Survival on Array

Immobilization of bacteria onto microarrays holds little research value if the process of isolating them also kills them. In order to check the viability of immobilized bacteria, several tests were designed and performed. Arrays with immobilized bacteria were submerged in lysogeny broth growth medium (LB-medium) and subjected to a live-dead assay. The goal was to ascertain the viability of the array under different conditions and provide an assessment of whether the technique is viable as a means of isolating single bacteria for study.

5.4.1 In Liquid Growth Medium

By submerging the array in liquid growth media the bacteria are protected from desiccation and starvation. Daughter cells may adhere to PD islands or may escape to move through the liquid nutrient medium. While some mother cells are likely to escape the printed islands, as may be seen in Figure 5.9, others are likely to remain.

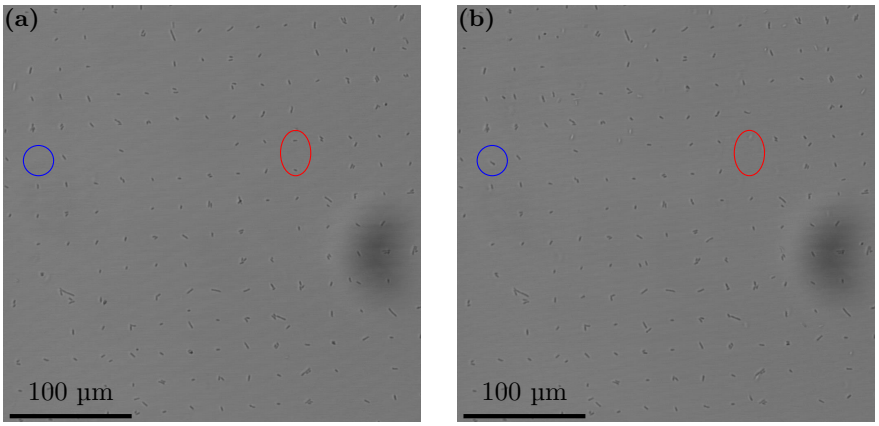

Figure 5.9: Images from timelapse recording. Repeated from Figure 4.15 for clarity. Images show areas where bacteria tore free from the array during the experiment (red ellipse) or adhered to it during the experiment (blue circle). These images were taken 18 minutes apart.

To assess the viability of a bacterial array while submerged in liquid nutrient media, LB-medium was added to existing bacterial microarrays and observed in a Leica SP5 CLSM over time. Given that the bacteria used in this experiment were not fluorescently labeled, transmission mode was used on the CLSM. For this mode, the Leica SP5 does not have a pinhole restricting light from entering the collector. This means light outside the focal point contributed significantly to the image, and some bacteria in the liquid immediately above the array were seen as clearly as the ones adhering to it. This may be seen in Figure 4.15, (a) and (d). Figure 5.9 reveals some of the changes seen in the array during the experiment. The marked areas show bacteria leaving the array, and bacteria adhering to it. What was not seen was bacteria appearing to elongate during this time. Given that only a small area was chosen and the sample allowed to dry somewhat before liquid nutrient media was added, it is possible, however unlikely, that the chosen area was practically devoid of live bacteria. The entire sample did not solely contain dead bacteria however. As may be seen in Figure 4.15(d) and Appendix D the nutrient media eventually filled with free bacteria, obscuring the array. Moreover, the video in Appendix D shows some bacteria on the array that are clearly motile and alive. Additionally, it is possible the cell division was halted due to temperature shock. A short time prior to being added to the array, the bacteria had been in an incubator set to 30°C, whereas ambient temperature in the lab was approximately 20°C. Sudden temperature changes such as this can stop cell division in bacteria for a time. A sudden temperature change will delay growth and increase generation time. For example, for *P. putida* KT2440 a change from 30°C to 10°C lead to a cessation of growth for 6 to 7 hours, and a subse-

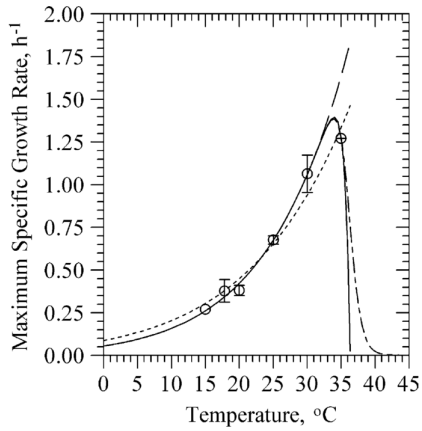

Figure 5.10: This figure is excerpted from Alagappan and Cowan [30]. The figure shows "The Effect of temperature on the maximum specific growth rate of *P. putida* F1 grown on non-inhibitory toluene concentration: (solid line) Topiwala–Sinclair model fit [93]; (long dash) Arrhenius model fit to the first five points (15–30°C); (short dash) Arrhenius model fit to all the data points (15–35°C), and (dash dot dash) Mayo model [94]." Citations to the Topiwala-Sinclair and Mayo models were added to this quote, which otherwise is extracted verbatim from Alagappan and Cowan [30].

quent generation time of 5 hours, ± 20 minutes, according to Fonseca, Moreno, and Rojo [29]. If we use data from [30], specifically Figure 4, which is repeated here as Figure 5.10 for clarity, we see that a change from 30 to 25°C would constitute a change in generation time from 56 minutes to 1 hour and 57 minutes. Alagappan and Cowan used a different *P. putida* strain and different growth conditions, which makes their results less applicable as a parallel to the results in this thesis, yet the work illustrates the significant difference in generation times experienced as a result of changing growth conditions. This difference should be applicable despite differing nutritional parameters. The time-lapse recording of the arrays submerged in growth medium does, after slightly less than 40 minutes, show a sudden arrival of a large multitude of bacteria. Some of these move in a fashion suggesting they are alive and motile, as opposed to just subject to Brownian motion and currents in the medium, which may or may not indicate death. Others move consistently with a current, possibly due to drying, and Brownian motion. These exhibit no apparent motility, which would be the case for dead bacteria, but also immotile bacteria which for other reasons do not display motility. Most of the bacteria appear to fall in the non-motile, group. Given the information available in the time-lapse, a conclusion cannot be drawn. Submerging the array in LB-medium and observing over time does not appear to provide sufficient information on bacterial viability over time. Further experimentation is needed to properly examine the portion of live versus dead bacteria isolated on the arrays. For this purpose, an analysis with live-dead assays should paint a clearer picture of the survival of bacteria immobilized on arrays.

5.4.2 Live-Dead Assay

The results discussed up to this point have revealed that *P. putida* may readily be immobilized on patterns of PD. We have also demonstrated that this adhesion is rapidly initiated, and that it remains stable when submerged in LB-medium. While time-lapse recordings indicate some bacterial cells survive the adhesion process, it is not clear how many. To ascertain this, a live/dead assay may be used. These work by staining bacteria with different dyes depending on their condition. Life Technologies' *Bac*Light™ series of assays use cell wall integrity as a measure for life or death [87]. Live bacteria are assumed to have intact cell walls, whereas dead bacteria are assumed to have ruptured walls. While this gives a good indication, the assumption is not perfect; some bacteria scored as dead may still retain or restart metabolic function, whereas metabolism may have ceased in cells with intact cell walls [95].

Labeling arrays with the kit reveals that the vast majority of cells have intact cell walls after isolation on arrays. According to *Bac*Light^{TM} assays seen in Chapter 4.4, the process of isolation and cleaning does not kill the bacteria; approximately 99% of the isolated bacteria are scored as alive after immobilization. Repeated experiments with submersion in growth medium for a time reveals further that the bacteria remain viable even after 120 minutes.During the experiment we experienced severe roof collapse, meaning the quantitative potential inherent in the micro-array approach was lost, and only a qualitative analysis of longer term effects on bacterial viability could be obtained. Yet as seen in Figure 4.16, it appears evident that for the first 120 minutes there is very little change in bacterial viability. From 120 to 180 minutes, something appears to have changed, and a larger portion of the bacteria are stained red, meaning they are scored as dead by the *Bac*Light^{TM} assay. The samples were not agitated during the incubation period, nor was fresh medium added during it. This, coupled with the immobility of the bacteria, is likely to have caused a local buildup of metabolites/waste product around the bacteria as well as a local reduction in nutrient availability in the immediate vicinity of the immobilized bacterial cells. This may have been a factor contributing to the increased portion of bacteria with compromised membranes. As only one sample was subjected to a three hour incubation time, other factors outside of our control may also have been partially responsible for the outcome.

5.5 Price per Array

A goal of the developed method has been to keep the costs low. The cost of producing one master may vary greatly from case to case and is therefore discounted in this estimate. Given the specialized equipment and chemicals needed, we estimate this to be the most costly component by far. Dyes and substrates such as cover slips are also ignored from the following table as this may vary according to the needs of the experimenter. Considering the raw materials needed to produce an array, we can produce an estimate for the cost of one array. The costs are based on consumption levels used to obtain the results in this thesis.

Table 5.1: Cost estimates for raw materials used in the described micro-array. The price listed for PDMS assumes a stamp will only be used once, though it may be re-used many times.

Compound	Price (USD)	Qty (g)	Price per gram (USD)	Price per sample (USD)	Producer
PEG	485	0.5	970	$4.85 \cdot 10^{-2}$	Nanocs
PDMS	60.48	500	0.12	$2.05 \cdot 10^{-2}$	DowCorning[a]
PD	449.1	100	4.49	$9.36 \cdot 10^{-5}$	Sigma Aldrich
PVA	113.25	500	0.23	$1.13 \cdot 10^{-4}$	BDH

a: DowCorning does not sell PDMS directly. The listed price is retrieved from Ellsworth.

Price estimates are found in Table 5.1, which does not take into account the re-usability of the PDMS stamps. Moreover, it does not account for the substrates or growth medium used, which may vary greatly depending on the experimental setup. From this table, we can see that raw materials needed to print one 9 mm^2 PD array printed on a PEGylated surface costs approximately 0.07 USD at the time of writing. To print a similar array onto a PVA coated surface costs approximately 0.02 USD. These prices, while we consider them low, may be reduced further by streamlining the production, or purchasing higher quantities of the raw materials employed, thereby reducing the amount of raw material needed or cost per gram of required raw materials even further.

It may be of interest to compare the raw material costs per micro-array with other consumables used in similar experiments. To compare the prices of other products used in this work, we may for example consider WillCo-dishes or borosilicate cover slips. Glass bottomed WillCo-dish kit-5030 costs approximately 680 USD for 500 dishes at the time of writing. Fisher Scientific's pack of 200 borosilicate cover slips (20 by 20 mm. Product code 12302128) costs 19.22 USD at the time of writing. Hence we see the chemical costs are far below or comparable to other, related consumables.

5.6 Future Work

The developed method has been tested for two bacterial species: *P. putida* KT2440 and *E. coli* DH5alpha. Of these two species, the array successfully isolated only *P. putida*. A multitude of bacterial species exist, and testing the developed method on other species may help determine the applicability of the method as it is, as well as whether a modification of the used chemistry may make it more general than the current formulation permits. Should isolation/immobilization of *E. coli* be particularly desirable, this may be pursued by modifying the described method. *E. coli* does show some affinity for PD, yet also adheres to the PEG-coating. Bacteria often use flaws in the anti-adhesive film, and may compress a PEG brush in order to adhere [96]. It is therefore possible a denser and/or thicker PEG brush may reduce this undesired adhesion. Besides this, it may, given the apparent low affinity for PD exhibited by the strain, be beneficial to look into co-depositing PD with a charged polymer, such as PLL or PEI. This may conceivably increase the likelihood of adhesion to the adhesive islands, by encouraging adhesion by electrostatic interactions.

Further use of the arrays, as opposed to further optimization of them, may be attempted by encasing the arrays in a gel matrix. Examples of biopolymers which may be used for this purpose includes agar or, if the heat of melted agar causes unacceptable stress for the studied species, another biopolymer such as alginate may be used. By such encasing it should be possible to study cell division and colony formation on each separate array coordinate.

For studies in liquid environments, it may be beneficial to integrate the arrays into microfluidic devices, pumping nutrient fluid or other fluids across the array to observe for example bacterial reactions to changes in nutrient environments or to specific chemicals such as antibiotics diluted in the nutrient solution. Integration of ordered bacterial microarrays with microfluidic devices holds potential for affecting bacteria on the array itself. Such an integration could make use of other experimental systems downstream, studying the daughter cells of the bacteria isolated on the array. A similar approach to studying daughter cells has been proposed by Shaw et al. [97] for eukaryotic cells.

The developed method likely has potential beyond what the author envisions. The previously mentioned opportunities for improvement and future uses of the array is not intended to be an exhaustive list, but rather a select few, brief examples of possible future development of the method described in the current thesis.

Concluding Remarks

6

Formulating the goals of this project in a list form, we can say the goal was to produce arrays that

- immobilize bacteria on a well defined grid, preferably one bacterium per grid coordinate,
- are cheap to produce,
- cause minimal harm to the bacteria,
- do not require advanced skills or expensive lab equipment,
- can immobilize bacteria from different species.

In the following, the successfulness of meeting each of these goals is evaluated.

Immobilization of bacteria. Arrays of viable *P. putida* KT2440 can be produced using the method described in this thesis. The number of islands with one or more bacteria on it has been seen to be over 97% on most experiments using stamp design II, though the majority of these islands have more than one bacterium per island. The number of bacteria per island is related to the island's diameter. While an optimal island size for *P. putida* KT2440 was identified using the prototype stamp design, stamp design II, which was intended to produce islands of this size, did not produce islands with a consistent diameter, as may be seen in Figure 5.8. A likely cause is the increased space between punches as well as the increased total area of the stamp. These two factors likely contributed to decrease stamp stability which may contribute to pattern deformation or degradation. Consequently, consistent immobilization of single bacterial cells per array coordinate necessitates a revision of either stamp design, elastomer stiffness or both.

Costs. Consumable costs can be held low as the produced arrays can be made using well known chemicals that are readily available. Raw material costs are estimated to be well below one US Cent per micro-array (Table 5.1). While this does not account for production of the initial master, substrates, fluorescent dyes or catalysts such as acetic acid or tris, the method described herein can be considered low cost once the initial master production costs are met.

Toxicity. Bacteria isolated on the printed arrays have been observed to survive immobilization for extended periods of time, provided nutrients are available. Labeling immediately after isolation indicates that as much as approximately 99% of the isolated bacteria are alive at the moment of immobilization. The chemicals used, PEG, PVA and PD are all known to be biocompatible, as argued earlier in this thesis. Live/Dead assays of the arrays seem to indicate the bacteria are not adversely affected by isolation on the arrays, and that they remain largely unaffected for hours after isolation, supporting the hypothesis that the developed method has low toxicity for *P. putida*.

Expertise Requirements. The production of a master requires access to cleanroom facilities with photolithography equipment, the use of which does require a certain level of expertise. However, once the master is produced casting of stamps and the production of microarrays does not require cleanroom facilities and can be performed with minimal training and no specialized expertise; the method is easy to use, and requires specialized expertise and equipment only in an initial phase.

Robustness. Polydopamine binds to thiols, which are present in cysteine, and to amine moieties, which are present on many amino acids and all amino terminal ends of proteins. Such moieties may be present on extrusions from most bacterial cell walls, permitting and even encouraging bacterial adhesion to the PD islands. If PD alone is not sufficient, PD may be co-deposited with other chemicals, such as PLL or PEI to provide alternate means of adhesion. We therefore hypothesize the proposed method is perhaps most likely to fail where bacteria to be studied are able to adhere even to the anti-adhesive coating. This seems to have been the case for *E. coli* DH5 alpha. As good functionality was demonstrated for only one of two tested species, we do not have empirical basis for a conclusion in favor of inter-species robustness.

The developed method successfully meets several of the intended goals and may, with further work, meet others such as cellular resolution and ability to immobilize and organize bacteria from a broad array of species. From the results presented we believe the method is cheap, rapid and simple to a sufficient extent to hold potential as a method applied by microbiologists and researchers in related fields.

Glossary

cleanroom *A cleanroom is a laboratory (manufacturing or scientific) environment with low and controlled levels of particulate contaminants in the air.* vii, 2, 4, 8, 92

elastomer *An elastomer is a viscoelastic polymer, typically with a low Young's modulus.* . . . . . iii, v, 2, 7, 9, 10, 82, 87, 91

fluorophore *Also fluorochrome. A molecule that can emit light after excitation in a process known as fluorescence.* 22, 34, 43, 46, 51, 77

HyD *A HyD (Short for Hybrid Detector) is a hybrid of photomultipliers and avalanche photodiodes.* 27, 45, 51, 54

mask *Commonly used in photolithography, a mask is a transparent plate with opaque sections or patterns.* 5, 6

master *A patterned surface on which elastomer stamps can be cast. Also commonly referred to as a mold.* 2, 7, 8, 50–52, 78, 81, 87, 92

PEGylation *Chemical modification of a surface, macromolecule or compound by attachment of PEG chains.* 36, 52, 87

photolithography *A process by which a thin photoresist film can be patterned by selective exposure to light, typically UV light.* . . 2, 6, 7, 31, 32, 76, 80, 81, 92

photoresist *A chemical compund consisting of polymers that form or break crosslinks when exposed to certain wavelengths of electromagnetic radiation (light).* 3–6, 31, 32, 78, 80, 82

punch *A punch is a feature protruding from a stamp surface which, by design, deposits ink onto a substrate when the stamp is used.* . 7, 33, 43, 51, 73, 78, 80–82, 91

soft lithography *A family of lithography techniques using elastomeric materials to construct patterns, usually on the micro- to nanometer scale [98].* 3, 7, 8

Bibliography

[1] Michael Madigan et al. *Biology of Microorganisms*. Ed. by Deirdre Espinoza et al. 13th, Glob. San Francisco: Pearson Education, 2011. ISBN: 978-0-321-73551-5.

[2] Douglas B Weibel, Willow R Diluzio, and George M Whitesides. "Microfabrication meets microbiology." In: *Nature reviews. Microbiology* 5.3 (Mar. 2007), pp. 209–18. ISSN: 1740-1534. DOI: 10.1038/nrmicro1616.

[3] EJ Gangarosa et al. "Impact of anti-vaccine movements on pertussis control: the untold story". In: *The Lancet* 351.9099 (Jan. 1998), pp. 356–361. ISSN: 01406736. DOI: 10.1016/S0140-6736(97)04334-1.

[4] World Health Organization (WHO). "WHO | Antimicrobial resistance". In: (2014).

[5] Reinhard Renneberg. *Biotechnology for Beginners*. Academic Press, 2007, p. 360. ISBN: 0123735815.

[6] Tse-Wen Chang. "Binding of cells to matrixes of distinct antibodies coated on solid surface". In: *Journal of Immunological Methods* 65.1 (1983), pp. 217–223.

[7] Claudia Holz et al. "Bacterial motility and clustering guided by microcontact printing." In: *Nano letters* 9.12 (Dec. 2009), pp. 4553–7. ISSN: 1530-6992. DOI: 10.1021/nl903153c.

[8] Aline Cerf et al. "Nanomechanical properties of dead or alive single-patterned bacteria." In: *Langmuir : the ACS journal of surfaces and colloids* 25.10 (May 2009), pp. 5731–6. ISSN: 0743-7463. DOI: 10.1021/la9004642.

[9] Sergey Rozhok et al. "Methods for fabricating microarrays of motile bacteria." In: *Small (Weinheim an der Bergstrasse, Germany)* 1.4 (Apr. 2005), pp. 445–51. ISSN: 1613-6829. DOI: 10.1002/smll.200400072.

[10] J Ziauddin and D M Sabatini. "Microarrays of cells expressing defined cDNAs." In: *Nature* 411.6833 (May 2001), pp. 107–10. ISSN: 0028-0836. DOI: 10.1038/35075114.

[11] Ieong Wong et al. "Accurate and effective live bacteria microarray patterning on thick polycationic polymer layers co-patterned with HMDS". In: *RSC Advances* 2.20 (2012), p. 7673. DOI: 10.1039/c2ra20938a.

[12] Krisztián Papp, Zoltán Szittner, and József Prechl. "Life on a microarray: assessing live cell functions in a microarray format." In: *Cellular and molecular life sciences : CMLS* 69.16 (Aug. 2012), pp. 2717–25. ISSN: 1420-9071. DOI: 10.1007/s00018-012-0947-z.

[13] Jieun Kim et al. "Direct-write patterning of bacterial cells by dip-pen nanolithography." In: *Journal of the American Chemical Society* 134.40 (Oct. 2012), pp. 16500–3. ISSN: 1520-5126. DOI: 10.1021/ja3073808.

[14] S. Petersen et al. "Hold on at the Right Spot : Bioactive Surfaces for the Design of Live-Cell Micropatterns". In: *Bioactive Surfaces*. Ed. by Hans G. Börner and Jean-Francois Lutz. Vol. 240. Advances in Polymer Science July 2010. Berlin, Heidelberg: Springer Berlin Heidelberg, 2011, pp. 35–78. ISBN: 978-3-642-20154-7. DOI: 10.1007/12.

[15] James L Wilbur et al. "Microfabrication by Microcontact Printing of Self-Assembled Monolayers **". In: *Advanc* 6.7-8 (1994), pp. 600–604. DOI: DOI:10.1002.

[16] Luping Xu et al. "Microcontact printing of living bacteria arrays with cellular resolution." In: *Nano letters* 7.7 (July 2007), pp. 2068–72. ISSN: 1530-6984. DOI: 10.1021/nl070983z.

[17] Sami Alom Ruiz and Christopher S. Chen. "Microcontact printing: A tool to pattern". en. In: *Soft Matter* 3.2 (Jan. 2007), p. 168. ISSN: 1744-683X. DOI: 10.1039/b613349e.

[18] Vegar Ottesen. *On the Development of a Bacterial Microarray by Microcontact Printing*. Project paper. Norwegian University of Science and Technology (NTNU), 2013.

[19] Michael Quirk and Julian Serda. *Semiconductor Manufacturing Technology*. Pearson Education, 2000. ISBN: 9780130815200.

[20] Tobias Kaufmann and Bart Jan Ravoo. "Stamps, inks and substrates: polymers in microcontact printing". In: *Polymer Chemistry* 1.4 (2010), p. 371. ISSN: 1759-9954. DOI: 10.1039/b9py00281b.

[21] Daniel J. Graham, David D. Price, and Buddy D. Ratner. "Solution Assembled and Microcontact Printed Monolayers of Dodecanethiol on Gold: A Multivariate Exploration of Chemistry and Contamination". In: *Langmuir* 18.5 (Mar. 2002), pp. 1518–1527. ISSN: 0743-7463. DOI: 10.1021/la010059z.

[22] Dow Corning. *Sylgard® 184 Silicone Elastomer Kit*.

[23] Seok Woo Lee and Seung S. Lee. "Shrinkage ratio of PDMS and its alignment method for the wafer level process". In: *Microsystem Technologies* 14.2 (May 2007), pp. 205–208. ISSN: 0946-7076. DOI: 10.1007/s00542-007-0417-y.

[24] Anne M. Ruminski et al. "Topological Control of Porous Silicon Photonic Crystals by Microcontact Printing". In: *Advanced Optical Materials* 1.7 (July 2013), pp. 510–516. ISSN: 21951071. DOI: 10.1002/adom.201300014.

[25] Emmanuel Delamarche et al. "Stability of molded polydimethylsiloxane microstructures". In: *Advanced Materials* 9.9 (1997), pp. 741–746. ISSN: 0935-9648. DOI: 10.1002/adma.19970090914.

[26] C.Y. Hui et al. "Constraints on Microcontact Printing Imposed by Stamp Deformation". In: *Langmuir* 18.4 (Feb. 2002), pp. 1394–1407. ISSN: 0743-7463. DOI: 10.1021/la0113567.

[27] Joseph E Petrzelka and David E Hardt. "Static load-displacement behavior of PDMS microfeatures for soft lithography". en. In: *Journal of Micromechanics and Microengineering* 22.7 (July 2012), p. 075015. ISSN: 0960-1317. DOI: 10.1088/0960-1317/22/7/075015.

[28] Juan-Luis Ramos, ed. *Pseudomonas Volume 1 Genomics, Life Style and Molecular Architecture*. Springer, 2004. ISBN: 978-1-4419-9086-0.

[29] Pilar Fonseca, Renata Moreno, and Fernando Rojo. "Growth of Pseudomonas putida at low temperature: global transcriptomic and proteomic analyses." In: *Environmental microbiology reports* 3.3 (June 2011), pp. 329–39. ISSN: 1758-2229. DOI: 10.1111/j.1758-2229.2010.00229.x.

[30] Gunaseelan Alagappan and Robert M Cowan. "Effect of temperature and dissolved oxygen on the growth kinetics of Pseudomonas putida F1 growing on benzene and toluene." In: *Chemosphere* 54.8 (Feb. 2004), pp. 1255–65. ISSN: 0045-6535. DOI: 10.1016/j.chemosphere.2003.09.013.

[31] Stephen Cooper and Charles E. Helmstetter. "Chromosome replication and the division cycle of Escherichia coli Br". In: *Journal of Molecular Biology* 31.3 (1968), pp. 519–540.

[32] C S Harwood, K Fosnaugh, and M Dispensa. "Flagellation of Pseudomonas putida and analysis of its motile behavior." In: *Journal of bacteriology* 171.7 (July 1989), pp. 4063–6. ISSN: 0021-9193.

[33] Juan-Luis Ramos and Alain Filloux. *Pseudomonas: Volume 5: A Model System in Biology*. Ed. by Juan-Luis Ramos and Alain Filloux. Springer, 2007. ISBN: 9780306483752.

[34] M. Espinosa-Urgel, A. Salido, and J.-L. Ramos. "Genetic Analysis of Functions Involved in Adhesion of Pseudomonas putida to Seeds". In: *Journal of Bacteriology* 182.9 (May 2000), pp. 2363–2369. ISSN: 0021-9193. DOI: 10.1128/JB.182.9.2363-2369.2000.

[35] Joerg C. Tiller. "Antimicrobial Surfaces, Bioactive Surfaces Chapter 7". In: *Bioactive Surfaces*. Ed. by Hans G. Börner and Jean François Lutz. Berlin, Heidelberg: Springer, 2010. Chap. 7, pp. 193–216. DOI: 10.1007/12_2010_101.

[36] Dirk Linke and Adrian Goldman, eds. *Bacterial Adhesion*. Vol. 715. Advances in Experimental Medicine and Biology. Dordrecht: Springer Netherlands, 2011, p. 374. ISBN: 978-94-007-0939-3. DOI: 10.1007/978-94-007-0940-9.

[37] Prof. Masahito Taya, Katsutoshi Hori, and Shinya Matsumoto. "Bacterial adhesion: From mechanism to control". In: *Biochemical Engineering Journal* 48.3 (2010), pp. 424–434.

[38] Alexander J B Zehnder. "Adhesion of the positively charged bacterium Stenotrophomonas (Xanthomonas) maltophilia 70401 to glass and Teflon . Adhesion of the Positively Charged Bacterium Stenotrophomonas (Xanthomonas) maltophilia 70401 to Glass and Teflon". In: (1996).

[39] J W Costerton et al. "Biofilms, the customized microniche." In: *Journal of bacteriology* 176.8 (Apr. 1994), pp. 2137–42. ISSN: 0021-9193.

[40] Christian Mayer et al. "The role of intermolecular interactions: studies on model systems for bacterial biofilms". In: *International Journal of Biological Macromolecules* 26.1 (1999), pp. 3–16.

[41] C J van Oss. "Energetics of cell-cell and cell-biopolymer interactions." In: *Cell biophysics* 14.1 (Feb. 1989), pp. 1–16. ISSN: 0163-4992. DOI: 10.1007/BF02797387.

[42] Haeshin Lee et al. "Mussel-inspired surface chemistry for multifunctional coatings." In: *Science (New York, N.Y.)* 318.5849 (Oct. 2007), pp. 426–30. ISSN: 1095-9203. DOI: 10.1126/science.1147241.

[43] Haeshin Lee, Norbert F Scherer, and Phillip B Messersmith. "Single-molecule mechanics of mussel adhesion." In: *Proceedings of the National Academy of Sciences of the United States of America* 103.35 (Aug. 2006), pp. 12999–3003. ISSN: 0027-8424. DOI: 10.1073/pnas.0605552103.

[44] Dong Soo Hwang, Sung Bo Sim, and Hyung Joon Cha. "Cell adhesion biomaterial based on mussel adhesive protein fused with RGD peptide." In: *Biomaterials* 28.28 (Oct. 2007), pp. 4039–46. ISSN: 0142-9612. DOI: 10.1016/j.biomaterials.2007.05.028.

[45] Jürgen Liebscher et al. "Structure of polydopamine: a never-ending story?" In: *Langmuir : the ACS journal of surfaces and colloids* 29.33 (Aug. 2013), pp. 10539–48. ISSN: 1520-5827. DOI: 10.1021/la4020288.

[46] Daniel R. Dreyer et al. "Perspectives on poly(dopamine)". en. In: *Chemical Science* 4.10 (Aug. 2013), p. 3796. ISSN: 2041-6520. DOI: 10.1039/c3sc51501j.

[47] Kang Sun et al. "Using self-polymerized dopamine to modify the antifouling property of oligo(ethylene glycol) self-assembled monolayers and its application in cell patterning." In: *Langmuir : the ACS journal of surfaces and colloids* 27.10 (May 2011), pp. 5709–12. ISSN: 1520-5827. DOI: 10.1021/la2012099.

[48] Haeshin Lee et al. "Mussel-inspired surface chemistry for multifunctional coatings." In: *Science (New York, N.Y.)* 318.5849 (Oct. 2007), pp. 426–30. ISSN: 1095-9203. DOI: 10.1126/science.1147241.

[49] Haeshin Lee et al. "Mussel-inspired surface chemistry for multifunctional coatings." In: *Science (New York, N.Y.)* 318.5849 (Oct. 2007), pp. 426–30. ISSN: 1095-9203. DOI: 10.1126/science.1147241.

[50] Haeshin Lee, Junsung Rho, and Phillip B Messersmith. "Facile Conjugation of Biomolecules onto Surfaces via Mussel Adhesive Protein Inspired Coatings." In: *Advanced materials (Deerfield Beach, Fla.)* 21.4 (Jan. 2009), pp. 431–434. ISSN: 1521-4095. DOI: 10.1002/adma.200801222.

[51] Bruce P Lee et al. "Mussel-Inspired Adhesives and Coatings." en. In: *Annual review of materials research* 41 (Aug. 2011), pp. 99–132. ISSN: 1531-7331. DOI: 10.1146/annurev-matsci-062910-100429.

[52] Yanlan Liu et al. "Dopamine-melanin colloidal nanospheres: an efficient near-infrared photothermal therapeutic agent for in vivo cancer therapy." In: *Advanced materials (Deerfield Beach, Fla.)* 25.9 (Mar. 2013), pp. 1353–9. ISSN: 1521-4095. DOI: 10.1002/adma.201204683.

[53] Rifang Luo et al. "In vitro investigation of enhanced hemocompatibility and endothelial cell proliferation associated with quinone-rich polydopamine coating." In: *ACS applied materials & interfaces* 5.5 (Mar. 2013), pp. 1704–14. ISSN: 1944-8252. DOI: 10.1021/am3027635.

[54] Yanlan Liu, Kelong Ai, and Lehui Lu. "Polydopamine and Its Derivative Materials: Synthesis and Promising Applications in Energy, Environmental, and Biomedical Fields." In: *Chemical reviews* (Feb. 2014). ISSN: 1520-6890. DOI: 10.1021/cr400407a.

[55] Sook Hee Ku, Joon Seok Lee, and Chan Beum Park. "Spatial control of cell adhesion and patterning through mussel-inspired surface modification by polydopamine." In: *Langmuir : the ACS journal of surfaces and colloids* 26.19 (Oct. 2010), pp. 15104–8. ISSN: 1520-5827. DOI: 10.1021/la102825p.

[56] Hsiu-Wen Chien et al. "Tunable micropatterned substrates based on poly(dopamine) deposition via microcontact printing." In: *Langmuir : the ACS journal of surfaces and colloids* 28.13 (Apr. 2012), pp. 5775–82. ISSN: 1520-5827. DOI: 10.1021/la300147p.

[57] Anran Liu et al. "Polypyrrole actuator with a bioadhesive surface for accumulating bacteria from physiological media." In: *ACS applied materials & interfaces* 1.4 (May 2009), pp. 951–5. ISSN: 1944-8244. DOI: 10.1021/am9000387.

[58] B E Rabinow et al. "Biomaterials with permanent hydrophilic surfaces and low protein adsorption properties." In: *Journal of biomaterials science. Polymer edition* 6.1 (Jan. 1994), pp. 91–109. ISSN: 0920-5063.

[59] Maria Laura Immordino, Franco Dosio, and Luigi Cattel. "Stealth liposomes: review of the basic science, rationale, and clinical applications, existing and potential." In: *International journal of nanomedicine* 1.3 (Jan. 2006), pp. 297–315. ISSN: 1176-9114.

[60] Hwankyu Lee et al. "A coarse-grained model for polyethylene oxide and polyethylene glycol: conformation and hydrodynamics." In: *The journal of physical chemistry. B* 113.40 (Oct. 2009), pp. 13186–94. ISSN: 1520-6106. DOI: 10.1021/jp9058966.

[61] Raphaël Barbey et al. "Polymer brushes via surface-initiated controlled radical polymerization: synthesis, characterization, properties, and applications." In: *Chemical reviews* 109.11 (Nov. 2009), pp. 5437–527. ISSN: 1520-6890. DOI: 10.1021/cr900045a.

[62] Stéphanie Pasche et al. "Effects of ionic strength and surface charge on protein adsorption at PEGylated surfaces." In: *The journal of physical chemistry. B* 109.37 (Sept. 2005), pp. 17545–52. ISSN: 1520-6106. DOI: 10.1021/jp050431+.

[63] D Mantzavinos et al. “Catalytic wet air oxidation of polyethylene glycol”. In: *Applied Catalysis B: Environmental* 11.1 (Dec. 1996), pp. 99–119. ISSN: 09263373. DOI: 10.1016/S0926-3373(96)00037-9.

[64] Seongok Han, Chongyoup Kim, and Dongsook Kwon. “Thermal/oxidative degradation and stabilization of polyethylene glycol”. In: *Polymer* 38.2 (Jan. 1997), pp. 317–323. ISSN: 00323861. DOI: 10.1016/S0032-3861(97)88175-X.

[65] D A Herold, K Keil, and D E Bruns. “Oxidation of polyethylene glycols by alcohol dehydrogenase.” In: *Biochemical pharmacology* 38.1 (Jan. 1989), pp. 73–6. ISSN: 0006-2952.

[66] Kai M Beckwith and Pawel Sikorski. “Patterned cell arrays and patterned co-cultures on polydopamine-modified poly(vinyl alcohol) hydrogels”. en. In: *Biofabrication* 5.4 (Dec. 2013), p. 045009. ISSN: 1758-5082. DOI: 10.1088/1758-5082/5/4/045009.

[67] D. A. Barrett et al. “Resistance to Nonspecific Protein Adsorption by Poly(vinyl alcohol) Thin Films Adsorbed to a Poly(styrene) Support Matrix Studied Using Surface Plasmon Resonance”. In: *Analytical Chemistry* 73.21 (Nov. 2001), pp. 5232–5239. ISSN: 0003-2700. DOI: 10.1021/ac010368u.

[68] J. Koziarz and H. Yamazaki. “Stabilization of poly vinyl alcohol coating of polyester cloth for reduction of bacterial adhesion”. In: *Biotechnology Techniques* 13.4 (1999), pp. 221–225. ISSN: 0951208X.

[69] Thomas Peterbauer et al. “Simple and versatile methods for the fabrication of arrays of live mammalian cells.” en. In: *Lab on a chip* 6.7 (July 2006), pp. 857–63. ISSN: 1473-0197. DOI: 10.1039/b601803c.

[70] Emanuele Ostuni et al. “Selective Deposition of Proteins and Cells in Arrays of Microwells”. In: *Langmuir* 17.9 (May 2001), pp. 2828–2834. ISSN: 0743-7463. DOI: 10.1021/la001372o.

[71] Pascal Jonkheijm et al. “Chemical strategies for generating protein biochips.” In: *Angewandte Chemie (International ed. in English)* 47.50 (Jan. 2008), pp. 9618–47. ISSN: 1521-3773. DOI: 10.1002/anie.200801711.

[72] Ute Böhme and Ulrich Scheler. “Effective charge of bovine serum albumin determined by electrophoresis NMR”. In: *Chemical Physics Letters* 435.4 (2007), pp. 342–345.

[73] Emilie Bulard et al. “Competition of bovine serum albumin adsorption and bacterial adhesion onto surface-grafted ODT: in situ study by vibrational SFG and fluorescence confocal microscopy.” In: *Langmuir : the ACS journal of surfaces and colloids* 28.49 (Dec. 2012), pp. 17001–10. ISSN: 1520-5827. DOI: 10.1021/la302976u.

[74] W.C. Bigelow, D.L. Pickett, and W.A. Zisman. “Oleophobic monolayers”. In: *Journal of Colloid Science* 1.6 (Dec. 1946), pp. 513–538. ISSN: 00958522. DOI: 10.1016/0095-8522(46)90059-1.

[75] T Materne, F de Buyl, and GL Witucki. “Organosilane Technology in Coating Applications: Review and Perspectives”. In: *Dow Corning Corporation, USA* (2006).

[76] CRC Press. *Nanotechnology in Biology and Medicine: Methods, Devices, and Applications (Google eBook)*. Ed. by Tuan Vo-Dinh. CRC Press, 2007, p. 792. ISBN: 1420004441.

[77] Clifford A. Schlecht and Joshua A. Maurer. “Functionalization of glass substrates: mechanistic insights into the surface reaction of trialkoxysilanes”. en. In: *RSC Advances* 1.8 (Nov. 2011), p. 1446. ISSN: 2046-2069. DOI: 10.1039/c1ra00421b.

[78] P. Silberzan et al. “Silanation of silica surfaces. A new method of constructing pure or mixed monolayers”. In: *Langmuir* 7.8 (Aug. 1991), pp. 1647–1651. ISSN: 0743-7463. DOI: 10.1021/la00056a017.

[79] M Minsky. “Microscopy apparatus”. In: *US Patent 3,013,467* (1961).

[80] JB Pawley, ed. *Handbook of biological confocal microscopy*. Third. Springer, 2006, p. 985. ISBN: 038725921X.

[81] Life Technologies. *Fluorescence SpectraViewer*. 2014.

[82] William G. Lawrence et al. “A comparison of avalanche photodiode and photomultiplier tube detectors for flow cytometry”. In: ed. by Daniel L. Farkas, Dan V. Nicolau, and Robert C. Leif. Feb. 2008, pages. DOI: 10.1117/12.758958.

[83] Kenneth R. Spring and Michael W. Davidson. *Olympus Microscopy Resource Center | Digital Imaging in Optical Microscopy - Concepts in Digital Imaging - Avalanche Photodiodes*. 2012.

[84] Frank Schreiber, Holger Birk, and Rolf T. Borlinghaus. “Sensors for True Confocal Scanning”. In: (Aug. 2012).

[85] R F Egerton. *Physical Principles of Electron Microscopy*. An Introduction to TEM, SEM, and AEM. New York : Springer Science+Business Media, 2005. ISBN: 9780387258003.

[86] WillCo Wells. *WillCo-dish Kit Assembly Instructions*. 2009.

[87] Life Technologies. *Live/Dead BacLight Bacterial Viability Kits*. 2004.

[88] Peter Eaton and Paul West. *Atomic Force Microscopy*. Oxford University Press, Mar. 2010. ISBN: 9780199570454. DOI: 10.1093/acprof:oso/9780199570454.001.0001.

[89] CRC Press. *Atomic Force Microscopy in Nanobiology*. CRC Press, 2014, p. 458. ISBN: 978-981-4411-58-5.

[90] Yang Leng. *Materials Characterization*. Introduction to Microscopic and Spectroscopic Methods. Wiley, 2009. ISBN: 9780470822999.

[91] Michael L Davis et al. "2D motility tracking of Pseudomonas putida KT2440 in growth phases using video microscopy." en. In: *Journal of bioscience and bioengineering* 111.5 (May 2011), pp. 605–11. ISSN: 1347-4421. DOI: 10.1016/j.jbiosc.2011.01.007.

[92] Elizabeth A. Wilder et al. "Measuring the Modulus of Soft Polymer Networks via a Buckling-Based Metrology". In: *Macromolecules* 39.12 (June 2006), pp. 4138–4143. ISSN: 0024-9297. DOI: 10.1021/ma060266b.

[93] H Topiwala and C G Sinclair. "Temperature relationship in continous culture." In: *Biotechnology and bioengineering* 13.6 (Nov. 1971), pp. 795–813. ISSN: 0006-3592. DOI: 10.1002/bit.260130606.

[94] Aloice W. Mayo. "Effects of temperature and pH on the kinetic growth of unialga *Chlorella vulgaris* cultures containing bacteria". In: *Water Environment Research* 69.1 (Jan. 1997), pp. 64–72. ISSN: 10614303. DOI: 10.2175/106143097X125191.

[95] D B Roszak and R R Colwell. "Survival strategies of bacteria in the natural environment." In: *Microbiological reviews* 51.3 (Sept. 1987), pp. 365–79. ISSN: 0146-0749.

[96] S Gon et al. "How Bacteria Adhere to Brushy PEG Surfaces: Clinging to Flaws and Compressing the Brush." In: *Macromolecules* 45.20 (Oct. 2012), pp. 8373–8381. ISSN: 0024-9297. DOI: 10.1021/ma300981r.

[97] Josephine Shaw et al. "A microfluidic "baby machine" for cell synchronization." en. In: *Lab on a chip* 12.15 (Aug. 2012), pp. 2656–63. ISSN: 1473-0189. DOI: 10.1039/c2lc40277g.

[98] Younan Xia and George M. Whitesides. “Soft Lithography”. en. In: *Angewandte Chemie International Edition* 37.5 (Mar. 1998), pp. 550–575. ISSN: 1433-7851. DOI: 10.1002/(SICI)1521-3773(19980316)37:5<550::AID-ANIE550>3.0.CO;2-G.

Appendices

Fluorophore Arrays, Prototype Design

A

In addition to the array shown in Figure 4.4, the arrays shown in Figure A.1 were used to collect the data tabulated in Table 4.1 and shown in a histogram in Figure 4.5.

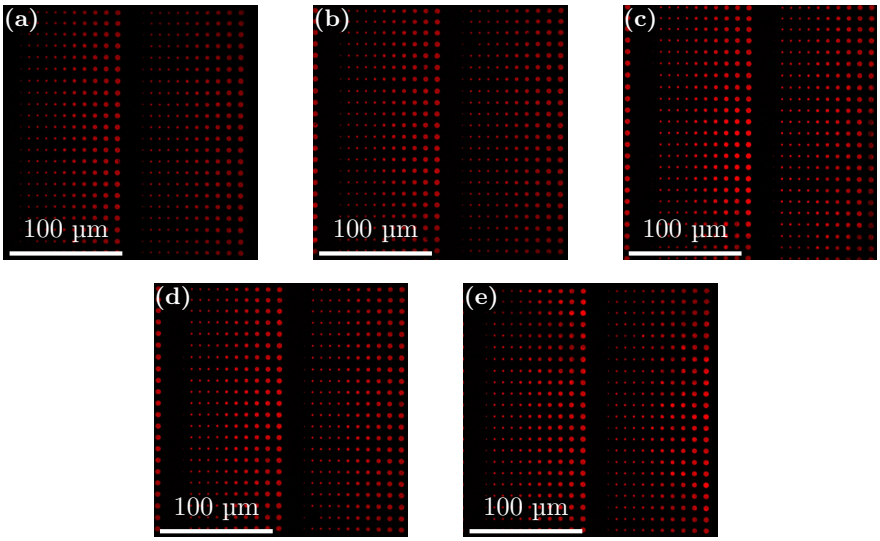

Figure A.1: Fluorophores (QD655) stamped using the prototype stamp design. The arrays in these micrographs were used along with the micrograph in Figure 4.4 to generate the data tabulated in Table 4.1 and shown in a histogram in Figure 4.5. Parameters and microscope used are identical to what is detailed for Figure 4.4

Bacterial Arrays

B

In addition to the bacterial array in Figure 4.11 the arrays in Figure B.1 were used to collect data for Figure 4.12 and Table 4.3.

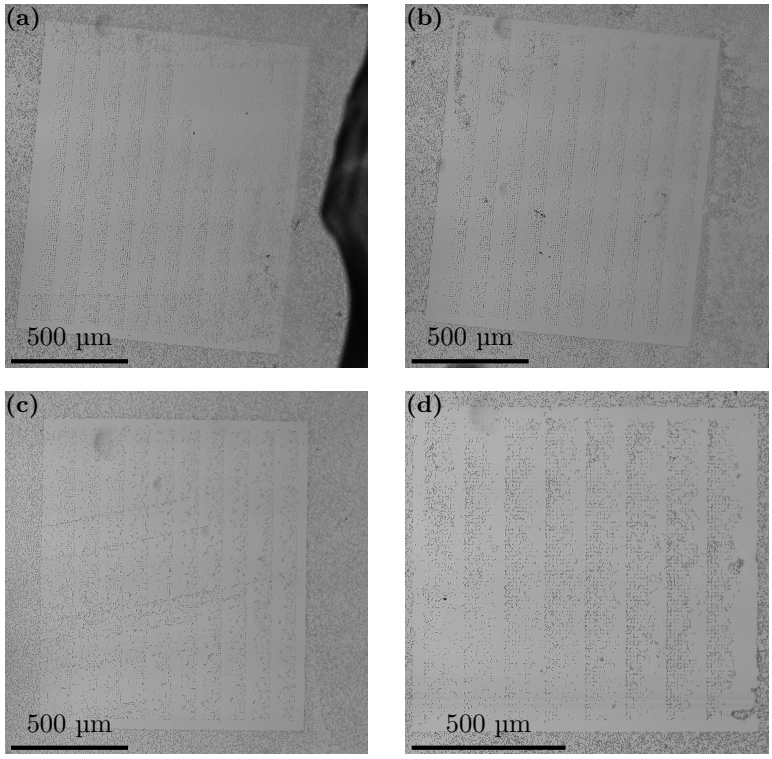

Figure B.1: *P. putida* adhering to polydopamine arrays printed on a PVA film. These arrays were, in addition to the array shown in Figure 4.11, used in collecting data for Figure 4.12 and Table 4.3. Note that areas with large numbers of bacteria adhering outside the PD islands were omitted in the analysis. These micrographs were recorded with the same settings as are detailed for Figure 4.11.

Fluorophore Arrays, Stamp Design II

C

In Figure 4.7 fluorophores stamped using stamp design II is shown. Together with that array, the arrays in Figure C.1 were used to generate the histograms shown in figures 4.8 and 5.8.

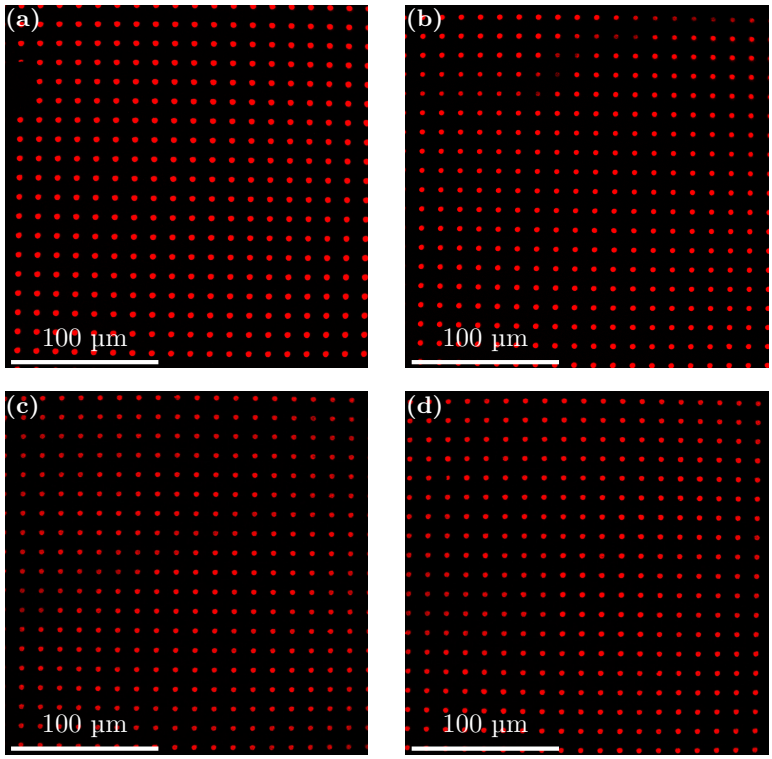

Figure C.1: QD655 stamped onto borosilicate cover slips using stamp design II. These micrographs, in addition to Figure 4.7, were used to obtain the data displayed in figures 4.8 and 5.8. Parameters and microscope used are identical to what is detailed for Figure 4.7.

Time-lapse Recording

D

Figure D.1 shows a time-lapse recording of *Pseudomonas putida* KT2440 adhering to PD islands printed on PVA. The figure is a video if the thesis is viewed digitally on Adobe's own PDF readers.

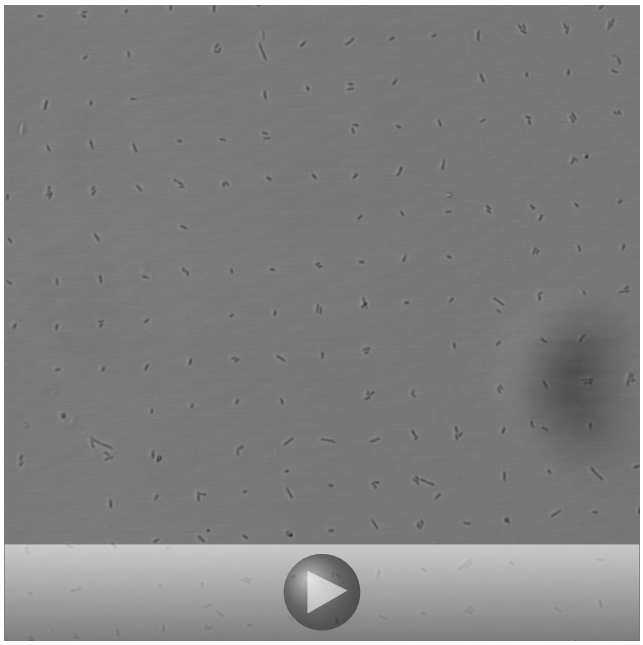

Figure D.1: Recorded time-lapse of *P. putida* isolated on PD, printed on PVA. Images excerpted from this video are seen in figures 4.15 and 5.9. Video available at time of writing only when using Adobe's own PDF readers with Flash plugin, currently available for Microsoft Windows and Mac OS X exclusively. For space conservation reasons the video is clipped at beginning and, more significantly, end. A Leica TCS SP5 was used to obtain these images. Transmitted light was collected in a photomultiplier tube (PMT) and is shown as greyscale. The objective used was a Leica HCX PL APO CS 10.0x0.40 dry UV. A diode-pumped solid-state laser (DPSS) laser emitting with a wavelength of 561 nm was used. Compression, clipping and conversion to mp4 done by MPEG Streamclip by Squared5.

Live Dead Assays

E

Live dead assays performed in this thesis utilized two different dyes, fluorescing with different wavelengths. The two dyes can then be picked up in different channels on the microscope. These channels can be seen combined into a single image, as in Figure 4.16 or they can be seen separately, as in Figure E.1.

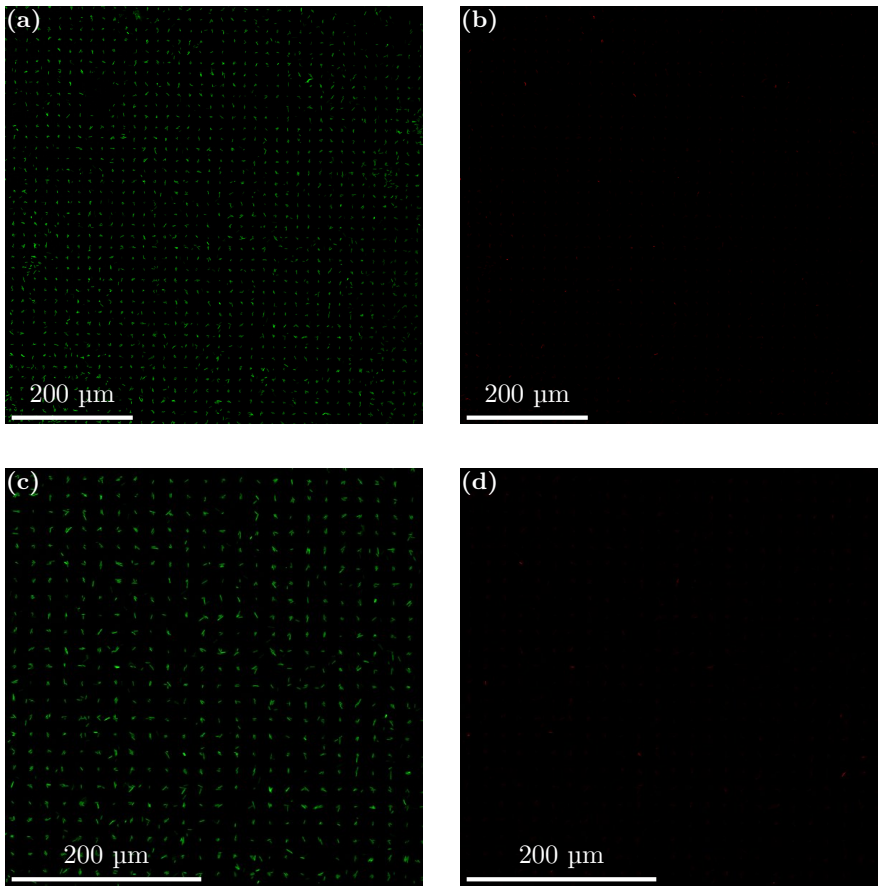

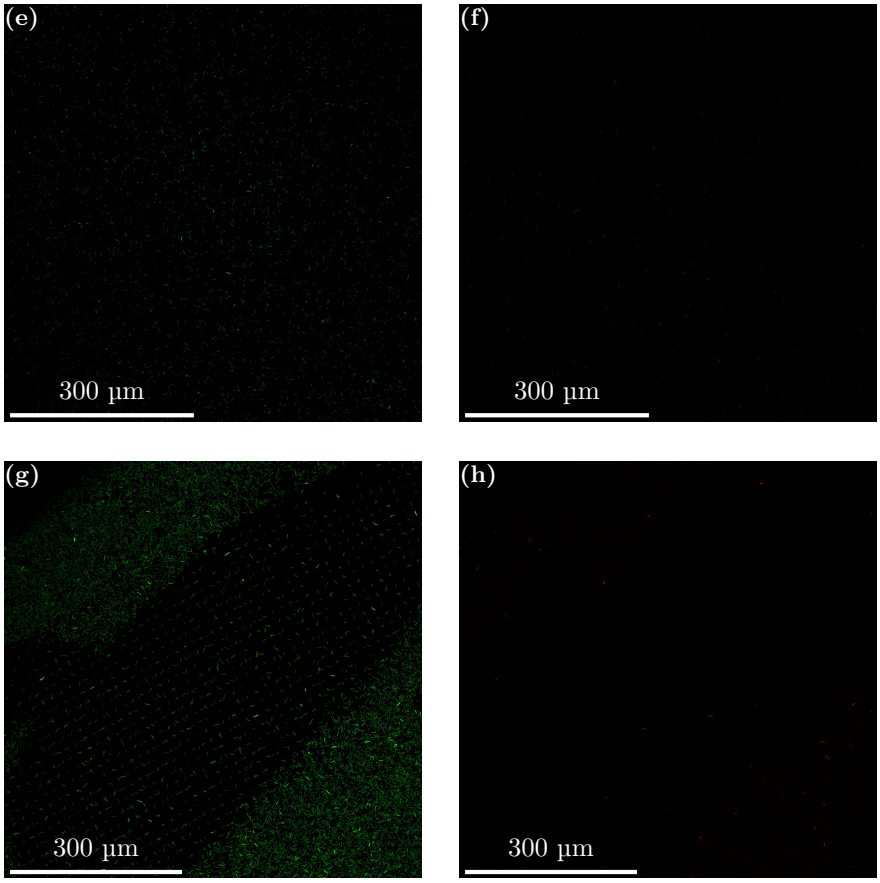
(e)
300 µm
(f)
300 µm
(g)
300 µm
(h)
300 µm

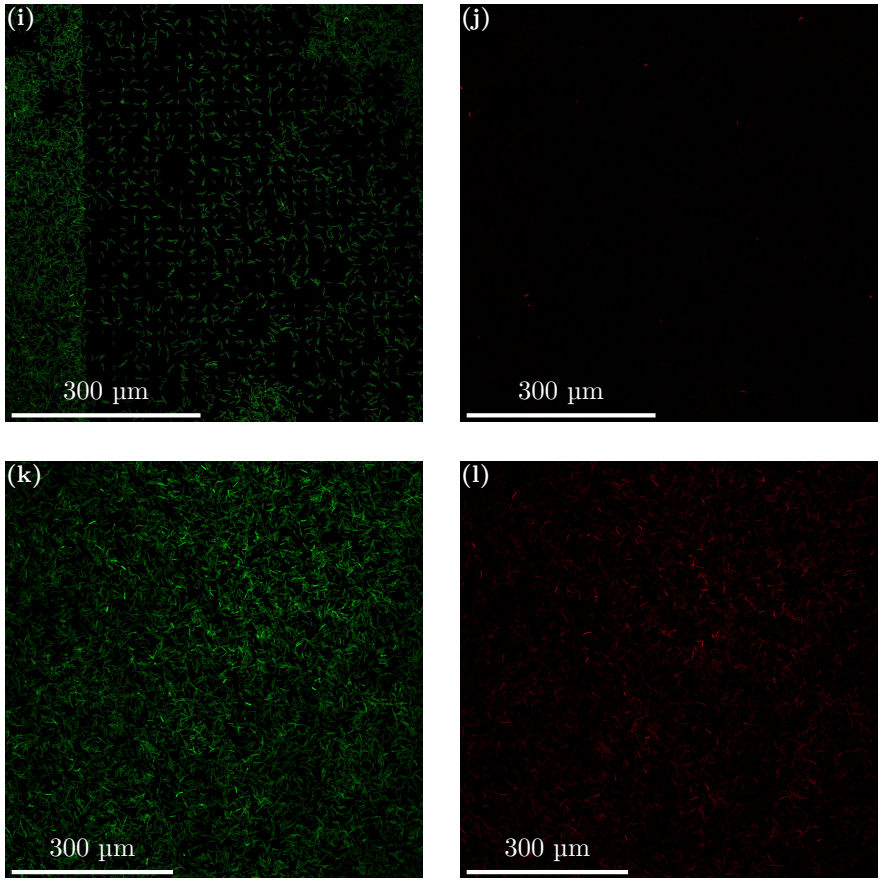

Figure E.1: Split fluorescent channels from Live/Dead assays. The channels are merged in Figure 4.16. Subfigures (a), (c), (e), (g), (i) and (k) show bacteria with intact cell walls, assumed to be alive. The other subfigures show bacteria with permeable cell walls, assumed dead. (a) and (b) are from Figure 4.15(a). (a) and (d) are from Figure 4.15(b). (e) and (f) are from Figure 4.15(c). (g) and (h) are from Figure 4.15(d). (i) and (j) are from Figure 4.15(e). (k) and (l) are from Figure 4.15(f). Note that figures (g) through (l) were taken by Nina Bjørk Arnfinnsdottir.